Drug Discoveries & Therapeutics

ISSN 1881-7831 Online ISSN 1881-784X
Volume 3, Number 6, December 2009
www.ddtjournal.com

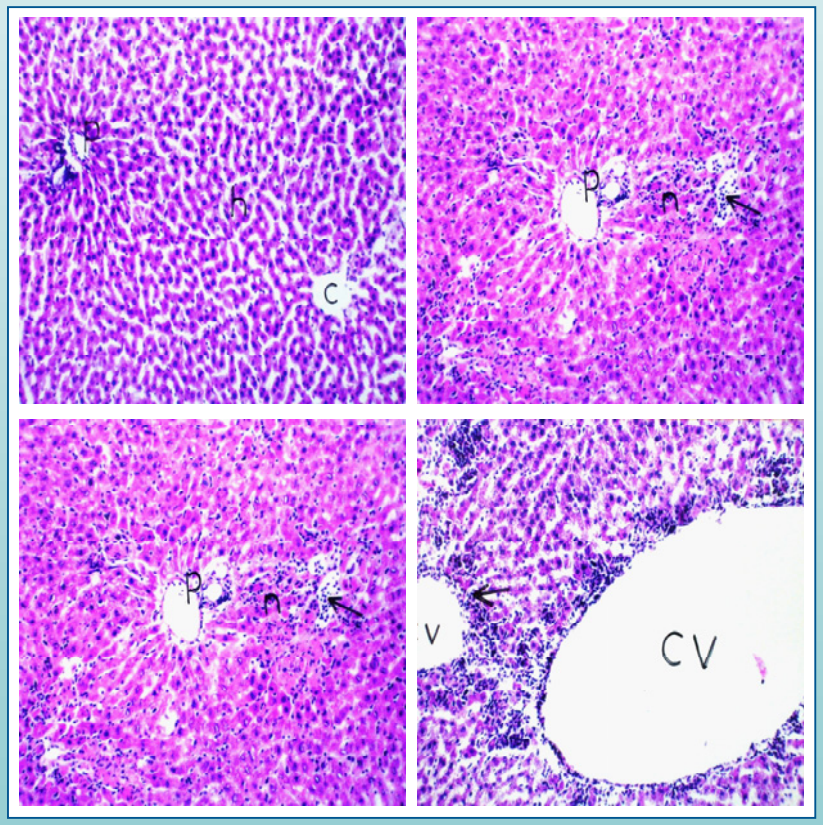

Shandong University China-Japan Cooperation Center for Drug Discovery & Screen
International Advancement Center for Medicine & Health Research

Drug Discoveries & Therapeutics

Drug Discoveries & Therapeutics is a peer-reviewed international journal published bimonthly by *Shandong University China-Japan Cooperation Center for Drug Discovery & Screen* (SDU-DDSC) and *International Advancement Center for Medicine & Health Research Co., Ltd.* (IACMHR Co., Ltd.).

Drug Discoveries & Therapeutics mainly publishes articles related to basic and clinical pharmaceutical research such as pharmaceutical and therapeutical chemistry, pharmacology, pharmacy, pharmacokinetics, industrial pharmacy, pharmaceutical manufacturing, pharmaceutical technology, drug delivery, toxicology, and traditional herb medicine. Studies on drug-related fields such as biology, biochemistry, physiology, microbiology, and immunology are also within the scope of this journal.

Subject Coverage: Basic and clinical pharmaceutical research including Pharmaceutical and therapeutical chemistry, Pharmacology, Pharmacy, Pharmacokinetics, Industrial pharmacy, Pharmaceutical manufacturing, Pharmaceutical technology, Drug delivery, Toxicology, and Traditional herb medicine.

Language: English
Issues/Year: 6
Published by: IACMHR and SDU-DDSC
ISSN: 1881-7831 (**Online ISSN** 1881-784X)
CODEN: DDTRBX

Editorial and Head Office

Wei TANG, MD PhD
Executive Editor
Drug Discoveries & Therapeutics

TSUIN-IKIZAKA 410,
2-17-5 Hongo, Bunkyo-ku,
Tokyo 113-0033, Japan.
Tel: 03-5840-9697
Fax: 03-5840-9698
E-mail: office@ddtjournal.com
URL: www.ddtjournal.com

IACMHR CO., LTD.

Drug Discoveries & Therapeutics

Editorial Board

CONTENTS

Volume 3, Number 6, 2009

Brief Report

Original Articles

CONTENTS (*Continued*)

Index

Guide for Authors

Copyright

Brief Report

Ivermectin inactivates the kinase PAK1 and blocks the PAK1-dependent growth of human ovarian cancer and NF2 tumor cell lines

Hisashi Hashimoto[1,2], Shanta M. Messerli[3], Tamotsu Sudo[1], Hiroshi Maruta[4,*]

[1] *Hyogo Cancer Center, Akashi, Hyogo, Japan;*
[2] *Department of Obstetrics and Gynecology, Ehime University School of Medicine, Ehime, Japan (Present address);*
[3] *Marine Biological Laboratory, Woods Hole, Mass, USA;*
[4] *NF Cure Japan, Melbourne, Australia.*

ABSTRACT: Ivermectin is an old anti-parasitic antibiotic which selectively kills nematodes at a very low dose (0.2 mg/kg) by inhibiting their gamma-aminobutyric acid (GABA) receptor, but not mammalian counterpart. Interestingly, several years ago it was reported by a Russian group that Ivermectin can suppress almost completely the growth of human melanoma and a few other cancer xenografts in mice at the much higher doses (3-5 mg/kg) without any adverse effect on mice. However, its anti-cancer mechanism still remained to be clarified at the molecular levels, that would determine the specific type of cancers susceptible to this drug. The first hint towards its anti-PAK1 potential was a recent finding that Ivermectin at its sublethal doses dramatically reduces the litter size (number of eggs laid) of the tiny nematode *C. elegans*. Interestingly, either a PAK1-deficiency (gene knock-out) or treatment with natural anti-PAK1 products such as caffeic acid phenethyl ester (CAPE) and artepillin C (ARC), the major anti-cancer ingredients in propolis, also causes the exactly same effect on this nematode, suggesting the possibility that the kinase PAK1 might be a new target of Ivermectin. This kinase is required for the growth of more than 70% of human cancers such as pancreatic, colon, breast and prostate cancers and neurofibromatosis (NF) tumors. Here we demonstrate for the first time that Ivermectin blocks the oncogenic kinase PAK1 in human ovarian cancer and NF2-deficient Schwannoma cell lines to suppress their PAK1-dependent growth in cell culture, with the IC_{50} between 5-20 μM depending on cell lines.

Keywords: Ivermectin, PAK1, ovarian cancer, neurofibromatosis type 2 (NF2), *C. elegans*

**Address correspondence to:*
Dr. Hiroshi Maruta, NF Cure Japan, Melbourne, Australia.
e-mail: julie8860@gmail.com

1. Introduction

Ivermectin/Avermectin is an antibiotic of macrolide family isolated in 1979 from a filamentous bacterium called *Streptomyces avermitilis* (*1*), and further developed by Merck and Kitasato Institute during mid-1980s as the exceptionally potent and most broad spectrum anti-parasitic drug which kills the intestinal worms (nematodes) in human and several other mammals such as horse and dog at a very low dose (0.2 mg/kg) (*2*). It blocks selectively the worms' GABA (γ-aminobutyric acid) receptor (*3*), but not mammalian counterpart. In 1987 it was found that Ivermectin is a muscle relaxant which blocks the phosphorylation of the regulatory light chain of myosin II (double-headed myosin) in tonic Ascaris suum muscle (*4*), indicating that this drug somehow inhibits a kinase(s) responsible for the phosphorylation of this myosin light chain. The tiny nematode *C. elegans* swallows its food, bacteria, by pharyngeal pumping. In 1990 it was reported that Ivermectin at sublethal doses reduces dramatically the rate of this pumping, leading to a near starvation/fast (*5*), indicating that this drug relaxes the pharyngeal smooth muscle of this nematode. In 2004 a Russian group demonstrated that Ivermectin can suppress the growth of human melanoma and a few other cancer xenografts in mice at the higher doses (3-5 mg/kg) almost completely without any adverse effect on mice (*6*). This prompted us to determine the detailed molecular mechanism underlying its anti-cancer action.

Interestingly, prior to this investigation of ours, an Australian group reported that Ivermectin at sublethal doses reduces the litter size (number of eggs laid) of *C. elegans* by almost 90% (Grant W *et al*., unpublished observation). This phenomenon is almost identical to our own observation with either PAK1-deficiency (in the *C. elegans* strain RB689) or treatment of this nematode with anti-PAK1 drugs such as CAPE (caffeic acid phenethyl ester) and ARC (artepillin C), the major anti-cancer ingredients in NZ (New Zealand) and Brazilian green propolis (*7-9*), suggesting that the major oncogenic kinase PAK1 could be a new target

of Ivermectin. This notion is compatible with the previous observation that the regulatory light chain of myosin II is phosphorylated by PAK1 (*10*). Finally in the study presented here we provide the first direct evidence indicating that Ivermectin indeed inactivates the PAK1 in human ovarian cancer and NF2-deficient Schwannoma cell lines in cell culture, and can suppress the PAK1-dependent growth of these tumor cell lines, with the IC_{50} between 5-20 μM depending on cell lines.

2. Materials and Methods

2.1. *Cell lines and reagents*

Human ovarian cancer cell lines TYK-nu, KOC7c, SKOV3 and RMUG-S as well as human NF2-deficient Schwannoma cell line (HEI-193) were maintained under the standard cell culture conditions as described previously (*8,9*). Human normal embryonic kidney cell line (HEK-293) was obtained from American Type Culture Collection (ATCC). Ivermectin was purchased from Sigma-Aldrich (Cat #18898). Monoclonal antibody against p-Raf1 (Ser 338) was obtained from Cell Signaling (p-c-Raf Ser 338 #9427).

2.2. *Assay for the kinase activity of PAK1 in cell culture*

The phosphorylated level of the kinase Raf1 at Ser 338 (p-Raf1) was monitored by means of the monoclonal antibody against p-Raf1 (×1,000 dilution), as the direct indicator of the kinase activity of PAK1 in ovarian cancer cell lines, TYK-nu and RMUG-S, cultured in the presence or absence of Ivermectin (0-40 μM) for 48 h. Immunoblot analysis was performed as described previously (*9*), and the actin level was used as an internal control for the cellular protein loading at each gel slot.

2.3. *Cell growth inhibition by Ivermectin*

2.0×10^3 cells of ovarian cancer cell lines or 10^3 cells of Schwannoma cell line were seeded per well, and cultured for 3 and 6 days, respectively, in the presence or absence of Ivermectin, at various concentrations and their growth was monitored by MTT method, measuring the optical density at 550 nm as described previously (*8,9*).

3. Results and Discussion

3.1. *Inactivation of PAK1 by Ivermectin*

Since Ser 338 of the kinase RAF1 is the major target site by the phosphorylation of PAK1 and its phosphorylation is essential for the activation of the former (*9,11*), we monitored the kinase activity of PAK1 in each ovarian cancer cell line by measuring the phosphorylation levels of RAF-1 using the antibody specific for the phosphorylated (p)-Raf-1 (Ser 338). As shown in Figure 1, Ivermectin inhibits the phosphorylation of RAF-1 at Ser 338 in cell lines TYK-nu and RMUG-S with IC_{50} around 5 and 20 μM, respectively, clearly indicating that Ivermectin inactivates PAK1 somehow in these cancer cells.

3.2. *Inhibition of growth of ovarian cancer and NF2-deficient Schwannoma cells*

To see whether Ivermectin can suppress the growth of human ovarian cancer cell lines which requires the kinase PAK1 (*12*), we determine the IC_{50} of Ivermectin for their growth. As shown in Figure 2, Ivermectin inhibits the growth of 4 distinct cancer ovarian cell lines including TYK-nu and RMUG-S with IC_{50} around 10 and 20 μM, respectively. Since the IC_{50} of Ivermectin for both PAK1 and growth are roughly the same in each cell line, it is most likely that the growth inhibition of these cell lines is mainly due to the inactivation of PAK1 by Ivermectin.

To further confirm this notion, we have tested the effect of Ivermectin on the growth of NF2-deficient Schwannoma cell line (HEI-193) which has been established to require the kinase PAK1 and inhibited by a variety of anti-PAK1 drugs such as CEP-1347,

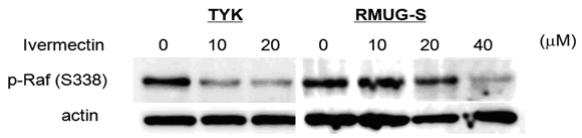

Figure 1. Ivermectin down-regulates the phosphorylation of Raf1 at Ser 338 (p-Raf1) by inactivating the kinase PAK1 in two different ovarian cancer cell lines, TYK-nu and RMUG-S. The p-Raf1 levels were estimated by the monoclonal antibody against p-Raf1 as described under "Materials and Methods".

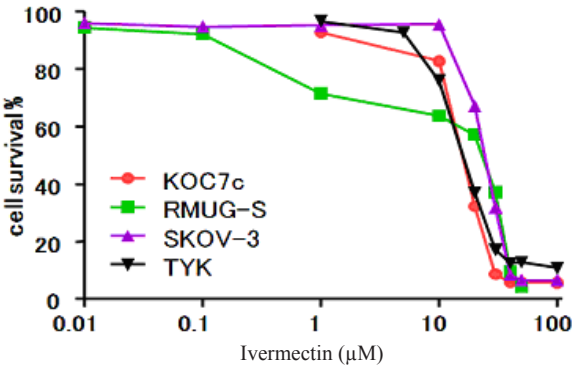

Figure 2. Ivermectin inhibits the growth of four different human ovarian cancer cell lines at the indicated concentrations. For detail, see "Materials and Methods".

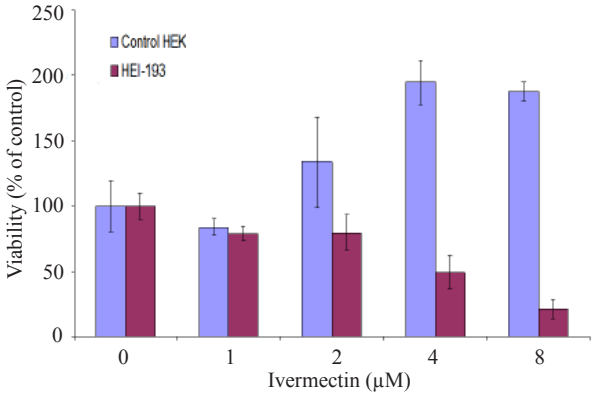

Figure 3. Ivermectin inhibits the growth of human Schwannoma cell line HEI-193, but not the normal cell line HEK-293. Statistical analysis indicates a significant difference in the viability between the control HEK-293 and HEI-193 at 4-8 μM of Ivermectin ($p < 0.001$).

FK228, CAPE, and ARC (*8,9,13,14*). The NF2 gene product called Merlin is a direct inhibitor of PAK1, and therefore in the NF2-deficient cell lines, PAK1 is abnormally activated (*13,14*). As shown in Figure 3, the PAK1-dependent growth of this Schwannoma cell line was selectively inhibited by Ivermectin with the IC_{50} around 5 μM, whereas Ivermectin at these tested concentrations showed no toxicity on the control normal human embryonic kidney cell line (HEK-293) at all, confirming again that PAK1 is not essential for the normal cell growth. These data altogether strongly suggest that Ivermectin would be potentially useful for the treatment of both ovarian cancers and NF2 tumors as well as many other PAK1-dependent cancers such as pancreatic, colon, gastric, breast, prostate, cervical, lung, and thyroid cancers, melanoma, MM (multiple-myeloma), glioma, hepatoma, and NF1-deficient cancer such as MPNST (*12-19*).

As the effective therapeutics for these PAK1-dependent cancers or tumors, only the bee products "propolis" such as CAPE-based Bio 30 and ARC-based Brazillian green propolis extract (GPE) have been available on the market. Furthermore, Ivermectin turned out to be the sole chemically defined anti-PAK1 drug which is available on the market inexpensively so far. Although Bio 30 is the most effective and inexpensive, it causes an allergic reaction to 1-2% of population, whereas GPE causes no allergic reaction, but is far more expensive and less effective than Bio 30 (*8,9*). Thus, Ivermectin could be an inexpensive alternative of Bio 30 for those who are allergic to CAPE in Bio 30. The reasonably low price (around a dollar or so for daily treatment) is in particular important for NF and TSC (Tuberous Sclerosis) tumor patients, because these rare disorders are genetic diseases and their treatment which often starts in early childhood would be life-long, unlike cancer treatment which usually starts at much older ages and lasts for only a short time period.

Acknowledgements

This work was funded by the NF Cure Award to S. M. M. and also supported by the NIH Biocurrents Research Center at MBL (P41 RR001395).

References

1. Burg RW, Miller BM, Baker EE, Birnbaum J, Currie SA, Hartman R, Kong YL, Monaghan RL, Olson G, Putter I, Tunac JB, Wallick H, Stapley EO, Oiwa R, Omura S. Avermectins, a new family of potent anthelminthic agents: Producing organism and fermentation. Antimicrob Agents Chemother. 1979; 15:361-367.
2. Omura S, Crump A. The life and times of ivermectin: a success story. Nature Rev Microbiol. 2004; 2:894-899.
3. Wang CC, Pong SS. Actions of avermectin B1a on GABA nerves. Prog Clin Biol Res. 1982; 97:373-395.
4. Martin R, Donahue M. Correlation of myosin light chain phosphorylation and GABA receptors in Ascaris suum muscle. Comp Biochem Physiol C. 1987; 87:23-29.
5. Avery L, Horvitz HR. Effects of starvation and neuroactive drugs on feeding in *Caenorhabditis elegans*. J Exp Zool. 1990; 253:263-270.
6. Drinyaev VA, Mosin VA, Kruglyak EB, Novik TS, Sterlina TS, Ermakova NV, Kublik LN, Levitman MKh, Shaposhnikova VV, Korystov YN. Antitumor effect of avermectins. Eur J Pharmacol. 2004; 501:19-23.
7. Maruta H. An innovated approach to *in vivo* screening for the major anti-cancer drugs. In: Cancer Screening. Nova Publishing, 2009; in press.
8. Demestre M, Messerli SM, Celli N, Shahhossini M, Kluwe L, Mautner V, Maruta H. CAPE (caffeic acid phenethyl ester)-based propolis extract (Bio 30) suppresses the growth of human neurofibromatosis (NF) tumor xenografts in mice. Phytother Res. 2009; 23:226-230.
9. Messerli SM, Ahn MR, Kunimasa K, Yanagihara M, Tatefuji T, Hashimoto K, Mautner V, Uto Y, Hori H, Kumazawa S, Kaji K, Ohta T, Maruta H. Artepillin C (ARC) in Brazilian green propolis selectively blocks oncogenic PAK1 signaling and suppresses the growth of NF tumors in mice. Phytother Res. 2009; 23:423-427.
10. Chew T, Masaracchia R, Goeckeler Z, Wysolmerski R. Phosphorylation of non-muscle myosin II regulatory light chain by PAK. J Muscle Res Cell Motil. 1998; 19:839-854.
11. Zang M, Hayne C, Luo Z. Interaction between active Pak1 and Raf-1 is necessary for phosphorylation and activation of Raf-1. J Biol Chem. 2002; 277:4395-4405.
12. Khabele D, Son DS, Parl AK, Goldberg GL, Augenlicht LH, Mariadason JM, Rice VM. Drug-induced inactivation or gene silencing of class I histone deacetylases suppresses ovarian cancer cell growth: implications for therapy. Cancer Biol Ther. 2007; 6:795-801.
13. Hirokawa Y, Tikoo A, Huynh J, Utermark T, Hanemann CO, Giovannini M, Xiao GH, Testa JR, Wood J, Maruta H. A clue to the therapy of neurofibromatosis type 2: NF2/merlin is a PAK1 inhibitor. Cancer J. 2004; 10:20-26.
14. Hirokawa Y, Nakajima H, Hanemann CO, Kurtz A, Frahm S, Mautner V, Maruta H. Signal therapy of NF1-

deficient tumor xenograft in mice. Cancer Biol Ther. 2005; 4:379-381.
15. Sasakawa Y, Naoe Y, Inoue T, Sasakawa T, Matsuo M, Manda T, Mutoh S. Effects of FK228, a novel histone deacetylase inhibitor, on tumor growth and expression of p21 and c-myc genes *in vivo*. Cancer Lett. 2003; 195:161-168.
16. Hirokawa Y, Arnold M, Nakajima H, Zalcberg J, Maruta H. Signal therapy of breast cancers by the HDAC inhibitor FK228 that blocks the activation of PAK1 and abrogates the tamoxifen-resistance. Cancer Biol Ther. 2005; 4:956-960.
17. Hirokawa Y, Levitzki A, Lessene G, Baell J, Xiao Y, Zhu H, Maruta H. Signal therapy of human pancreatic cancer and NF1-deficient breast cancer xenograft in mice by a combination of PP1 and GL-2003, anti-PAK1 drugs (Tyr-kinase Inhibitors). Cancer Lett. 2007; 245:242-251.
18. Maruta H, Ohta T. Signal Therapy: Propolis and Pepper Extracts as Cancer Therapeutics. In: Complementary and Alternative Therapies and the Aging Population (Watson RR, ed). Elsevier, Inc., San Diego, CA, USA, 2008; pp. 523-539.
19. Messerli S, Li XN, Maruta H. Bio 30, the anti-PAK1 extract of NZ (New Zealand) propolis, blocks the growth of glioma from both adults and children grafted in mice. Manuscript in preparation, 2009.

(*Received October 25, 2009; Accepted October 27, 2009*)

Original Article

Pyrrolizidine alkaloid clivorine-induced oxidative stress injury in human normal liver L-02 cells

Qingning Liang[1,2], Tianyu Liu[2], Lili Ji[2,3,*], Yang Min[1], Yuye Xia[1,*]

[1] *The Department of Pharmacology, Shanghai Institute of Pharmaceutical Industry, Shanghai, China;*
[2] *The MOE Key Laboratory for Standardization of Chinese Medicines and the SATCM Key Laboratory for New Resources and Quality Evaluation of Chinese Medicines, Institute of Chinese Materia Medica, Shanghai University of Traditional Chinese Medicine, Shanghai, China;*
[3] *Shanghai R&D Centre for Standardization of Chinese Medicines, Shanghai, China.*

ABSTRACT: Clivorine is an otonecine-type pyrrolizidine alkaloid isolated from the traditional Chinese medicine *Ligularia hodgsonii* Hook. Pyrrolizidine alkaloids (PAs) are well-known hepatotoxins widely distributed around the world. The present study sought to evaluate clivorine-induced oxidative injury in human normal liver L-02 cells. After cells were treated with various concentrations of clivorine for 48 h, cellular total antioxidant capacity, glutathione-S-transferase (GST) and glutathione reductase (GR) were determined to evaluate oxidative injury. Results showed that cellular total antioxidant capacity and GST activity both increased in clivorine-treated L-02 cells, while clivorine decreased GR activity in cells. Further, the protective effects of some antioxidants such as ascorbic acid (vitamin C, Vc), Trolox, dithiothreitol (DTT) and mannitol against clivorine-induced cytotoxicity were observed. Results showed that Trolox, which is an analogue of tocopherol (vitamin E, Ve), prevented clivorine-induced cytotoxicity in L-02 cells. Taken together, these results revealed clivorine-induced oxidative injury in human liver L-02 cells. These results also indicated the possible use of Trolox in the reduction of clivorine-induced hepatotoxicity.

Keywords: Pyrrolizidine alkaloid, clivorine, oxidative injury, antioxidant, Trolox

**Address correspondence to:*
Dr. Lili Ji, The MOE Key Laboratory for Standardization of Chinese Medicines and the SATCM Key Laboratory for New Resources and Quality Evaluation of Chinese Medicines, Institute of Chinese Materia Medica, Shanghai University of Traditional Chinese Medicine, 1200 Cai Lun Road, Shanghai 201203, China.
e-mail: jll_syc@yahoo.com.cn

Dr. Yuye Xia, The Department of Pharmacology, Shanghai Institute of Pharmaceutical Industry, 1111 Zhong Shan Bei Yi Road, Shanghai 200437, China.
e-mail: xiayuye2004@126.com

1. Introduction

Mammalian cells are generally kept in a reducing environment that is maintained by various antioxidants. The overproduction of reactive oxygen species (ROS) will occur after the disruption of the cellular oxidant/antioxidant balance by exogenous oxidative injury and thus leading to cell death by the damage of cellular macromolecules such as lipids, proteins, and nucleic acids (*1*). The cellular redox balance is maintained by both enzymatic and nonenzymatic antioxidant systems to maintain the normal reducing environment in cells. Cellular nonenzymatic antioxidants primarily include α-tocopherol, ascorbic acid, and dithiothreitol (DTT), while the enzymatic antioxidant system includes catalase, superoxide dismutase, and reduced glutathione (GSH)-related enzymes such as glutathione S-transferase (GST), glutathione reductase (GR), glutathione peroxidase (GPx) (*2*). Many studies have found that oxidative stress injury was involved in hepatotoxin-induced toxicity in hepatocytes involving alcohol, acetaminophen, carbon tetrachloride, *etc*. (*3-5*).

Pyrrolizidine alkaloids (PAs) are natural hepatotoxins widely distributed in various species of plants around the world. Due to their serious liver injury, the U.S. Food and Drug Administration (FDA) proposed a series of research programs and instructions to alert people to the toxicity of PAs-containing herbs, while the British Medicines Healthcare Products Regulatory Agency (MHRA) and bodies in other European countries all formulated standards to limit the dosage of PAs per day. The hepatotoxicity of PAs has been widely investigated around the world. Clivorine is an otonecine-type PA abundant in *Ligularia hodgsonii* Hook and *Ligularia dentata* Hara, which are generally used to treat coughs, hepatitis, and inflammation in traditional Chinese medicine (*6,7*). Previous studies by the current authors have found that clivorine inhibited cell growth and induced cell apoptosis in normal human liver L-02 cells *via* cellular mitogen-activated protein kinases and mitochondrial-mediated apoptotic signal

pathways (*6,8,9*).

The present study was designed to observe clivorine-induced oxidative injury in human liver L-02 cells and protection provided by various antioxidants.

2. Materials and Methods

2.1. *Cells and reagents*

A L-02 cell line was derived from adult normal human livers (*10,11*) (Cell Bank, Type Culture Collection of Chinese Academy of Sciences), and cells were cultured in RPMI1640 supplemented with 10% (v/v) fetal bovine serum. Clivorine (Figure 1) was isolated from *Ligularia hodgsonii* Hook with a purity ≥ 99.5%. GSH, oxidized glutathione (GSSG), and NADPH were purchased from Roche Diagnostics GmbH (Mannheim, German). Unless indicated, other reagents were from Sigma Chemical Co. (St. Louis, MO, USA).

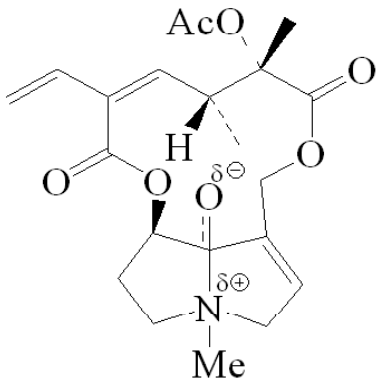

Clivorine, $C_{21}H_{27}NO_7$

Figure 1. The chemical structure of clivorine.

2.2. *Cell viability assay*

After various treatments, cells were incubated with 500 μg/mL 3-(4,5-dimethyl-thiazol-2-yl) 2,5-diphenyltetrazolium bromide (MTT) for 4 h. The functional mitochondrial dehydrogenases in surviving cells converted MTT to blue formazan, which was dissolved in 10% SDS-5% iso-butanol-0.01 M HCl (*12*). The optical density was measured at 570 nm, with 630 nm as a reference, and cell viability was normalized as a percentage of the control.

2.3. *Measurement of cellular total antioxidant capacity*

The ferric reducing antioxidant power (FRAP) assay is a simple and reliable colorimetric method commonly used to measure total antioxidant capacity (*13*). After treatment, cells were harvested in cold phosphate buffer (pH 7.0) and sonicated (2 × 5 sec) on ice and then centrifuged at 5,000 × g for 10 min. The supernatant was transferred to new tubes for determination. The FRAP testing buffer consisted of 300 mM acetate buffer (pH 3.6), 20 mM ferric chloride and 10 mM TPTZ in 40 mM hydrochloric acid. The three above solutions were mixed together at a ratio of 25:2.5:2.5 (v/v/v), and the absorbance of the reaction mixture at 593 nm was measured after incubation with the supernatant at 25°C for 10 min. The FRAP values, expressed in mmol $FeSO_4$ per mg protein, were derived from a prepared standard curve.

2.4. *Measurement of cellular glutathione S transferase*

After treatment, cells were harvested in cold phosphate buffer (pH 7.0) and sonicated (2 × 5 sec) on ice and then centrifuged at 5,000 × g for 10 min. The supernatant was used for enzymatic assays. GST activity was measured in accordance with a previously reported method (*14*) using 1-chloro-2,4-dinitrophenol (CDNB) as the substrate. A unit of GST activity is defined as the amount of enzyme catalyzing the formation of 1 μM of product per min under the conditions of the specific assay. Specific GST activity is defined as the units of enzyme activity per mg of protein. Protein concentrations were determined by the Bradford method (*15*) with bovine serum albumin as a standard.

2.5. *Measurement of cellular glutathione reductase*

After treatment, cells were harvested in cold phosphate buffer (pH 7.0) and sonicated (2 × 5 sec) on ice and then centrifuged at 5,000 × g for 10 min. The supernatant was used for enzymatic assays. The glutathione reductase (GR) activity was assayed according to a reported method (*16*). The enzymatic activity of GR was expressed as mU/mg protein, where 1 unit of GR activity is defined as 1 mmol GSSG catalyzed per minute.

2.6. *Statistical analysis*

For all experiments, data were expressed as means ± SEM. Statistical comparisons were subjected to an analysis of variance (ANOVA) and LSD-test using SPSS version 11.5, and $p < 0.05$ was considered as statistically significant difference. All statistical analysis were performed using SigmaPlot version 10.0 software.

3. Results

Previous studies have revealed the cytotoxicity of clivorine on human liver L-02 cells (*6,8*). As shown in Figure 2, clivorine at a concentration of 100 μM increased cellular total antioxidant capacity, which may be due to the cellular defense against the oxidative stress injury induced by clivorine.

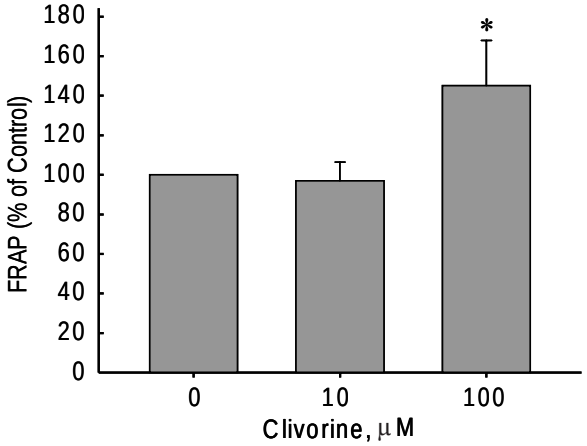

Figure 2. Effects of clivorine on cellular total antioxidant capacity in L-02 cells. Cells were treated with 10 μM and 100 μM clivorine for 48 h, and then cellular total antioxidant capacity was analyzed as described in "Materials and Methods". The results (means ± SEM, $n = 6$) are expressed as a percent of the control in the absence of clivorine.* $p < 0.05$ in comparison to the absence of clivorine.

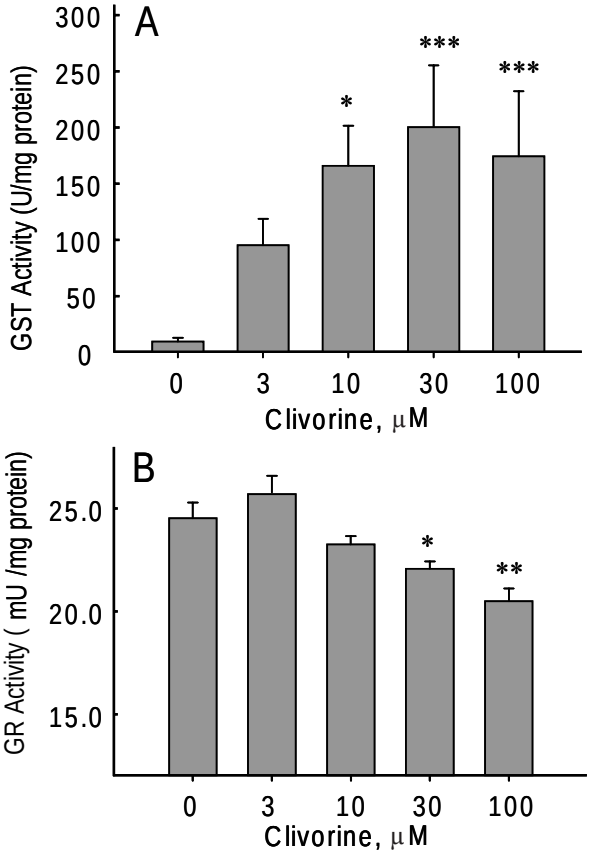

Figure 3. Effects of clivorine on GST (A) and GR (B) activity in L-02 cells. (A) Cells were treated with various concentrations of clivorine for 48 h, and then cellular GST activity was analyzed as described in "Materials and Methods". **(B)** Cells were treated with various concentrations of clivorine for 48 h, and then cellular GR activity was analyzed as described in "Materials and Methods". Data are means ± SEM ($n = 6$). * $p < 0.05$, ** $p < 0.01$, *** $p < 0.001$ in comparison to the absence of clivorine.

L-02 cells were treated with various concentrations of clivorine (3, 10, 30, and 100 μM) for 48 h. As shown in Figure 3A, clivorine significantly increased GST activity in a concentration-dependent manner, while clivorine decreased GR activity (Figure 3B).

The effect of several well-known antioxidants, such as ascorbate (Vc), Trolox, mannitol, and DTT, on clivorine-induced cytotoxicity was also observed in L-02 cells. As shown in Figure 4A, cell viability decreased to 60% of the control after cells were incubated with 50 μM clivorine for 48 h. When cells were pretreated with Trolox (50 μM) for 15 min, clivorine-induced cytotoxicity significantly reversed, and cell viability increased from 60% to 90% of the control. The effect of various concentrations of Trolox on clivorine-induced cytotoxicity was also observed. As shown in Figure 4B, the protection provided by

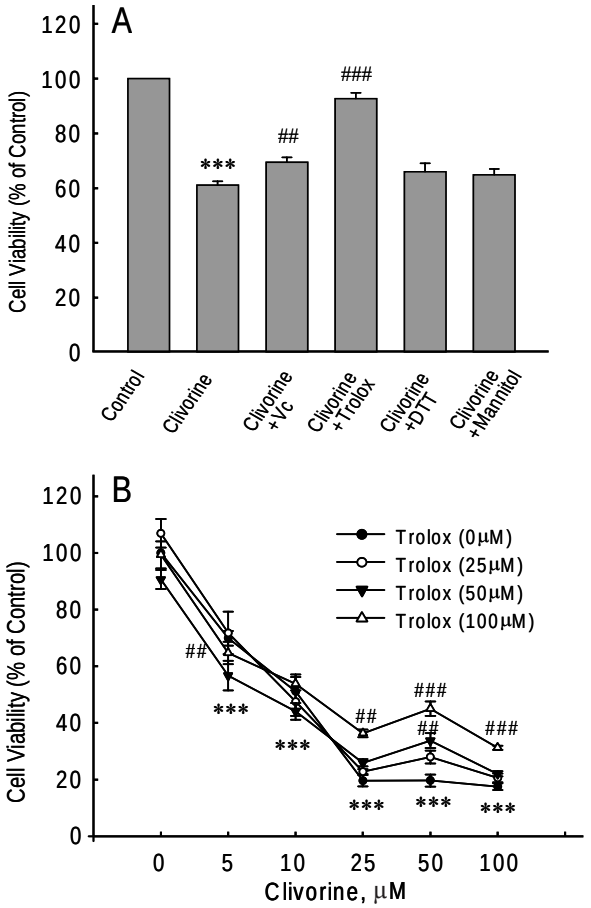

Figure 4. Effects of various antioxidants on clivorine-induced cytotoxicity in L-02 cells. (A) Cells were pretreated with Vc (500 μM), Trolox (50 μM), DTT (500 μM), or mannitol (500 μM) for 15 min and then incubated with clivorine (50 μM) for another 48 h. The number of viable cells was determined by MTT assay. **(B)** Cells were pretreated with various concentrations of Trolox (0, 25, 50, and 100 μM) for 15 min and then incubated with clivorine (50 μM) for another 48 h. The number of viable cells was determined by MTT assay. All the results (means ± SEM, $n = 6$) are expressed as a percent of the control in the absence of clivorine. *** $p < 0.001$ versus control in the absence of clivorine, ## $p < 0.01$, ### $p < 0.001$ in comparison to clivorine.

100 μM Trolox was better than that provided by 50 μM and 25 μM Trolox.

4. Discussion

Clivorine is an otonecine-type PA that is abundant in the traditional Chinese medicines *Ligularia hodgsonii* Hook and *Ligularia dentata* Hara. Previous reports by the current authors have shown their direct toxicity on human normal liver L-02 cells (*6*,*8*). The ferric reducing antioxidant power (FRAP) assay is a simple and reliable colorimetric method commonly used to measure total antioxidant capacity (*13*). The FRAP assay has been used to test for free radical scavenging and antioxidant activity in tissues (*17*). The present study showed that clivorine increased FRAP values in cells, which indicated that clivorine changed the redox balance in hepatocytes.

GSTs are enzymes of a multi-gene family that is involved in eliminating xenobiotic hepatotoxins. GSTs have the capacity to catalyze the conjugation of cellular GSH with electrophilic compounds, thereby decreasing their reactivity with important cellular macromolecules (*18*). The current results showed that clivorine increased GST activity in a concentration-dependent manner, which suggests that cellular GST may play a critical role in regulating clivorine-induced hepatotoxicity. Mammalian soluble GSTs are primarily divided into 4 main classes, Alpha (A), Mu (M), Pi (P), and theta (T) (*19*), and further research is needed to determine which types of GSTs are crucial to clivorine-induced toxicity.

GR is an important enzyme that helps replenish the key cellular antioxidant GSH *via* reduction of GSSG into GSH (*16*). A previous study by the current authors showed that clivorine decreased cellular GSH. S-adenosyl-L-methionine (SAM), which is a precursor of cellular GSH, significantly prevented clivorine-induced hepatotoxicity (*20*). As shown in Figure 3B, clivorine decreased GR activity in a concentration-dependent manner, which may explain the reduced amounts of GSH.

The cellular antioxidant system consists of enzymes and numerous nonenzymatic antioxidants including vitamins A, E, and C, ubiquinone, and flavonoids. Next, we observed the protection from clivorine-induced cytotoxicity provided by various antioxidants. As shown in Figure 4A, both Trolox and Vc prevented the cytotoxicity of clivorine, and Trolox provided better protection than Vc, while other antioxidants such as DTT and mannitol had no protective effect. As shown in Figure 4B, various concentrations of Trolox all protected cells from clivorine-induced cytotoxicity, and 100 μM Trolox provided the best protection.

Ve is a naturally occurring antioxidant in biological systems, and Trolox is a chemical analogue of Ve. Many studies have examined the protection from oxidative stress injury provided by Ve (*21*,*22*). The current results are the first to demonstrate the potential use of Trolox or Ve in the reduction of clivorine-induced hepatotoxicity. The present study helps to direct the search for alexipharmic substances for use in the clinical removal of clivorine or other PAs.

Acknowledgements

This work was financially supported by the National Natural Science Foundation of China (30801544), Shanghai Rising-Star Program (07QA14049), and the Open Fund of Key Laboratory Project for Standardization of Chinese Medicines sponsored by the Chinese Ministry of Education (ZK0801).

References

1. Sies H. Biochemistry of oxidative stress. Angew Chem Int Ed Engl. 1986; 25:1058-1071.
2. Jones DP. Redefining oxidative stress. Antioxid Redox Signal. 2006; 8:1865-1879.
3. Bailey SM, Cunningham CC. Contribution of mitochondria to oxidative stress associated with alcohol liver disease. Free Radic Biol Med. 2002; 32:11-16.
4. Jaeschke H, Bajt ML. Intracellular signaling mechanisms of acetaminophen-induced liver cell death. Toxicol Sci. 2006; 89:31-41.
5. Reinke LA, Towner RA, Janzen EG. Spin trapping of free radical metabolites of carbon tetrachloride *in vitro* and *in vivo*: effect of acute ethanol administration. Toxcol Appl Pharmacol. 1992; 112:17-23.
6. Ji LL, Zhang M, Sheng YC, Wang ZT. Pyrrolizidine alkaloid clivorine induces apoptosis in human normal liver L-02 cells and reduces the expression of p53 protein. Toxicol *In Vitro*. 2005; 19:41-46.
7. Kuhara K, Takanashi H, Hirono I, Furuya T, Asada Y. Carcinogenic activity of clivorine, a pyrrolizidine alkaloid isolated from *Ligularia Dentata*. Cancer Lett. 1980; 10:117-122.
8. Ji LL, Zhao XG, Chen L, Zhang M, Wang ZT. Pyrrolizidine alkaloid clivorine inhibits human normal liver L-02 cells growth and activates p38 mitogen-activated protein kinase in L-02 cells. Toxicon. 2002; 40:1685-1690.
9. Ji LL, Chen Y, Liu TY, Wang ZT. Involvement of Bcl-xL degradation and mitochondrial-mediated apoptotic pathway in pyrrolizidine alkaloids-induced apoptosis in hepatocytes. Toxicol Appl Pharmacol. 2008; 231:393-400.
10. Yeh HJ, Chu TH, Shen TW. Ultrastructure of continuously cultured adult human liver cell. Acta Biologiac Experimentalis Sinica. 1980; 13:361-364.
11. Zhang B, Zhang Y, Wang J, Zhang Y, Chen J, Pan Y, Ren L, Hu Z, Zhao J, Liao M, Wang S. Screening and identification of a targeting peptide to hepatocarcinoma from a phage display peptide library. Mol Med. 2007; 13:246-254.
12. Hansen MB, Nielsen SE, Berg K. Re-examination and further development of a precise and rapid dye method for measuring cell growth/cell kill. J Immunol Methods. 1989; 119:203-210.
13. Benzie IF, Strain JJ. The ferric reducing ability of plasma

(FRAP) as a measure of "antioxidant power": the FRAP assay. Anal Biochem. 1996; 239:70-76.
14. Habig WH, Pabst MJ, Jakoby WB. Glutathione S-transferases. The first enzymatic step in mercapturic acid formation. J Biol Chem. 1974; 249:7130-7139.
15. Bradford MM. A rapid and sensitive method for the quantitation of microgram quantities of protein utilizing the principle of protein dye binding. Anal Biochem. 1976; 72:248-254.
16. Carlberg I, Mannervik B. Glutathione reductase. Methods Enzymol. 1985; 113:484-490.
17. Sun L, Gao YH, Tian DK, Zheng JP, Zhu CY, Ke Y, Bian K. Inflammation of different tissues in spontaneously hypertensive rats. Acta Physiologica Sinica. 2006; 58:318-323.
18. Eaton DL, Bammler TK. Concise review of the glutathione S-transferases and their significance to toxicology. Toxicol Sci. 1999; 49:156-164.
19. Mannervik B, Board PG, Hayes JD, Listowsky I, Pearson WR. Nomenclature for mammalian soluble glutathione transferases. Methods Enzymol. 2005; 401:1-8.
20. Ji LL, Chen Y, Wang ZT. Protection of S-adenosyl methionine against the toxicity of clivorine on hepatocytes. Environ Toxicol Pharm. 2008; 26:331-335.
21. Servais S, Letexier D, Favier R, Duchamp C, Desplanches D. Prevention of unloading-induced atrophy by vitamin E supplementation: Links between oxidative stress and soleus muscle proteolysis. Free Radic Biol Med. 2007; 42:627-635.
22. Oh TY, Yeo M, Han SU, Cho YK, Kim YB, Chung MH, Kin YS, Cho SW, Hahm KB. Synergism of *Helicobacter pylori* infection and stress on the augmentation of gastric mucosal damage and its prevetion with α-tocopherol. Free Radic Biol Med. 2005; 38:1447-1457.

(*Received August 24, 2009; Revised September 11, 2009; Accepted September 12, 2009*)

Original Article

Induction of immune responses to a human immunodeficiency virus type 1 epitope by novel chimeric influenza viruses

Naoki Takizawa[1,2], Mayuko Morita[1], Kei Adachi[1], Ken Watanabe[1], Nobuyuki Kobayashi[1,3,*]

[1] *Laboratory of Molecular Biology of Infectious Agents, Graduate School of Biomedical Sciences, Nagasaki University, Nagasaki, Japan;*
[2] *Institute of Tropical Medicine, Nagasaki University, Nagasaki, Japan;*
[3] *Central Research Center, AVSS Corporation, Nagasaki, Japan.*

ABSTRACT: Mucosal and systemic immune responses play an important role in the prevention of infections, including infection with human immunodeficiency virus type 1 (HIV-1). Influenza virus can efficiently induce mucosal and systemic immune responses, and thus, chimeric influenza viruses expressing the peptides derived from HIV-1 proteins have been generated to elicit immune responses against the inserted peptide. Novel chimeric influenza viruses were generated with full length of the V3-loop of gp120 or cytotoxic T-lymphocyte epitope of gag from HIV-1 inserted into the stalk of NA (NA-V3 and NA-gag, respectively) and the V3-loop was inserted into the intracellular domain of M2 (M2-V3). The immune responses of mice infected with these chimeric influenza viruses were investigated. The intranasal infection of NA-gag induced gag epitope-specific CTLs and the intranasal infection of NA-V3 and M2-V3 induced V3-specific antibodies. The serum from mice infected with NA-V3 neutralized a clinical isolate of HIV-1 and the infection of NA-V3 induced V3-specific secretory antibodies. These results suggest that intranasal infection of these chimeric influenza viruses could induce both humoral and cellular immune responses against an inserted foreign peptide and therefore could be a potential candidate for use as an HIV-1 vaccine.

Keywords: Influenza virus, HIV-1, vaccine, gag, V3-loop

1. Introduction

Recent vaccine development against human immunodeficiency virus type 1 (HIV-1) is intended to stimulate a strong cellular immune response. In the case of HIV-1 infection, HIV-specific cytotoxic T lymphocytes (CTLs) have been detected before neutralizing antibodies are generated (*1,2*). Specific CTL activity correlates with the clinical stage of disease in infected individuals (*3,4*). Therefore, it is thought that the induction of strong CTL responses against HIV-1 could be important to prevent the onset of acquired immune deficiency syndrome (AIDS). HIV-1 gag is one of the most conserved antigens of HIV-1. Many studies towards development of an HIV vaccine are based on induction of a CTL against gag because several reports have shown that long-term nonprogressors have higher levels of gag-specific CTLs (*4*). Neutralizing antibodies may play only a limited role on primary HIV replication because it has proven difficult to induce broadly neutralizing antibodies due to its unusual neutralization-resistant mechanisms, such as masking of neutralizing epitopes and the high mutation rate of HIV-1 (*5,6*). However, neutralizing antibodies controlled primary virus replication in a macaque AIDS model (*7*). Therefore, it is thought that induction of effective neutralizing antibodies would be important for preventing HIV-1 infection as well as controlling primary virus replication. The epitopes that are known to induce neutralizing antibodies include the membrane proximal external region of gp41, the CD4 binding site on gp120, complex glycans on gp120, the CD4-induced epitope in and around the gp120 bridging sheet, and the V3-loop of gp120 (*8*). The V3-loop which is critical for co-receptor recognition is a highly immunogenic region of the virus envelope. In addition, the neutralizing epitope of the V3-loop is formed by a continuous stretch of amino acids in comparison to other neutralizing epitopes. Therefore, the V3-loop has been targeted for the development of vaccines to induce neutralizing antibodies against HIV-1.

The induction of strong CTL responses and neutralizing antibodies against HIV-1 would be required for an HIV vaccine. However, inoculation of recombinant epitopes with adjuvant and inactivated viruses do not efficiently induce mucosal and cellular immune responses. A virus vector has been developed

**Address correspondence to:*
Dr. Nobuyuki Kobayashi, Laboratory of Molecular Biology of Infectious Agents, Graduate School of Biomedical Sciences, Nagasaki University, Bunkyo-machi 1-14, Nagasaki 852-8521, Japan.
e-mail: nobnob@nagasaki-u.ac.jp

to induce both mucosal and cellular immune responses. Influenza A virus is a segmented negative-strand RNA virus and may be a candidate for the development of effective vaccine vectors against various diseases. Reverse-genetics methods have been developed to manipulate the influenza virus genome (*9-11*). Influenza virus can induce the maturation of strong virus-specific CTLs and the secretion of neutralizing antibodies. Significantly, influenza virus elicits mucosal immunity which is thought to be important for preventing the infection of infectious agents, such as HIV-1, through mucosal tissues. Therefore, chimeric influenza viruses have been engineered to express foreign antigens. Influenza virus has two membrane-spanning glycoproteins, hemagglutinin (HA) and neuraminidase (NA), on the envelope. In many cases, foreign antigens have been inserted into HA or NA because HA and NA are viral membrane proteins and anti-HA and anti-NA antibodies that neutralize influenza virus are induced in infected animals. To examine the potential of chimeric influenza virus as a vaccine for HIV-1, a 12-amino-acid peptide derived from the V3-loop of gp120 was inserted into the loop of antigenic site B of the HA and a 15-amino-acid peptide derived from the V3-loop of gp120 was inserted into the stalk of NA. These chimeric viruses can induce both a humoral and a cell-mediated immune response against HIV-1 (*12,13*). Furthermore, a 8-amino-acid peptide derived from gp41 was inserted into the loop of antigenic site B of the HA and the chimeric virus could induce inserted peptide-specific IgA in respiratory, intestinal, and vaginal secretions (*14,15*).

Some chimeric influenza viruses that are candidates for HIV-1 vaccine have been generated, but no chimeric influenza viruses have been generated with the full length of the V3-loop and CTL epitope of gag inserted into viral protein. The foreign peptides were inserted into only NA or HA and whether foreign peptides can be inserted into other viral proteins is not known. In this study, three chimeric influenza A viruses were generated that expressed the V3-loop of HIV-1 env in the NA stalk (NA-V3) and in the intracellular domain of matrix protein 2 (M2), a viral membrane protein, intracellular domain (M2-V3), respectively, and the CTL epitope derived from gag (H-2K^d) in the NA stalk (NA-gag). The infection of NA-gag could induce gag specific CTL and the infection of M2-V3 could induce specific antibodies to the V3-loop by intranasal infection, and the infection of NA-V3 induced antibodies that could neutralize a clinical HIV-1 strain. These experiments demonstrated that chimeric influenza virus expressing the CTL epitope of gag could induce a cell-mediated immune response for gag and chimeric influenza viruses and that full length of the V3-loop inserted into NA and M2 could be generated and induce V3-specific antibodies by intranasal infection.

2. Materials and Methods

2.1. *Cells and viruses*

Cultures of 293T (*16*) and MAGIC-5 (*17*) cells were maintained in Dulbecco's modified Eagle's medium (DMEM; Invitrogen) containing 10% fetal bovine serum (FBS). MDCK and MDBK cells were maintained in Eagle's minimal essential medium (MEM; Invitrogen) containing 10% FBS. LB27.4 cells (H-2b/d) were maintained in RPMI1640 (Invitrogen) containing 10% FCS, 5 mM β-mercaptoethanol, and 1 mM pyruvic acid. Influenza A/WSN/33 (H1N1) virus was grown at 34°C for 48 h in allantoic sacs of 11-day-old embryonated eggs, and the virus titer was determined by a plaque assay.

2.2. *Mouse infection and serum collection*

Six- to 10-week-old female BALB/c mice were housed under conventional conditions and were provided with standard diet and water ad libitum. The mice were anesthetized with diethyl ether and infected intranasally with influenza virus (1.0×10^4 PFU/20 μL) to induce antibodies. Blood was collected from the tail and was allowed to clot for 4 h at room temperature. Thereafter, the sample was centrifuged and the serum was collected. The lungs from infected mice were suspended in saponin extraction buffer (2% saponin in PBS) to permeabilize the cell membrane (*18*), and then incubated at 4°C for 18 h. The mixture was centrifuged and the supernatant was collected as a lung extract.

2.3. *Chimeric influenza viruses*

Chimeric influenza virus expressing the V3-loop of HIV-1 isolate, 2088E34t kindly provided by Dr. T. Shioda (Oosaka University) (*19*), envelope protein (Genebank: #AB002930) in the NA stalk (NA-V3) was generated based on the RNP transfection method (*20*). The pT3NAv, containing the NA gene of A/WSN/33, and A/WSN-HK virus were kindly provided by Dr. P. Palese (*20,21*). A C to G mutation was introduced into NA gene position 184 by PCR to create an *Nsi*I site in pT3NAv (pT3NAv-NsiI). To make pT3NAvENV51, the env fragment was amplified by RT-PCR from the HIV-1 genome. The amplified product was digested with *Nsi*I and inserted into the *Nsi*I site of pT3NAv-NsiI.

Chimeric influenza viruses expressing the V3-loop in the M2 intracellular domain (M2-V3) and expressing the CTL epitope derived from the HIV-1 IIIB gag protein (H-2K^d) in the NA stalk (NA-gag) were generated based on a plasmid-based reverse genetics system (*11*). Vectors for plasmid-based reverse genetics were kindly provided by Dr. Y. Kawaoka (Tokyo University). To make pHH-M2-V3, the V3 region fragment was amplified by PCR from pT3NAvENV51.

The amplified product was digested with *Nsi*I and inserted into the *Nsi*I site of pHH21-M. To make the *Nsi*I site in pHH-NA (pHH-NA-NsiI), a C to G mutation was introduced into the NA gene position 184 by PCR. To make pHH-NA-gag, a primer pair, NsiI-gag198-206f (5′-TCGCCATGCAAATGTTAAAAGAG ACCATCTGCA-3′) and NsiI-gag198-206r (5′-GATGG TCTCTTTTAACATTTGCATGGCGATGCA-3′), were hybridized and inserted into the *Nsi*I site of pHH21-NA-NsiI.

2.4. *CTL assay*

Groups of female BALB/c mice (H-2d), from 8 to 10 weeks old, were anesthetized with diethyl ether and infected intranasally with influenza virus (WSN; 1.0 × 10^4 PFU/50 μL). Spleen cells were prepared from the mice 16 days after infection, and were cultured in the presence of a peptide specific to NP (H-2K^d, TYQRTRALV) or gag (H-2K^d, AMQMLKETI; 10 μM) for 5 days, and used as effector cells. LB27.4 cells pulsed with the same peptide were incubated with increasing numbers of effector cells for 4 h (*22*), and the LDH levels in the cell culture supernatants were measured according to the manufacturer's protocol (Takara, Kyoto, Japan).

2.5. *ELISA*

Antigens diluted with coating buffer (10 mM carbonate buffer; pH 9.5) were plated onto a 96-well ELISA plate, and then incubated at 37°C for 2 h. Blocking buffer (0.05% Tween-20 and 1% BSA in PBS) was added to the plate, and then incubated at room temperature for 2 h. Serial dilutions of sera in blocking buffer were added to the plate, and incubated at 4°C for 18 h. Bound antibodies were detected with goat anti-mouse IgG antibody conjugated with alkaline phosphatase or goat anti-mouse IgA antibody conjugated with alkaline phosphatase. The plate was stained with *p*-nitrophenyl phosphate as a substrate.

2.6. *MAGI assay*

The neutralization activity was determined by an infection assay (MAGI assay) using MAGIC-5 cells (*17,23*). MAGIC-5 cells, which are derived from HeLa-CD4-LTR-β-gal (MAGI) cells and express CCR5, were seeded and cultured in a 96-well plate (1 × 10^4 cells/well). After removal of the medium, the cells were infected with the virus in the presence of sera diluted with DMEM to 1/50 for 1 h and washed with the culture medium. The cells were cultured in the medium for 48 h, and then fixed with 1% formaldeyde-0.2% glutaraldehyde in PBS for 5 min. The fixed cells were stained with X-gal. Blue-stained cells were counted under a light microscope.

3. Results

3.1. *Pathogenesis of chimeric viruses*

Three chimeric influenza A viruses were generated, one expressing the V3-loop of HIV-1 env (residues 288 to 331) in the NA stalk (NA-V3), another expressing the V3-loop (residues 288 to 339) in the M2 intracellular domain (M2-V3), and a third expressing the CTL epitope derived from gag (residues 198 to 206; H-2K^d) in the NA stalk (NA-gag; Figure 1A). We planned

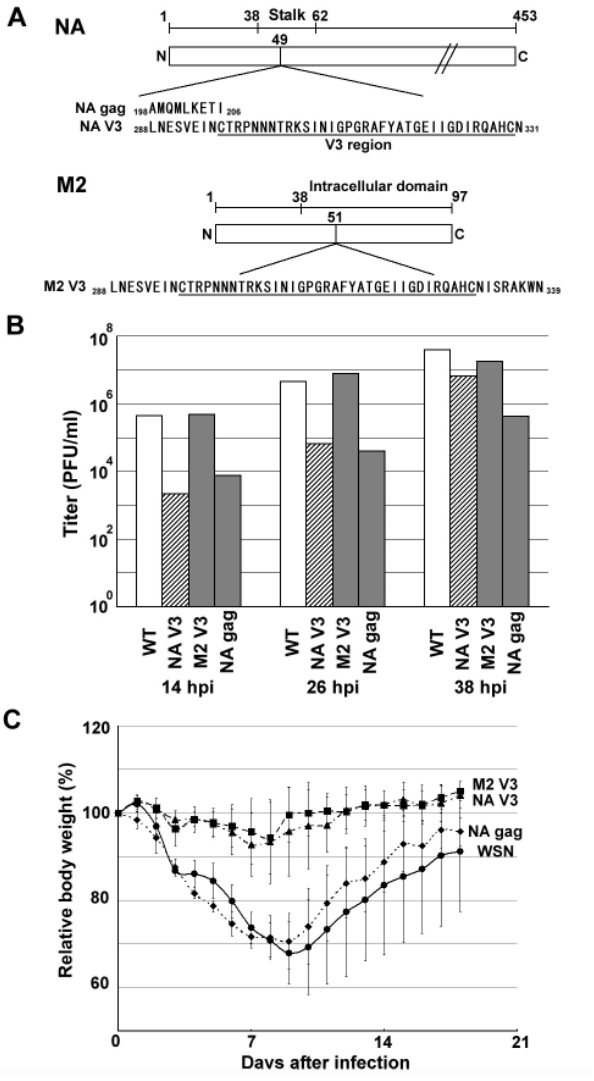

Figure 1. Chimeric influenza viruses containing the gag epitope and V3-loop. (A) Chimeric influenza viruses generated in this study. A 9-amino-acid peptide derived from gag was inserted into the stalk region of NA (NA-gag). A 44-amino-acid peptide derived from env was inserted into the stalk region of NA (NA-env). A 51-amino-acid peptide derived from env was inserted into the intracellular domain of M2. Underline indicates the V3 region in the HIV env. **(B)** Titer of the chimeric influenza viruses. MDBK cells were infected with the viruses at an MOI of 0.01 and the supernatant was collected at 14, 26, and 38 hpi. The titers in the supernatant were determined by a plaque assay. The titers represent the average of two independent experiments. **(C)** Virulence of the chimeric influenza viruses. 1.0 × 10^4 PFU of the viruses were infected into BALB/c mice. The relative body weight of the mice was calculated before infection as 100%.

to generate the chimeric virus which contained a 51-amino-acid peptide derived from env in the NA stalk but three chimeric viruses that contained a 51-amino-acid peptide, a 44-amino-acid peptide, and a 33-amino-acid peptide in the NA stalk were collected. The chimeric virus which contained the 44-amino-acid peptide was well propagated compared to the virus containing the 51-amino-acid peptide. These results suggest that the virus which contained the 44-amino-acid peptide in the stalk of NA was more stable than that containing the 51-amino-acid peptide. Thus, we used the chimeric virus containing the 44-amino-acid peptide in this study. In NA-gag, the virus that lacked the inserted nucleotide was generated after several passages from the first transfection supernatant. But, the virus which lacked the inserted sequence was not generated in several passages after plaque isolation of NA-gag from the mixture. The virus that lacked the inserted epitope might be generated in transfected cells and the inserted peptide in NA-gag was stable at least for several passages. M2-V3 and NA-V3 were stable for several passages. To examine the pathogenesis of the chimeric viruses, the virus titer of the supernatant from cells infected with the viruses was determined and the body weight of mice infected with these viruses was measured. The virus titer in the supernatant at 14 hours post infection (hpi) was 4.5×10^5 PFU/mL (wild type:WT), 2.2×10^3 PFU/mL (NA-V3), 4.9×10^5 PFU/mL (M2-V3), and 7.7×10^3 PFU/mL (NA-gag), respectively (Figure 1B). The virus titer at 38 hpi was 3.9×10^7 PFU/mL (WT), 6.6×10^6 PFU/mL (NA-V3), 1.8×10^7 PFU/mL (M2-V3), and 4.3×10^5 PFU/mL (NA-gag), respectively (Figure 1B). These results suggest that the insertion of a foreign peptide into NA and M2 tends to reduce the growth of the viruses at the early stage of replication but a significant amount of viruses could be recovered 38 h after infection. Next, BALB/c mice were infected with 1.0×10^4 PFU of WT, NA-V3, M2-V3, and NA-gag, respectively, and weight loss was monitored. As shown in Figure 1C, mice infected with either NA-gag or WT virus showed significant weight loss but mice infected with either NA-V3 or M2-V3 did not show any apparent weight loss. These results suggest that NA-V3 and M2-V3 are attenuated in BALB/c mice.

3.2. *Gag-specific CTL response in mice infected with NA-gag*

A CTL assay was performed to examine the gag-specific CTL response in mice infected with NA-gag. The infection of the viruses in mice was confirmed by monitoring weight loss (data not shown). Spleen cells from mice infected with NA-gag were activated with epitope peptide and mixed with LB27.4 cells treated with epitope peptide. Cytotoxity was detected in 15.8% of target cells treated with NP epitope peptide using effector cells derived from mice infected with WT and NA-gag whereas cytotoxity was not detected using effector cells derived from mock-infected mice (Figure 2A). This result suggests that an NP-specific CTL response was detected in cells from mice infected with WT and NA-gag. Cytotoxity was detected in 34.5% of target cells treated with gag epitope peptide using effector cells derived from mouse infected with NA-gag whereas cytotoxity was detected in 10.4% or 13.2% of the target cells using effector cells derived from mock-infected mice and mice infected with WT, respectively. This result suggests that a gag-specific CTL response was detected only in cells from mice infected with NA-gag and the infection of NA-gag can induce a gag-specific CTL response.

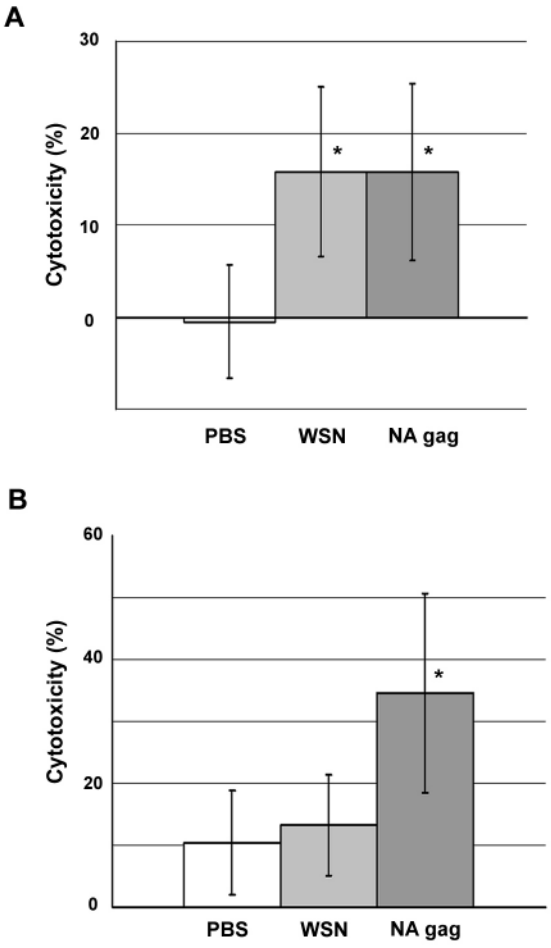

Figure 2. The induction of a specific CTL response by infection with NA-gag. (A) The induction of a specific CTL response against NP. The mice (n = 3) were mock-infected (PBS) or infected intranasally with 1.0×10^4 PFU of WT or NA-gag, and the specific CTL activity was then determined in the spleens. Spleen cells were stimulated for 6 days *in vitro* with 10 μM NP epitope peptide and examined for CTL activity against peptide-coated target cells. E:T ratios were 60:1. *, $p < 0.05$ *vs*. PBS infected mouse. **(B)** The induction of a specific CTL response against gag. The mice (n = 6: PBS and NA-gag and n = 4: WSN) were mock-infected (PBS) or infected intranasally with 1.0×10^4 PFU of WT or NA-gag, and the specific CTL activity was then determined in the spleens. Spleen cells were stimulated for 6 days *in vitro* with 10 μM gag epitope peptide and examined for CTL activity against peptide-coated target cells. E:T ratios were 60:1. *, $p < 0.05$ *vs*. PBS infected mouse.

3.3. *V3-specific antibodies in serum from mice infected with NA-V3 and M2-V3*

The subsequent experiments investigated whether infection of NA-V3 and M2-V3 in mice would induce antibodies specific for the V3 region. Sera from mice infected with NA-V3 and M2-V3 was prepared and V3-specific IgG in the serum was detected by ELISA. The induction of specific antibodies in infected mice (positive mice) was evaluated by comparison of the value obtained from ELISA assays using the serum from infected mice with the maximum value using sera from mock-infected mice. HA-specific IgG was detected in serum from 100% (57 of the positive mice/57 of the infected mice) of mice infected with WSN and V3-specific IgG was not detected in the serum from the mice infected with WSN (Figure 3). HA-specific IgG was detected in the serum from 100% (76 of the positive mice/76 of the mice infected with NA-V3 and 20 of the positive mice/20 of the mice infected with M2-V3) of the mice infected with NA-V3 and M2-V3 and V3-specific IgG was detected from 33% (25 of the positive mice/76 of the mice infected with NA-V3) and 25% (5 of the positive mice/20 of the mice infected with M2-V3), respectively (Figure 3). These results suggest that the infection of NA-V3 and M2-V3 can induce specific antibodies for the V3 region.

3.4. *Secretory antibodies in mice infected with NA-V3 and M2-V3*

Secretory antibodies are important for preventing viral infection. Therefore, V3-specific IgA was measured in serum and lung extracts from mice infected with NA-V3 and M2-V3 by ELISA. V3-specific IgA in serum was detected from 3% (2 of the positive mice/76 of the mice infected with NA-V3) and 5% (1 positive mouse/20 of the mice infected with M2-V3), respectively (Figure 3). HA-specific IgA was detected in the lung extract from 94% (29 of the positive mice/31 of the mice infected with WSN), 98% (54 of the positive mice/55 of the mice infected with NA-V3), and 100% (20 of the positive mice/20 of the mice infected with M2-V3), respectively (Figure 4). No V3-specific IgA was detected in the extract from mice infected with WSN and was detected in the extract from 18% (10 of the positive mice/55 of the mice infected with NA-V3) and 5% (1 positive mouse/20 of the mice infected with M2-V3), respectively (Figure 4). These results suggest that an infection with NA-V3 and M2-V3 can induce the secretion of V3-specific IgA in lungs.

3.5. *Neutralization of clinically isolated HIV-1*

A neutralization assay was performed to determine whether these antibodies have neutralization activity

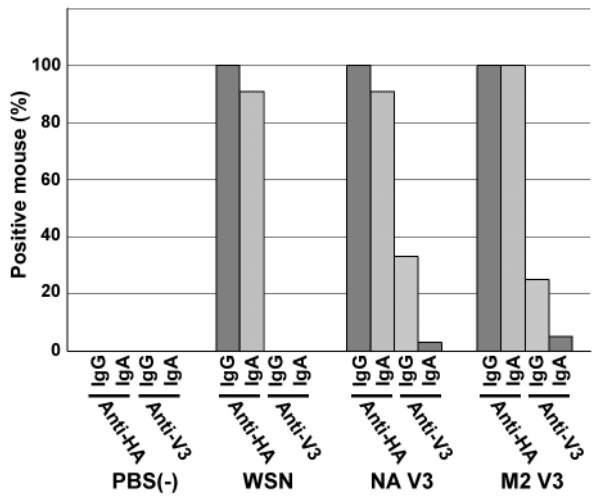

Figure 3. The induction of systemic antibodies by infection with NA-env and M2-env virus. The mice were infected intranasally with 1.0×10^4 PFU of each virus. Serum was collected 12 weeks after infection. Anti-HA IgG and IgA and anti-V3 IgG and IgA in the serum were detected by ELISA.

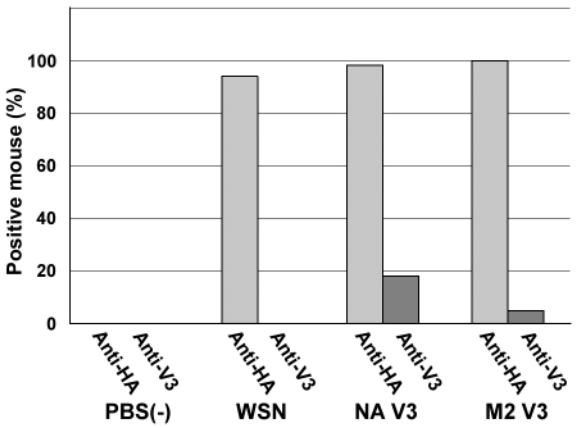

Figure 4. The induction of mucosal antibodies by infection with NA-env and M2-env virus. The mice were infected intranasally with 1.0×10^4 PFU of each virus. Lung extracts were prepared 12 weeks after infection. Anti-HA IgA and anti-V3 IgA were detected by ELISA.

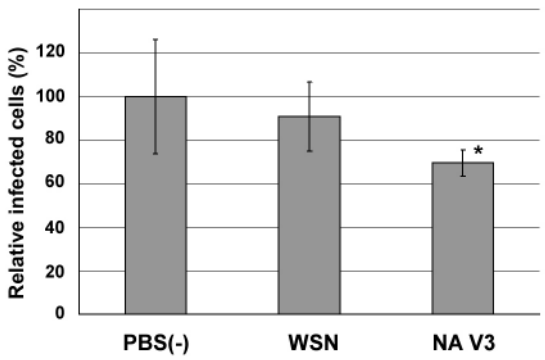

Figure 5. Neutralizing activities against a clinically isolated strain of HIV. The sera from the mice infected with each virus was diluted 50-fold and co-cultured with an isolated strain of HIV, YU-20, for 1 h. The efficiency of HIV infection was estimated by a MAGI assay. The infectious units resulting from the serum of the PBS infected mouse were calculated as 100%. *, $p < 0.05$ *vs*. PBS mock-infected and WSN infected mouse.

against clinically isolated HIV-1. The cells were infected with the clinically isolated HIV-1 in the presence of serum from the mouse infected with NA-V3. MAGIC-5 cells that were derived from MAGI cells were used to stain infected cells by MAGI assay (*17*,*23*). No neutralization activity to HIV-1 was detected in serum from the mouse infected with WSN (Figure 5). The number of infected cells decreased to 69.5% when the cells were infected with the HIV-1 in the presence of the serum from mice infected with NA-V3 (Figure 5). This result suggests that the V3-specific antibodies induced in mice infected with NA-V3 and the sera from mice infected with NA-V3 partially neutralized the infection of clinically isolated HIV-1.

4. Discussion

Chimeric influenza viruses expressing a part of the V3-loop inserted into NA or HA were generated and examined for their immunogenicity in mice. In this paper, the novel chimeric influenza viruses possessing full length of the V3-loop or CTL epitope of gag were generated and examined for their immunogenicity. These results, for the first time, demonstrated that a foreign peptide could be inserted into the M2 intracellular domain and the chimeric influenza virus could induce antibodies against the inserted peptide. M2 functions as a proton channel and the intracellular domain of M2 is essential for the function of the M2 channel (*24*,*25*). In M2-V3, the V3-loop was inserted into the region that connects the transmembrane domain to the C-terminal amphipathic helix (*26*). Therefore, the inserted peptide did not apparently affect the proton channel function of M2. NA-V3 was highly attenuated in mice but NA-gag was not (Figure 1C). The length of NA stalk affects the host range of the influenza virus (*27*,*28*). NA has neuraminidase activity and, thus, is important for releasing progeny virus from the cells. The virus which has mutations in segment 6 to reduce the synthesis of NA mRNA was attenuated in mice, suggesting that the activity of NA is one important factor for attenuation in mice (*29*). In addition, the WSN strain can replicate without trypsin because the NA of the WSN strain binds to serum plasminogen (*30*). The insertion of a foreign peptide into the NA stalk affects the activities of NA and, consequently, the pathogenesis of these chimeric viruses for mice is changed. The virus containing FLAG tag sequence (7 amino acids) in NA stalk was attenuated in mice (*28*) but NA-gag was not. These results suggest that not only length but also amino acid sequence of NA stalk affects the activity of NA.

The infection of NA-gag could induce a gag-specific CTL response (Figure 2). The cytotoxicity against cells expressing the gag epitope was about 25% and this rate was lower than that of a previous study (*31*). The cytotoxicity against cells expressing NP epitope was induced by the infection of NA-gag but the rate was also lower than that of a previous study (*32*). In this study, CTLs were detected using non-RI method. The sensitivity for detection of cell death with a non-RI method is slightly lower than that with an RI-method, and thus, the cytotoxicity in this study is slightly lower than that in the previous study. In spite of slightly lower sensitivity, a non-RI method is used for CTL detection because of its safety. It was reported that the specific CTL against NP epitopes in influenza infected mice was detected by a non-RI method (*33*). Thus, we concluded that specific CTLs against the NP epitope and gag epitope were induced by the infection of NA-gag.

Secretory IgAs were induced in 20% of mice infected with NA-V3 and in 5% of mice infected with M2-V3 (Figure 4). The V3-loop was inserted into the intracellular domain of M2 in M2-V3 but into the extracellular domain of NA in NA-V3. Mucosal immunity is important for preventing viral infection and neutralizing antibodies are induced to the domains that are outside of the viral membrane. Thus, the infection of M2-V3 could not induce secretory IgAs efficiently in comparison to that of NA-V3. In addition, the chimeric virus expressing the gag epitope inserted into the stalk of NA could induce a gag-specific CTL response (Figure 2). Chimeric influenza virus expressing a foreign peptide inserted into the stalk of NA is a candidate for an effective vaccine against various diseases because this chimeric virus can induce both systemic and mucosal immunity. The infection of M2-V3 induced anti-V3 IgG in serum (Figure 3). The vaccination of M2-V3 would not prevent mucosal infection of HIV-1 but would prevent infection in blood. The infection of M2-V3 could not induce secretory IgA against V3 efficiently but chimeric influenza virus expressing different foreign peptides inserted into the stalk of NA and the intracellular domain of M2 could be generated and the infection of these chimeric viruses could induce immune responses against both foreign peptides. Although the percentage of IgA-induced mice was limited in the present experiment, a combination with any adjuvant will increase the immunological response of mice. Further experiments are presently on going to explore this possibility.

This study demonstrated that about 50-amino-acids of a foreign peptide could be inserted into the intracellular domain of M2 and the stalk of NA and these chimeric influenza viruses could induce immune responses against foreign peptides. The improvement of reverse-genetics methods to manipulate the influenza virus genome generates influenza viruses that express the full-length of foreign proteins (*34*,*35*). However, the advantage of chimeric influenza viruses with foreign peptides inserted into viral proteins is that the immune response against chimeric influenza virus is almost the same as that against wild type influenza virus.

Therefore, a chimeric influenza virus vaccine could be safely used in a manner similar to that of an attenuated influenza virus vaccine. The chimeric influenza virus may therefore be a potentially promising vaccine candidate, not only against HIV, but also against other infectious diseases.

Acknowledgements

This research was supported in part by the Program of Founding Research Centers for Emerging and Reemerging Infectious Diseases, MEXT, Japan and the Global COE program of Nagasaki University, MEXT, Japan.

References

1 Koup RA, Safrit JT, Cao Y, Andrews CA, McLeod G, Borkowsky W, Farthing C, Ho DD. Temporal association of cellular immune responses with the initial control of viremia in primary human immunodeficiency virus type 1 syndrome. J Virol. 1994; 68:4650-4655.
2 Pantaleo G, Demarest JF, Soudeyns H, *et al*. Major expansion of CD8+ T cells with a predominant V beta usage during the primary immune response to HIV. Nature. 1994; 370:463-467.
3 Hoffenbach A, Langlade-Demoyen P, Dadaglio G, Vilmer E, Michel F, Mayaud C, Autran B, Plata F. Unusually high frequencies of HIV-specific cytotoxic T lymphocytes in humans. J Immunol. 1989; 142:452-462.
4 Klein MR, van Baalen CA, Holwerda AM, Kerkhof Garde SR, Bende RJ, Keet IP, Eeftinck-Schattenkerk JK, Osterhaus AD, Schuitemaker H, Miedema F. Kinetics of Gag-specific cytotoxic T lymphocyte responses during the clinical course of HIV-1 infection: a longitudinal analysis of rapid progressors and long-term asymptomatics. J Exp Med. 1995; 181:1365-1372.
5 Kwong PD, Doyle ML, Casper DJ, *et al*. HIV-1 evades antibody-mediated neutralization through conformational masking of receptor-binding sites. Nature. 2002; 420:678-682.
6 Wei X, Decker JM, Wang S, Hui H, Kappes JC, Wu X, Salazar-Gonzalez JF, Salazar MG, Kilby JM, Saag MS, Komarova NL, Nowak MA, Hahn BH, Kwong PD, Shaw GM. Antibody neutralization and escape by HIV-1. Nature. 2003; 422:307-312.
7 Yamamoto H, Kawada M, Takeda A, Igarashi H, Matano T. Post-infection immunodeficiency virus control by neutralizing antibodies. PLoS ONE. 2007; 2:e540.
8 Zolla-Pazner S. Identifying epitopes of HIV-1 that induce protective antibodies. Nat Rev Immunol. 2004; 4:199-210.
9 Enami M, Enami K. Characterization of influenza virus NS1 protein by using a novel helper-virus-free reverse genetic system. J Virol. 2000; 74:5556-5561.
10 Luytjes W, Krystal M, Enami M, Parvin JD, Palese P. Amplification, expression, and packaging of foreign gene by influenza virus. Cell. 1989; 59:1107-1113.
11 Neumann G, Watanabe T, Ito H, Watanabe S, Goto H, Gao P, Hughes M, Perez DR, Donis R, Hoffmann E, Hobom G, Kawaoka Y. Generation of influenza A viruses entirely from cloned cDNAs. Proc Natl Acad Sci U S A. 1999; 96:9345-9350.
12 Li S, Polonis V, Isobe H, Zaghouani H, Guinea R, Moran T, Bona C, Palese P. Chimeric influenza virus induces neutralizing antibodies and cytotoxic T cells against human immunodeficiency virus type 1. J Virol. 1993; 67:6659-6666.
13 Garulli B, Kawaoka Y, Castrucci MR. Mucosal and systemic immune responses to a human immunodeficiency virus type 1 epitope induced upon vaginal infection with a recombinant influenza A virus. J Virol. 2004; 78:1020-1025.
14 Muster T, Ferko B, Klima A, *et al*. Mucosal model of immunization against human immunodeficiency virus type 1 with a chimeric influenza virus. J Virol. 1995; 69:6678-6686.
15 Muster T, Guinea R, Trkola A, Purtscher M, Klima A, Steindl F, Palese P, Katinger H. Cross-neutralizing activity against divergent human immunodeficiency virus type 1 isolates induced by the gp41 sequence ELDKWAS. J Virol. 1994; 68:4031-4034.
16 DuBridge RB, Tang P, Hsia HC, Leong PM, Miller JH, Calos MP. Analysis of mutation in human cells by using an Epstein-Barr virus shuttle system. Mol Cell Biol. 1987; 7:379-387.
17 Mochizuki N, Otsuka N, Matsuo K, Shiino T, Kojima A, Kurata T, Sakai K, Yamamoto N, Isomura S, Dhole TN, Takebe Y, Matsuda M, Tatsumi M. An infectious DNA clone of HIV type 1 subtype C. AIDS Res Hum Retroviruses. 1999; 15:1321-1324.
18 Kang SM, Yaq Q, Guo L, Compans RW. Mucosal immunization with virus-like particles of simian immunodeficiency virus conjugated with cholera toxin subunit B. J Virol. 2003; 77:9823-9830.
19 Shioda T, Oka S, Xin X, Liu H, Harukuni R, Kurotani A, Fukushima M, Hasan MK, Shiino T, Takebe Y, Iwamoto A, Nagai Y. *In vivo* sequence variability of human immunodeficiency virus type 1 envelope gp120: association of V2 extension with slow disease progression. J Virol. 1997; 71:4871-4881.
20 Enami M, Palese P. High-efficiency formation of influenza virus transfectants. J Virol. 1991; 65:2711-2713.
21 Enami M, Luytjes W, Krystal M, Palese P. Introduction of site-specific mutations into the genome of influenza virus. Proc Natl Acad Sci U S A. 1990; 87:3802-3805.
22 Tsunoda I, Sette A, Fujinami RS, Oseroff C, Ruppert J, Dahlberg C, Southwood S, Arrhenius T, Kuang LQ, Kubo RT, Chesnut RW, Ishioka GY. Lipopeptide particles as the immunologically active component of CTL inducing vaccines. Vaccine. 1999; 17:675-685.
23 Kimpton J, Emerman M. Detection of replication-competent and pseudotyped human immunodeficiency virus with a sensitive cell line on the basis of activation of an integrated beta-galactosidase gene. J Virol. 1992; 66:2232-2239.
24 Tobler K, Kelly ML, Pinto LH, Lamb RA. Effect of cytoplasmic tail truncations on the activity of the M(2) ion channel of influenza A virus. J Virol. 1999; 73:9695-9701.
25 Pinto LH, Lamb RA. The M2 proton channels of influenza A and B viruses. J Biol Chem. 2006; 281:8997-9000.
26 Schnell JR, Chou JJ. Structure and mechanism of the M2 proton channel of influenza A virus. Nature. 2008; 451:591-595.

27 Castrucci MR, Kawaoka Y. Biologic importance of neuraminidase stalk length in influenza A virus. J Virol. 1993; 67:759-764.
28 Castrucci MR, Bilsel P, Kawaoka Y. Attenuation of influenza A virus by insertion of a foreign epitope into the neuraminidase. J Virol. 1992; 66:4647-4653.
29 Solorzano A, Zheng H, Fodor E, Brownlee GG, Palese P, Garcia-Sastre A. Reduced levels of neuraminidase of influenza A viruses correlate with attenuated phenotypes in mice. J Gen Virol. 2000; 81:737-742.
30 Goto H, Kawaoka Y. A novel mechanism for the acquisition of virulence by a human influenza A virus. Proc Natl Acad Sci U S A. 1998; 95:10224-10228.
31 Mata M, Travers PJ, Liu Q, Frankel FR, Paterson Y. The MHC class I-restricted immune response to HIV-gag in BALB/c mice selects a single epitope that does not have a predictable MHC-binding motif and binds to Kd through interactions between a glutamine at P3 and pocket D. J Immunol. 1998; 161:2985-2993.
32 Bodmer HC, Pemberton RM, Rothbard JB, Askonas BA. Enhanced recognition of a modified peptide antigen by cytotoxic T cells specific for influenza nucleoprotein. Cell. 1988; 52:253-258.
33 Corr M, Lee DJ, Carson DA, Tighe H. Gene vaccination with naked plasmid DNA: mechanism of CTL priming. J Exp Med. 1996; 184:1555-1560.
34 Machado AV, Naffakh N, van der Werf S, Escriou N. Expression of a foreign gene by stable recombinant influenza viruses harboring a dicistronic genomic segment with an internal promoter. Virology. 2003; 313:235-249.
35 Fujii Y, Goto H, Watanabe T, Yoshida T, Kawaoka Y. Selective incorporation of influenza virus RNA segments into virions. Proc Natl Acad Sci U S A. 2003; 100:2002-2007.

(*Received September 4, 2009; Revised September 25, 2009; Accepted October 3, 2009*)

Original Article

A microplate-based screening assay for neuraminidase inhibitors

Aifeng Li[1], Weihong Wang[1,*], Wenfang Xu[2], Jianzhi Gong[2]

[1] *Department of Pharmaceutical Analysis, School of Pharmacy, Shandong University, Ji'nan, Shandong, China;*
[2] *Department of Medicinal Chemistry, School of Pharmacy, Shandong University, Ji'nan, Shandong, China.*

ABSTRACT: Neuraminidase (NA) represents a highly promising new target for drug development in influenza virus genes. Rapid screening of enzyme inhibitors is a key method for the identification of leading compounds. In order to speed up the screening for enzyme inhibitors of natural and synthetic origin, effective and fast assays are needed. 2'-(4-Methylumbelliferyl)-α-D-*N*-acetylneuraminic acid (4-MUNANA) was selected as substrate for development of a microplate-based assay. The enzymatic reaction conditions were optimized as follows: in a 100 μL reaction mixture, the final concentrations were 32.5 mM sodium acetate (pH 3.5), 20 μM 4-MUNANA, 0.005% (w/v) bovine serum albumin, and 0.42 μg/mL NA. In the study, the dose-response relationship of oseltamivir carboxylate to NA activity was observed. In addition, an overall Z' value of 0.8 proved the systems robustness and potential for screening. The assay system developed will be a valuable tool to discover new structures for the therapeutic inhibition of NA used to treat Influenza.

Keywords: Neuraminidase, 4-MUNANA, microplate-based, screening assays, NA inhibitors

1. Introduction

Influenza is an acute viral infection of the upper respiratory tract that can affect millions of people every year. It is a high-priority and attractive area for drug discovery to develop effective anti-influenza agents. The influenza virus surface glycoprotein antigen neuraminidase (NA) has been proven as a valid therapeutic target for antiviral drugs due to its essential role in the viral replication cycle (*1,2*). NA catalyzes removal of terminal sialic acid linked to glycoproteins and glycolipids, which promotes influenza virus release from infected cells and facilitates virus spread within the respiratory tract. Despite the homologous identity of NA in different strains being only about 30%, the catalytic site of NA in all influenza A and B viruses is completely conserved (*3*). The enzymatic active site of NA contains four anti-parallel strands arranged in a propeller fashion. Each monomeric subunit has an active site cavity lined with 10 conserved residues and four water molecules. The inhibitors bind to the active site with the carboxylic acid binding to the triad guanidine groups of the three arginine residues, Arg 118, Arg 371, and Arg 292, which are located as a cluster on one side of the active site. Opposite to the guanidine triad, there is a hydrophobic pocket formed by side chains of Trp178, Ile 222, and part of Arg 224 (*4*) (Figure 1).

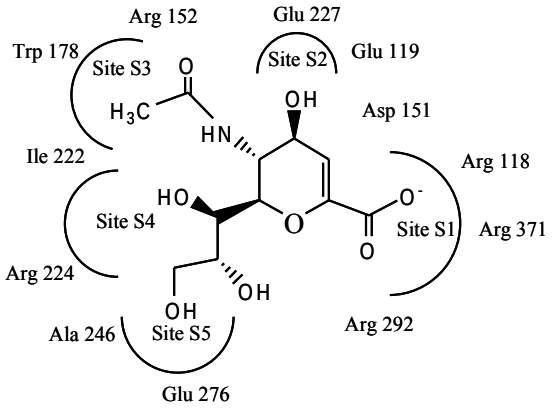

Figure 1. 'Airplane' model of NA active site (*5*)**.**

Therefore, NA has been regarded as an attractive target for antiviral drug development. So far, two NA inhibitors (zanamivir and oseltamivir) have been confirmed as effective and safe for the treatment of influenza and have been approved by FDA (*6*).

Rapid screening of enzyme inhibitors is a key method for the discovery of leading compounds. In order to speed up screening for enzyme inhibitors of natural and synthetic origin, effective and fast assays are necessary. The choice of an appropriate screening assay is crucial. Screening assays for enzyme inhibitors consist of *in vivo* and *in vitro* assay methods. *In vitro* screening assays include cell-based and biochemically-based

**Address correspondence to:*
Dr. Weihong Wang, Department of Pharmaceutical Analysis, School of Pharmacy, Shandong University, 44, Wenhuaxi Road, Ji'nan 250012, Shandong, China.
e-mail: wangwh@sdu.edu.cn

methods. In biochemically-based assays, the target is specific, and the drug action mechanism can be obtained directly. They allow for efficient logistics, and rapid screening of large libraries can be easily miniaturized, without suffering from off-target effects and toxicity issues. Biochemically-based assays can be performed with higher compound concentrations, thereby raising chances of finding inhibitors in novel chemical classes (*7*). Microplate-based assays are one form of biochemically-based assays, which have undergone a revolution and the field shows no signs of slowing down. This has been made possible through the introduction of high density microplates, small volume liquid handling robotics and associated detection technology. The common methods mainly use homogeneous formats that do not involve any solid phases or washing steps. The development of homogeneous mix-and-measure techniques was a necessary precondition for the current level of miniaturization and throughput in screening laboratories.

It was used to screen NA inhibitors using biochemically-based assays. Hong-Peng Cao and his partners have reported screening NA inhibitors using 4-MUNANA as substrate (*8*). NA was prepared from strain A (Yuefang 72-243 A and Jifang 90-15 A) and B (Sichuan 2000-38 B) influenza viruses. NA from different species has different reaction conditions. In this paper, we also chose 4-MUNANA as substrate to develop a microplate-based assay for neuraminidase inhibitors. NA was prepared from *Clostridium perfringens*, which has a high reaction activity. The reaction conditions were optimized. NA activity was monitored by using a synthetic substrate 4-MUNANA, which is hydrolyzed to yield a fluorescent product 4-methylumbelliferone (4-MU) that can be quantified using a fluorometric method (*9*). The intensity of fluorescence reflects the activity of NA sensitively.

2. Materials and Methods

2.1. *Enzyme and reagents*

NA, 4-MUNANA, and 4-MU were purchased from Sigma Chemicals (St. Louis, MO, USA). Black fluorescence 96-well plates were purchased from SPL chemical (South Korea). Tamiflu® capsules were obtained from F. Hoffmann, La Roche Ltd. (Basel, Switzerland, the labeled amount of 75 mg oseltamivir corresponded to 98.5 mg oseltamivir phosphate). The 20 chemical compounds were synthesized by Jianzhi Gong. All other chemicals were analytical-grade commercial preparations.

2.2. *Preparation of oseltamivir carboxylate*

Oseltamivir (Tamiflu®) is rapidly and extensively hydrolysed *in vivo* to its active metabolite oseltamivir carboxylate, which is a potent and selective inhibitor of influenza virus NA.

We transfered an accurately weighed portion of the contents of 5 opened Tamiflu® capsules, equivalent to about 25 mg of oseltamivir, to a 25-mL volumetric flask, added about 15 mL of water, and shook by mechanical means for about 15 min. We diluted with water to volume, and mixed. A portion of this solution was centrifuged, and 8.0 mL of the clear supernatant was transferred to a 20-mL round bottom flask, 2.0 mL of 10% sodium hydroxide was added, and mixed. The solution was refluxed for 3 h, cooled to room temperature, and adjusted to pH 7.5 with glacial acetic acid.

The hydrolyzed ratio of oseltamivir was determined using the method described by N. Lindegardh (*10*). The hydrolyzed ratio was calculated by comparing the peak area of oseltamivir in solution before and after hydrolyzation. We found that oseltamivir was hydrolyzed into oseltamivir carboxylate completely.

2.3. *Determination of the stability of NA*

NA (16.7 μg/mL) was prepared in redistilled water and 0.1% cold bovine serum albumin solution, respectively. The stability of NA in these solvents was monitored by determining the reaction activity of NA using optimized conditions.

2.4. *Determination of the stability of 4-MU*

4-MU (20 μM) was prepared in 0.15 M glycine-NaOH buffer (pH 10.4) and 50 mM sodium acetate buffer (pH 3.5), respectively. The intensity of fluorescence was measured at an excitation wavelength of 355 nm and an emission wavelength of 460 nm.

2.5. *Determination of neuraminidase activity*

The activity of NA was measured fluorometrically by determination of the degradation product 4-MU from the substrate 4-MUNANA. The reaction was performed under the following experimental conditions: 50 mM sodium acetate reaction buffer (pH 3.5), 0.2 mM 4-MUNANA, 0.15 M glycine-NaOH stop buffer (pH 10.4). The activity of the enzyme was measured in black fluorescence 96-well plates using the following procedure: 5 μL of NA (8.33 μg/mL) and 10 μL of 0.2 mM 4-MUNANA were added to 85 μL of 50 mM sodium acetate buffer (pH 3.5). The reaction mixture was gently stirred at 37°C for 15 min and 100 μL of stop buffer was added to the reaction solution. Meanwhile, a substrate blank control was set. Five μL of deactived NA (8.33 μg/mL) was added to the reaction mixture instead of 5 μL of NA (8.33 μg/mL). The fluorescence intensities were measured using an excitation wavelength of 355 nm and an emission wavelength of 460 nm.

2.6. *Validation of the assay*

The oseltamivir carboxylate solution was diluted into six concentrations with redistilled water: 783.9, 156.8, 31.36, 6.27, 1.25, and 0.25 μg/mL. Five μL of NA (8.33 μg/mL) was preincubated with 10 μL of oseltamivir carboxylate in 50 mM sodium acetate buffer (pH 3.5) at 37°C for 30 min, respectively. Ten μL of 0.2 mM 4-MUNANA was then added to each well. The terminal volume was 100 μL. The reaction was stopped after 15 min incubation by adding 100 μL of stop buffer. Meanwhile, substrate blank control (deactived NA) and enzyme activity control (no inhibitors) were set. The fluorescence intensities were measured using the method described above in order to obtain the inhibition ratio of oseltamivir carboxylate to NA activity.

$$\textbf{Inhibition ratio} = \frac{\mathbf{F}_{\text{enzyme activity control}} - \mathbf{F}_{\text{test}}}{\mathbf{F}_{\text{enzyme activity control}} - \mathbf{F}_{\text{black control}}} \times 100\%$$

2.7. *Inhibitor screening assays*

A total of 20 chemical compounds were used for screening and were dissolved in 50 mM sodium acetate buffer (pH 3.5) to a concentration of 2 mg/mL. Five μL of NA (8.33 μg/mL) was preincubated with 20 μL of various compounds (2 mg/mL) in 65 μL sodium acetate buffer (50 mM, pH 3.5) at 37°C for 30 min. Ten μL of substrate 4-MUNANA (0.2 mM) was then added to each well. The reaction was stopped after 15 min incubation by adding 100 μL of stop buffer. Meanwhile, substrate blank control (deactived NA) and enzyme activity control (no inhibitors) were set. The fluorescence intensities were measured using the method described above.

3. Results and Discussion

3.1. *Assay conditions and optimization*

Since the aim of this assay is the identification of small molecules that bind and inhibit the screened target, optimization translates into maximizing sensitivity towards inhibitors while maintaining good statistical quality and keeping reagent costs low.

3.1.1. *Stability of NA in solutions*

The activity of NA in solutions was not only retained but also increased as described according to the instructions. We, therefore, needed to investigate the stability of NA in different solvents and at different times to ensure that the NA solution was stable when used. When the enzyme was dissolved at a concentration of 16.7 μg/mL in redistilled water, it not only retained activity at 4°C but, actually increased activity in 10 days, and was comparatively stable from 11 to 15 days. When dissolved at 16.7 μg/mL in 0.1% cold bovine serum albumin solution, the activity of NA increased about 7 folds compared to activity in redistilled water. It was stable for 14 days before it increased in activity.

From the results, NA in 0.1% bovine serum albumin solution was stable for a much longer time. Meanwhile, the activity of NA increased compared to that in redistilled water. So, NA (8.33 μg/mL) prepared in 0.1% cold bovine serum albumin solution for 14 days was used.

3.1.2. *Stability of 4-MU in solution*

In 0.15 M glycine-NaOH buffer (pH 10.4), the fluorescence of 4-MU was constant for at least 10 h. In 50 mM sodium acetate buffer (pH 3.5), fluorescence was constant for at least 30 min. Therefore, 4-MU was stable in the reaction mixture, which meets the requirements for determination.

3.1.3. *Substrate concentrations*

In order to obtain the best reaction conditions, we determined the effect of substrate concentrations on NA activity. Various concentrations of 4-MUNANA (3, 6, 9, 18, 27, 36, and 54 μM) were incubated with the NA at 37°C for 5, 10, and 15 min, respectively. With the increase of substrate concentration the fluorescence intensity increased gradually (Figure 3). The enzymatic reaction rate was constant at 15 min when substrate concentration was 9, 18, 27, 36, and 54 μM. When substrate concentration was 9, 18, 27, and 36 μM, the

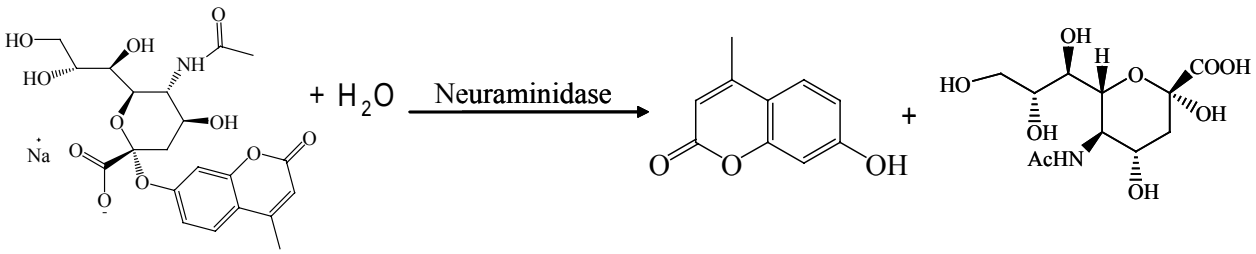

Figure 2. Reaction principle of microplate-based screening assay for NA inhibitors. NANA: *N*-Acetylneuraminic Acid.

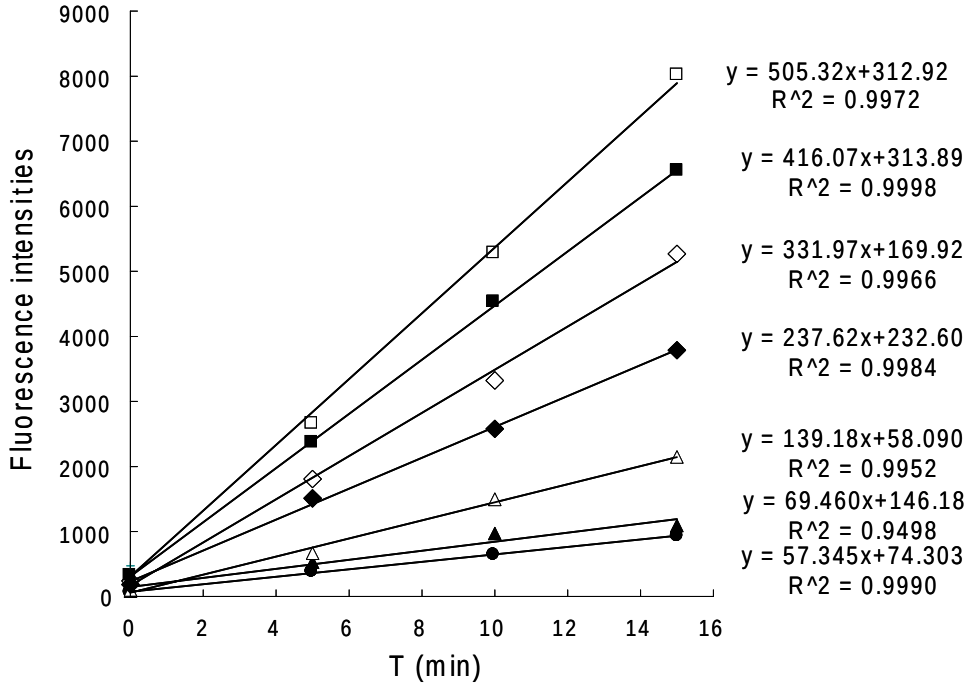

Figure 3. Effect of substrate concentrations on the NA activity. Substrate concentrations: 3 μM (●); 6 μM (▲); 9 μM (Δ); 18 μM (◆); 27 μM (◊); 36 μM (■); 54 μM (□).

values of B/S were smaller, and substrate fluorescence did not markedly interfere with the determination, which increased the sensitivity of detection (Figure 4). In order to reduce the interference and the cost, we chose 20 μM for the substrate concentration.

$$B/S = F_s / F_m \times 100\%$$

F_s and F_m are the fluorescence intensities measured after a 15 min incubation with deactivated and active enzyme.

3.1.4. *The pH of sodium acetate buffer*

Fifty mM sodium acetate buffer at various pHs (pH 3.0, 3.5, 4.0, 4.5, 5.0, 6.0, and 7.0) was used as reaction buffer to determine the activity of NA. The activity of NA increased from pH 3.0 to pH 3.5, and decreased when pH was changed from 3.5 to 7.0 (Figure 5). We chose 50 mM sodium acetate buffer (pH 3.5) as reaction buffer.

3.1.5. *Calcium ions*

Various concentrations of $CaCl_2$ prepared in 50 mM sodium acetate buffer (pH 3.5) were used to determine the activity of NA by the method described above. The reaction characteristics of NA vary with biological source. Only neuraminidase from Vibrio cholera requires calcium ions. However, the presence of calcium ions does not interfere with the activity of neuraminidases from other sources. In this study, NA

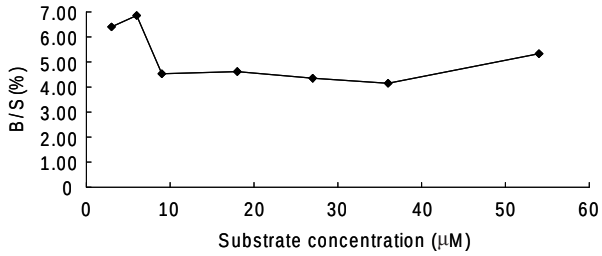

Figure 4. The interference of substrate concentrations on the determination.

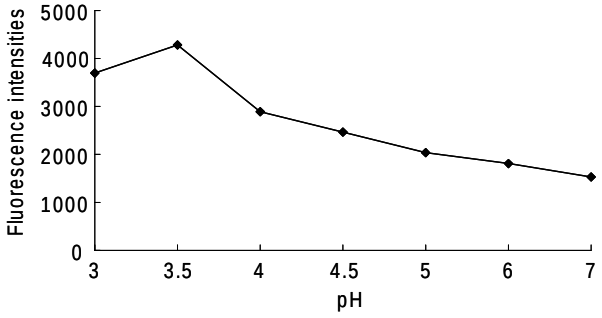

Figure 5. Effect of the pH of sodium acetate buffer on the determination of NA activity.

was prepared from *Clostridium perfringens*. The results demonstrated that NA from *Clostridium perfringens* does not require calcium ions for activity (Figure 6). This was in reasonable agreement with the published literature (*11*).

3.1.6. *Temperature*

The activity of NA was determined at various temperatures (25, 37, 40, 50, 60°C). The results demonstrated that the optimal temperature was 37°C.

3.1.7. *K_m value of the NA for 4-MUNANA*

K_m value of the NA for 4-MUNANA was determined by initial-rate enzyme assay. In order to ensure the progress of the reaction followed Michaelis-Menten kinetics, we chose 10 min as reaction time. The K_m value was calculated as 46.97 μM from a double-reciprocal plot (Figure 7).

3.2. *Assay validation*

We first investigated the assay's ability to identify known inhibitors. The IC_{50} value of previously characterized NA inhibitors was determined employing this assay by taking a fluorescent measurement after a reaction time of 15 min. Oseltamivir carboxylate was used as a known inhibitor for NA. The dose-response relationship of oseltamivir carboxylate to NA activity was observed. The IC_{50} value of oseltamivir carboxylate was 2.29 μM, which was in reasonable agreement with the published literature (*4*), thereby confirming its feasibility for screening.

Secondly, to quantify assay performance, we calculated the Z' factor, which was a main quality parameter in HTS, as described by Equation (1), where σ is the standard deviation and μ is the mean of the standard (s) or the negative (b) control (100% inhibition by a reference inhibitor) (*12*).

$$Z' = 1 - \frac{3\sigma_s + 3\sigma_b}{|\mu_s - \mu_b|} \qquad (1)$$

A Z' factor above 0.5 indicates a large separation band between the values for the positive and negative controls (100% and 0% activities, respectively). The Z' factor has the advantage of expressing the noise in relation to the signal window and, thus, gives a more complete estimation of assay quality than signal-to-background or signal-to-noise ratios alone would do (*7*). In this case, values between 0.8 and 0.9 were found, demonstrating that the assay holds a large separation band between samples and blank signals and thereby confirming its sensitivity for screening.

All of these findings establish the reliability and reproducibility of the developed fluorescent screening system for NA inhibition.

3.3. *Inhibitor screening assays*

Using the assay described above, 20 chemical compounds were used for screening. All the compounds were small molecule pyrrolidine derivatives, which were potencial NA inhibitors. In the primary screening, we found six compounds were active and the inhibition ratio was above 20%. For secondary screening, each of the six compounds was prepared in five concentrations. In our study, we observed a dose-response relationship of compound 10m for NA activity with an IC_{50} value of 2.96 mM (Figure 8). From the result, compound 10m (IC_{50} = 2.96 mM) was less effective against NA than oseltamivir carboxylate (IC_{50} = 2.29 μM), and will probably not be a leading compound. The synthesis and screening was continued in order to find leading compounds against NA.

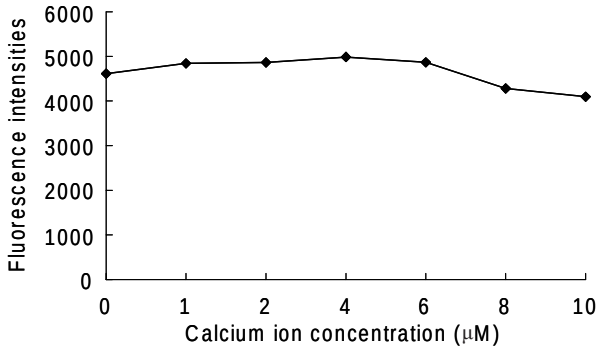

Figure 6. Effect of calcium ion on NA activity.

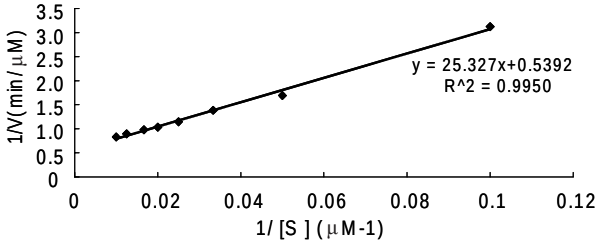

Figure 7. Assessment of K_m value of the NA for 4-MUNANA.

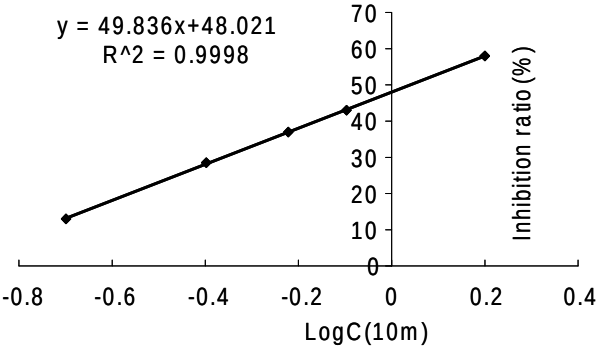

Figure 8. The inhibition curve of 10m to NA activity.

4. Conclusion

In the current study, we have developed and validated a fluorescent assay for the HTS of NA inhibition. This

test system will facilitate the HTS of large compound libraries with the objective to discover currently unknown potent NA inhibitors leading to novel drugs for influenza treatment. One shortage of this assay is that it is not suitable for screening mixtures. Further work will focus on screening for compounds synthesized by combinatorial chemistry. These results will be reported in future papers.

Acknowledgements

This research was supported in part by the Program of Founding Research Centers for Emerging and Reemerging Infectious Diseases, MEXT, Japan and the Global COE program of Nagasaki University, MEXT, Japan.

References

1. Noble GR. Basic and Applied Influenza Research. (Beare AS, ed). CRC Press, Boca Raton, FL, USA, 1980; p. 11.
2. Lamb RA. The Influenza Viruses. (Krug RM, ed). Plenum, New York, USA, 1989; p. 1.
3. Ghate AA, Air GM. Site-directed mutagenesis of catalytic residues of influenza virus neuraminidase as an aid to drug design. Eur J Biochem. 1998; 25:320-327.
4. Zhang J, Wang Q, Fang H, Xu WF, Liu AL, Du GH. Design, synthesis, inhibitory activity, and SAR studies of pyrrolidine derivatives as neuraminidase inhibitors. Bioorg Med Chem. 2007; 15:2749-2758.
5. Hanessian S, Bayrakdarian M, Luo X. Total synthesis of A-315675: a potent inhibitor of influenza neuraminidase. J Am Chem Soc. 2002; 124:4716-4721.
6. Stoll V, Stewart KD, Maring C. Influenza neuraminidase inhibitors: Structure-based design of a novel inhibitor series. J Biochem. 2003; 42:718-727.
7. von Ahsen O, Bömer U. High-throughput screening for kinase inhibitors. Chembiochem. 2005; 6:481-490.
8. Cao HP, Tao PZ, Du GH. Establishment and applicayion of high throughput screening model for influenza virus neuraminidase inhibitors *in vitro*. Acta Pharmacol Sin. 2002; 37:930-933.
9. Potier M, Mameli L, Belisle M, Dallaire L, Melancon SB. Fluorometric assay of neuraminidase with a sodium (4-methylumbelliferyl-alpha-D-*N*-acetylneuraminate) substrate. Anal Biochem. 1979; 94:287-296.
10. Lindegardh N, Hien TT, Farrar J, Singhasivanon P, White NJ, Day NPJ. A simple and rapid liquid chromatographic assay for evaluation of potentially counterfeit Tamiflu®. J Pharm Biomed Anal. 2006; 42:430-433.
11. Cassidy JT, Jourdian GW, Roseman S. The sialic acids. VI. Purification and properties of sialidase from *Clostridium perfringens*. J Biol Chem. 1965; 240:3501-3506.
12. Zhang JH, Chung TD, Oldenburg KR. A simple statistical parameter for use in evaluation and validation of high throughput screening assays. J Biomol Screen. 1999; 4:67-73.

(*Received September 17, 2009; Revised October 6, 2009; Accepted October 7, 2009*)

Original Article

In vitro evaluation of different transnasal formulations of sumatriptan succinate: A comparative analysis

Indrajeet D. Gonjari[1,*], Amrit B. Karmarkar[1], Pramod V. Kasture[2]

[1] *Govt. College of Pharmacy, Karad, MS, India;*
[2] *Padmashree. Dr. D. Y. Patil College of Pharmacy, Pimpri, Pune, MS, India.*

ABSTRACT: Sumatriptan succinate is an agonist for a vascular 5-hydroxytryptamine (5-HT)$_1$ receptor subtype (probably a member of the 5-HT$_{1D}$ family). It does not have significant affinity for the remaining 5-HT receptors. It does not have affinity for alpha$_1$, alpha$_2$ or beta-adrenergic, dopamine$_1$, dopamine$_2$, muscarinic or benzodiazepine receptors. The objective of the study was to evaluate the *in vitro* transnasal absorption of sumatriptan succinate through sheep nasal mucosa and to determine its *in vitro* permeation behavior from various formulations containing penetration enhancers. In this study four different thermoreversible gel formulations designed for nasal delivery of sumatriptan succinate were formulated. The formulations were prepared by using a poly(oxythylene) poly(oxypropylene) block copolymer (Pluronic F 127) based gel along with different permeation enhancers and a pluronic lecithin organogel base. The effect of different concentrations of sodium glycocolate, EDTA and transcutol on *in vitro* nasal diffusion of sumatriptan succinate was studied. The best permeation profile was obtained with a formulation containing transcutol at a concentration of 0.005% w/w. Pluronic lecithin organogel showed good gelling properties at a concentration in the 20% range.

Keywords: Sumatriptan succinate, Pluronic F 127, transcutol, sodium glycocolate, EDTA, pluronic lecithin organogel

1. Introduction

Migraine is currently thought to be a primary neural process. In the milieu of a hyperexcitable cortex, various stimuli probably produce disturbances in neuronal ion channel activity, resulting in a lowered threshold for external or internal factors to trigger "cortical spreading dysfunction (CSD)". This slowly propagating wave of neuronal depolarisation is most likely responsible for the migraine aura and activation of the trigemino-vascular system (*1*). Migraine treatment has evolved into the scientific arena, but opinions differ on whether migraine is primarily a vascular or a neurological dysfunction (*2*,*3*). Sumatriptan succinate (SS) is a potent and selective vascular 5-hydroxytryptamine1-receptor agonist effective for the treatment of migraine. It is rapidly but incompletely absorbed following oral administration and undergoes first-pass metabolism, resulting in a low absolute bioavailability of 14% in humans (*4*). In adults, intranasal SS is well absorbed and tolerated (*5*). For more than a decade intranasal SS has been a widely used drug for the treatment of acute migraine and has an excellent safety record (*6*,*7*). However, the problem associated with nasal delivery of SS solution is lower retention time in the nasal cavity (15 min) resulting in lower bioavailability as well as lower transfer of SS directly to the brain through the olfactory pathway. After 15 min, SS solution is swallowed and it enters the gastrointestinal tract (GIT), where the remaining dose is absorbed. Although SS nasal spray provides a faster onset effect than the tablet, it produces a similar headache response at 2 h (*8*).

The purpose of this work was to increase the nasal absorption of SS by increasing the residence time and increasing the absorption by using various penetration enhancers. We have formulated in situ gels using Pluronic F 127 (PF 127) and pluronic lecithin organogels (PLO) that can serve to improve drug delivery *via* the transnasal route. Different concentrations of absorption enhancers including: transcutol, sodium glycocolate, and EDTA were optimized. PLO is composed of isopropylpalmitate (or less commonly myristate), soya lecithin, water and PF 127.

2. Materials and Methods

2.1. *Materials*

Sumatriptan succinate was a gift sample from Dr. Reddys Lab. (Hydrabad, India). Transcutol and PF 127 was from ICPA Ltd. (Ankeleshwar, Gujarat, India).

**Address correspondence to:*
Dr. Indrajeet D. Gonjari, Govt. College of Pharmacy, Karad (Satara) 415110, MS, India.
e-mail: indrajeetgonjari@gmail.com

EDTA, sodium glycocolate, benzalkonium chloride, lecithin, and isopropyl palmitate chemicals were of analytical grade.

2.2. *Preparation of transnasal gels*

2.2.1. *Preparation of thermoreversible SS gel*

Preparation of thermoreversible gels was excellently reviewed by Karmarkar *et al.* (*9*). Thermoreversible gels were prepared using cold technique (*10*). PF 127 and SS were solubilized in distilled water containing PEG 4000, propylene glycol and benzalkonium chloride (BAC) in required quantities. The liquid was kept at 4°C until a clear solution was obtained to get a gelation temperature in the range of 36-37°C. Different thermoreversible gels containing permeation enhancers such as transcutol (0.01% w/w, 0.03% w/w, and 0.05% w/w concentrations), EDTA and sodium glycocolate (0.1% w/w, 0.3% w/w, and 0.5% w/w concentrations) were prepared. The concentration of EDTA (when a chelating agent is used, preferably, it is present in an amount within a range from about 0.005% to about 1% of the total weight of the composition, more preferably, from 0.01% to 0.5%, still more preferably, from about 0.05% to about 0.2% of the composition) (*11*) and sodium glycocolate was kept at 0.5% (1% SG was tried in humans for 60 mg/mL of gentamycin solution in saline) (*12*). The concentration of transcutol was reduced to 0.05% w/w because it was reported to be a non-irritant at the concentrations studied (0.005-0.03% w/w), while it produced slight irritation in rabbit eyes at a concentration of 0.05% w/w (*13*). To achieve the gelation temperature in the range of 35-37°C, optimization of the formulation was done by using different concentrations and PEG 4000 as shown in Tables 1-4 (formulation A3, A2, A1, A, B2, B1, B, C2, C1, C, D2, D1, and D).

2.2.2. *Preparation of sumatriptan pluronic lecithin organogel (PLO)*

Formulations were prepared by using factorial design. Twenty-seven batches of sumatriptan succinate PLO gel were prepared by dissolving SS in purified water, adding to it PF 127 and mixed. We incorporated the soya lecithin: isopropyl palmitate solution and mixed well. Sufficient water with mixing was added to get the final weight (*14*). The final weight of all formulations was adjusted to 10 g. The batches were prepared as shown in Tables 5 and 6. The batch of PLO with gelation near 37°C was considered for further evaluation. The batch containing P407 20%, soyalicithin 8%, isopropyl palmitate 5% along with drug 10% w/w and BAC 0.001% w/w had gelation at 35°C (Formulation IV-E). This was considered for further evaluation.

Table 1. Batches of PF 127 gel formulations containing SS

Formulation ingredients	A3	A2	A1	A
SS (% w/w)	10	10	10	10
PF 127 (% w/w)	20	20	20	20
PEG 4000 (% w/w)	1	1	2	2
PG (% w/w)	0.1	0.2	0.1	0.2
BAC (% w/w)	0.001	0.001	0.001	0.001
2 M NaOH	q.s.*	q.s.	q.s	q.s.
Distilled water	q.s.	q.s.	q.s	q.s.

* q.s., quantum sufficiat.

Table 2. Batches of PF 127 gel formulations containing SS with different concentrations of EDTA

Formulation ingredients	B2	B1	B
SS (% w/w)	10	10	10
PF 127 (% w/w)	20	20	20
PEG 4000 (% w/w)	2	2	2
PG (% w/w)	0.2	0.2	0.2
EDTA (% w/w)	0.1	0.3	0.5
BAC (% w/w)	0.001	0.001	0.001
2 M NaOH	q.s.*	q.s.	q.s
Distilled water	q.s.	q.s.	q.s

* q.s., quantum sufficiat.

Table 3. Batches of PF 127 gel formulations containing SS with different concentrations of SG

Formulation ingredients	C2	C1	C
SS (% w/w)	10	10	10
PF 127 (% w/w)	20	20	20
PEG 4000 (% w/w)	1	1	1
PG (% w/w)	0.2	0.2	0.2
SG (% w/w)	0.1	0.3	0.5
BAC (% w/w)	0.001	0.001	0.001
2 M NaOH	q.s.*	q.s.	q.s
Distilled water	q.s.	q.s.	q.s

* q.s., quantum sufficiat.

Table 4. Batches of PF 127 gel formulations containing SS with different concentrations of TC

Formulation ingredients	D2	D1	D
SS (% w/w)	10	10	10
PF 127 (% w/w)	20	20	20
PEG 4000 (% w/w)	2	2	2
PG (% w/w)	0.2	0.2	0.2
TC (% w/w)	0.01	0.03	0.05
BAC (% w/w)	0.001	0.001	0.001
2 M NaOH	q.s.*	q.s.	q.s
Distilled water	q.s.	q.s.	q.s

* q.s., quantum sufficiat.

2.3. *Evaluation of transnasal gels*

2.3.1. *Gelation temperature*

Gelation temperatures of the gels were measured according to the method described by Gilbert *et al.* (*15*). Two milliliter aliquots of the gel were transferred to test tubes sealed with parafilm and immersed in a water bath at 4°C. The temperature of the bath was increased in increments of 1°C and left to equilibrate for 15 min at each new setting. The samples were examined for gelation, which was said to have occurred when the meniscus would no longer

Table 5. Factorial design of PLO gel formulations containing SS

Coded levels	Values of variables		
	PF 127	SL	IIP
Low (-1)	10%	2%	4%
Medium (0)	20%	4%	5%
High (+1)	30%	8%	6%

Table 6. Formulation compositions of PLO gels using 3^3 factorial design

Batch Number	Values of variables			PF 127 (% w/w)	SL (% w/w)	IIP (% w/w)
1PLO	-1	-1	-1	10	2	4
2 PLO	-1	-1	-1	10	2	5
3 PLO	-1	-1	-1	10	2	6
4 PLO	-1	-1	-1	10	4	4
5 PLO	-1	-1	-1	10	4	5
6 PLO	-1	-1	-1	10	4	6
7 PLO	-1	-1	-1	10	8	4
8 PLO	-1	-1	-1	10	8	5
9 PLO	-1	-1	-1	10	8	6
10 PLO	0	0	0	20	2	4
11 PLO	0	0	0	20	2	5
12 PLO	0	0	0	20	2	6
13 PLO	0	0	0	20	4	4
14 PLO	0	0	0	20	4	5
15 PLO	0	0	0	20	4	6
16 PLO	0	0	0	20	8	4
17 PLO	0	0	0	20	8	5
18 PLO	0	0	0	20	8	6
19 PLO	1	1	1	30	2	4
20 PLO	1	1	1	30	2	5
21 PLO	1	1	1	30	2	6
22 PLO	1	1	1	30	4	4
23 PLO	1	1	1	30	4	5
24 PLO	1	1	1	30	4	6
25 PLO	1	1	1	30	8	4
26 PLO	1	1	1	30	8	5
27 PLO	1	1	1	30	8	6

To the above compositions, SS in a concentration of 10% w/w and BAC 0.001% w/w were added.

move when tilted through 90°. All measurements were performed in triplicate (n = 3).

2.3.2. *Content uniformity*

All optimized batches were checked for content uniformity. Weight of the gel equivalent to theoretical weight (Dose of drug *i.e.*, 20 mg) of the drug was taken and dissolved in water. The drug content was determined at 282 nm, using a Shimadzu 1700UV-VIS spectrophotometer (*16*) (Linearity range, 20 µg/mL to 100 µg/mL; Slope, 69.45; Intercept, -0.3692; R value, 0.9998).

2.3.3. *Measurement of gel strength*

A sample of 50 g of gel was placed in a 100 mL graduated cylinder and gelled in a thermostat at 37°C. The apparatus for measuring gel strength given by Choi *et al.* (*17*) was allowed to penetrate the gel. Gel strength *i.e.* the viscosity of the gels at physiological temperature was determined as the time (in seconds) for the apparatus to sink 5 cm through the prepared gel. All measurements were performed in triplicate (n = 3).

2.3.4. *Determination of bioadhesive force*

The bioadhesive force of all batches was determined by the method given by Choi *et al.* (*17*). A section of nasal mucosa was cut from the sheep nasal cavity and instantly fixed with mucosal side out onto each glass vial using a rubber band. The vials with nasal mucosa were stored at 37°C for 5 min. The next vial with a section of mucosa was connected to the balance in inverted position while the first vial was placed on a height adjustable pan. Nasal gel was added to the nasal mucosa of the first vial. The height of the second vial was adjusted so that the mucosal surfaces of both vials came into intimate contact. Two minutes of contact was allowed. Weight kept rising in the pan until the vials detached. Bioadhesive force was the minimum weight required to detach two vials. Nasal mucosa was changed for each measurement.

2.3.5. *Diffusion across nasal mucosa*

Noses of healthy sheep were obtained from the local slaughterhouse. It was cleaned and the mucosa was removed from the anterior nasal cavity. The mucosa was stored in normal saline with a few drops of gentamycin sulphate injection, to avoid bacterial growth. Phosphate buffer pH 7.4 was used as diffusion medium. *In vitro* diffusion studies were carried out in the nasal diffusion cell by the method of Pisal *et al.* (*18*). The outlet of the reservoir was maintained at 37 ± 0.5°C. About 1 mL of sample was withdrawn at a time interval of one hour from sampling port of receptor compartment and the same volume was then replaced with receptor fluid solution in order to maintain skin condition. The samples were appropriately diluted and the absorbance was measured at 282 nm using a Shimadzu 1700UV-VIS spectrophotometer.

3. Results and Discussion

3.1. *Gelation temperature*

It was previously proved that pluronics undergo thermal gelation or sol-gel transition at a temperature of about 25 to 35°C. Below the transition temperature pluronic solutions allow a comfortable and precise delivery in the nasal cavity where thermogelation occurs. Immediate gelling increases residence time and enhances bioavailability of drug (*19*). The gelation temperature of all batches is shown in Tables 7 and 8. All gel formulations containing PF 127 showed good gelling properties. Absorption enhancers have increased the gelation temperature of PF 127 base. For PLO

gels, the batches containing 10% PF 127 showed no gelation. Batches with 20% PF 127 indicated gelation in the range of 24-37°C whereas batches with 30% PF 127 concentrations did not have liquid consistency. At temperatures below 10°C batches containing 10% and 20% PF 127 exhibited a two-phase system. Increasing concentrations of soya lecithin decreased the gelation point in batches containing 20% PF 127. Batches containing 20% PF 127, 8% soya lecithin, and 5% isopropyl palmitate along with drug and BAC gelled at 35°C (Formulation E). This was considered for further evaluation.

Table 7. Gelation temperature of PF 127 gel formulations under various conditions

Sr. No.	Formulation*	Gelation temperature (°C)
1	A3	30.36 ± 0.15
2	A2	30.56 ± 0.05
3	A1	32.26 ± 0.20
4	A	34.50 ± 0.28
5	B2	35.23 ± 0.11
6	B1	35.36 ± 0.05
7	B	35.61 ± 0.10
8	C2	36.10 ± 0.20
9	C1	37.16 ± 0.40
10	C	37.60 ± 0.05
11	D2	36.80 ± 0.10
12	D1	37.20 ± 0.20
13	D	37.40 ± 0.17

* A3, A2, A1, and A, PF 127 gel formulations containing SS; B2, B1, and B, PF 127 gel formulations containing SS with different concentrations of EDTA; C2, C1, and C, PF 127 gel formulations containing SS with different concentrations of SG; D2, D1, and D, PF 127 gel formulations containing SS with different concentrations of TC in different concentrations. See Tables 1-4 for the composition of each formulation.

Table 8. Gelation temperature of formulations of SS in PLO gel

Batch No. of PLO*	Two phase	One phase	Gelation	Gel melting
1	< 10°C	15°C	No gelation	–
2	< 10°C	15°C	No gelation	–
3**	< 10°C	18°C	No gelation	–
4**	< 10°C	18°C	No gelation	–
5**	< 10°C	12°C	No gelation	–
6**	< 10°C	18°C	No gelation	–
7	< 10°C	19-20°C	No gelation	–
8	< 10°C	21°C	No gelation	–
9***	< 10°C	21°C	No gelation	–
10	< 10°C	21°C	27°C	90°C
11	< 10°C	16°C	25°C	75°C
12	< 10°C	21°C	25°C	90°C
13	< 10°C	20°C	25°C	90°C
14	< 10°C	18°C	25°C	90°C
15	< 10°C	19°C	25°C	90°C
16	< 10°C	25°C	38°C	90°C
17	< 10°C	22°C	35°C	91°C
18	< 10°C	25°C	30°C	90°C
19****			5°C	> 100°C
20****			5°C	> 100°C
21****			5°C	> 100°C
22****			5°C	> 100°C
23****			5°C	> 100°C
24****			5°C	> 100°C
25****			5°C	> 100°C
26****			5°C	> 100°C
27****			5°C	> 100°C

* See Table 6 for the formulation composition of each PLO batch; ** Batch numbers 3 to 6 of PLO became very viscous in the range of 25-35°C and gave very homogeneous mixtures at 40°C; *** Batch numbers 3 to 6 of PLO became very viscous in the range of 25-35°C; **** All the systems are in one phase. Gel at 5°C. Gel melting is above 100°C.

3.2. *Content uniformity*

Content uniformity of various formulations is summarized in Table 9.

3.3. *Measurement of gel strength*

Gel strength providing an indication of viscosity of gel formulations (*17*) was measured as described in "Materials and Methods". Results are shown in Table 9.

3.4. *Determination of bioadhesive force (detachment stress)*

The detachment stress and gel strength of PF 127 gel of SS was slightly decreased with the addition of absorption enhancers (effect seen at high concentrations). An increase in detachment stress was observed with PLO gel. PLO gel is Pluronic Lecithin Organogel. PLO was compounded from an aqueous phase, PF 127 and a lipid phase, lecithin and isopropyl palmitate. As the lipid content is increased in PLO the detachment stress of PLO gel is high. Results are shown in Table 9.

3.5. *Diffusion across nasal mucosa*

The percentage of drug diffusion of various formulations through nasal mucosa over a period of 8 h for formulations is shown in Figures 1-4.

In the initial phase, the rate of diffusion of SS from all batches containing EDTA was nearly the same. However, in the latter phase (time period more than 60 to 90 min), the amount of drug diffusion from the formulations containing higher concentrations of EDTA was greater and the cumulative amount of drug released was also greater. Thus, until a time period from 60 to

Table 9. Content uniformity, bioadhesion and gel strength of gel formulations

Formulation	Content uniformity	Detachment stress (dynes/cm^2)	Gel strength (sec)
A	99.9%	3792.41	118
B2	99.7%	3754.10	114
B1	99.8%	3734.95	115
B	99.9%	3723.46	115
C2	99.8%	3727.29	114
C1	99.9%	3719.63	115
C	100.1%	3715.80	116
D2	100.2%	3784.75	118
D1	99.8%	3773.26	117
D	99.8%	3769.43	117
E	100.2%	4290.40	131

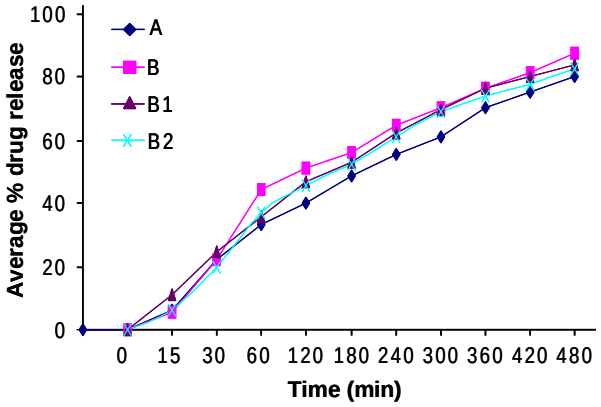

Figure 1. Plot of *in vitro* drug (SS) diffusion of various formulations (gels) containing PF 127 along with EDTA at different concentrations. See Tables 1 and 2 for composition of formulations A, B, B1, and B2.

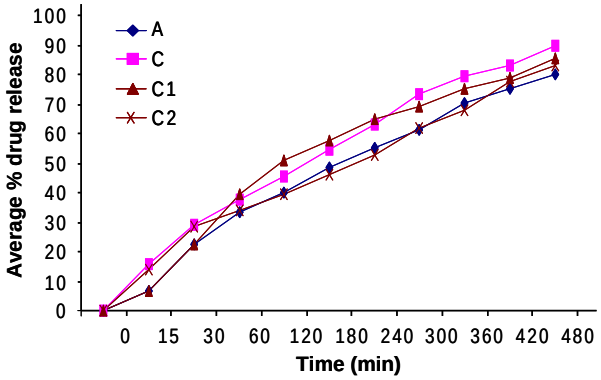

Figure 2. Plot of *in vitro* drug (SS) diffusion of various formulations (gels) containing PF 127 along with SG at different concentrations. See Tables 1 and 3 for the composition of formulations A, C, C1, and C2.

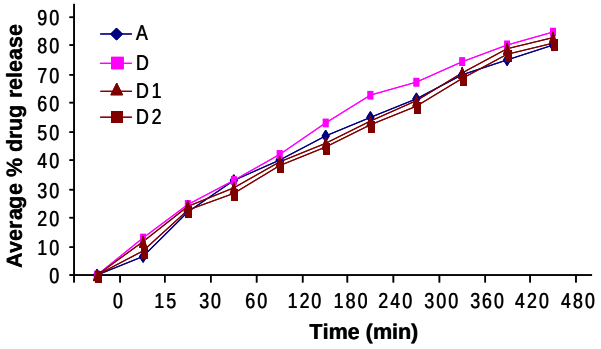

Figure 3. Plot of *in vitro* drug (SS) diffusion of various formulations (gels) containing PF 127 along with TC at different concentrations. See Tables 1 and 4 for the composition of formulations A, D, D1, and D2.

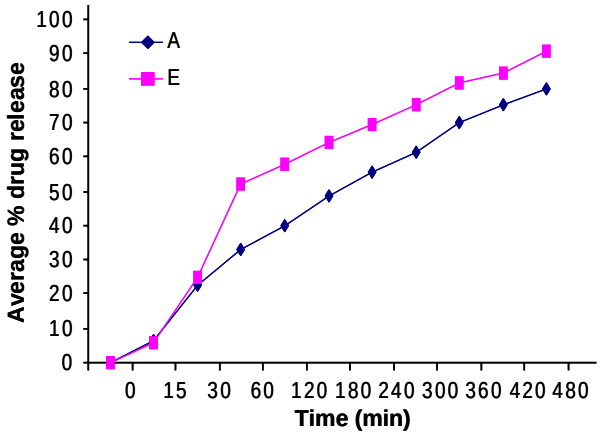

Figure 4. Plot of *in vitro* drug (SS) diffusion from PLO (Formulation E).

90 min EDTA fails to show a penetration enhancement effect. All the batches of SS in PF 127 gel along with the penetration enhancers followed a matrix model as the best-fit model for the release of drug. As compaired to EDTA, SG showed an increase in cumulative release of SS. The effect of penetration enhancement is concentration dependent. TC has also shown an increase in cumulative drug release from the formulations. This observed effect was also concentration dependent. This might be due to the hydrophilic nature of SS.

To our knowledge, no report has described the use of PLO gel as a penetration enhancer for a nasal drug delivery system. The aim of this study was to explore the use of PLO gel in a nasal drug delivery system. The *in vitro* diffusion of SS from PLO reveals that the *in vitro* transnasal transport of SS is greater than plain gel. The hypothesis that lecithin can increase mucosal drug transport was successfully evaluated for transnasal formulations from the above studies. Similar transnasal drug delivery of PLO gels with a suitable model drug can be further carried out to obtain desirable nasal drug delivery formulations.

The highest flux was shown by PLO gel formulations. The order of decreasing flux with different enhancers is as follows, PLO gel (63.25%) > 0.5% SG formulation (55.95%) > 0.5% EDTA (55.47%) > Plain PF 127 gel (53.14%) > 0.01% TC (46.33%).

4. Conclusion

The effect of different concentrations of sodium glycocolate, EDTA and transcutol on *in vitro* nasal diffusion of SS was studied. The effect of these absorption enhancers was found to be concentration dependent. The order of increasing absorption of SS caused by the enhancers was sodium glycocolate > EDTA at a concentration of 0.5%. Transcutol showed significant diffusion at concentration of 0.05%. Pluronic lecithin organogel showed good gelling properties with a concentration in the range of 20%. The pluronic lecithin organogel showed the highest release among all the formulations.

Acknowledgements

The authors are thankful to Dr. Reddy's Laboratories (Hydrabad, India) for providing a gift sample of Sumatriptan succinate and ICPA Ltd. (Ankeleshwar Gujarat India) for providing a gift sample of PF 127 and Transcutol.

References

1. Pietrobon D, Striessnig J. Neurobiology of migraine. Nat Rev. 2003; 4:386-398.
2. Humphrey PP, Feniuk W, Marriott AS, Tanner RJ, Jackson MR, Tucker ML. Preclinical studies on the anti-migraine drug: Sumatriptan. Eur Neurol. 1991; 31:282-290.
3. Pakalnis A, Kring D, Paolicchi J. Parenteral satisfaction with sumatriptan nasal spray in childhood migraine. J Child Neurol. 2003; 18:772-775.
4. Villalon CM, Centurion D, Valdivia LF, de Vries P, Saxena PR. Migraine: pathophysiology, pharmacology, treatment and future trends. Curr Vasc Pharmacol. 2003; 1:71-84.
5. Martindale K. The Complete Drug Reference. Pharmaceutical Press, London, UK, 1999; pp. 450-452.
6. Christensen ML, Mottern RK, Jabbour JT, Fuseau E. Pharmacokinetics of Sumatriptan nasal spray in adolescents. J Clin Pharmacol. 2003; 43:721-726.
7. Diamond S, Elkind A, Jackson T. Multiple attach efficacy and tolerability of sumatriptan nasal spray in the treatment of migraine. Arch Fam Med. 1998; 7:234-240.
8. Ryan R, Elkind A, Baker CC, Mullican W, DeBussey S, Asgharnejad M. Sumatriptan nasal spray for the treatment of acute migraine: results of two clinical studies. Neurology. 1997; 49:1225-1230.
9. Karmarkar AB, Gonjari ID, Hosmani AH. Poloxamers and their applications. Online international pharmaceutical journal Pharmainfo.net, 2008 (*http://www.pharmainfo.net)*.
10. Schmolka IR. Artificial skin. I: Preparation and properties of Pluronic F 127 gel for the treatment of burns. J Biomed Master Res. 1972; 6:571-582.
11. Williams RO, Zhang F, Koleng JJ, Pasternak GW, Kolesnikov YA. Methods and compositions for treating pain of the mucous membrane. US Patent 6509028. 2003.
12. Hussain AA, Hirai S, Bawarshi R. Nasal dosage forms of propranolol. US Patent 4394390. 1983.
13. Liu Z, Li J, Nie S, Guo H, Panm W. Effects of Transcutol P on the corneal permeability of drugs and evaluation of its ocular irritation of rabbit eyes. J Pharm Pharmacol. 2006; 58:45-50.
14. Allen LV Jr. Selegiline hydrochloride 10 mg/mL in pluronic lecithin organogel. Int J Pharm Compound. 2004; 8:59.
15. Gilbert JC, Richardson JL, Davies MC, Palin KJ, Hadgraft J. The effect of solutes and polymers on the gelation properties of Pluronic F 127 solutions for controlled drug delivery. J Control Release. 1987; 5:113-118.
16. Andersona BC, Pandit NK, Mallapragadaa SK. Understanding drug release from poly(ethylene oxide)-b poly(propylene oxide)-b-poly(ethylene oxide) gels. J Control Release. 2001; 70:157-167.
17. Choi HG, Jung JH, Ryu JM, Yoon SJ, Oh YK, Kim CK. Development of in situ gelling and mucoadhesive acetaminophen liquid suppository. Int J Pharm. 1998; 165:33-44.
18. Pisal S, Shelke V, Mahadik K, Kadam S. Effect of organogel components on *in vitro* nasal delivery of propranolol hydrochloride. AAPS PharmSciTech. 2004; 5: Article 63 (*http://www.aapspharmscitech.org*).
19. Koller C, Buri P. Properties and pharmaceuticae value of thermoreversible gels based on poloxamers and poloxamins. S.T.P. Pharma. 1987; 3:115-124. (in French)

(*Received October 11, 2009; Accepted November 2, 2009*)

Original Article

Positive inotropic effect of PHR0007 (2-(4-(4-(Benzyloxy)-3-methoxybenzyl)piperazin-1-)-*N*-(1-methyl-4,5-dihydro[1,2,4]triazolo[4,3-a]quinolin-7-yl) acetamide) on atrial dynamics in beating rabbit atria

Ying Lan[1], Huri Piao[2,3,*], Xun Cui[1,2,*]

[1] *Department of Physiology, School of Basic Medical Sciences, Ministry of Education, Yanbian University, Yanji, China;*
[2] *Key Laboratory of Natural Resources of Changbai Mountain & Functional Molecules (Yanbian University), Ministry of Education, Yanbian University, Yanji, China;*
[3] *College of Medicine, Yanbian University, Yanji, Jilin, China.*

ABSTRACT: The aim of the present study was to examine the positive inotropic effects and mechanism of action of PHR0007 (2-(4-(4-(Benzyloxy)-3-methoxybenzyl)piperazin-1-)-*N*-(1-methyl-4,5-dihydro[1,2,4]triazolo[4,3-a]quinolin-7-yl)acetamide) on beating rabbit atria. Atria were obtained from New Zealand white rabbits, and experiments performed using a perfused beating atrial model. The effects of PHR0007 (1, 30, or 100 μmol/L), and of the protein kinase inhibitors, staurosporine (1.0 μmol/L) or H-89 (10 μmol/L), plus PHR0007 (30 μmol/L), on atrial pulse pressure and stroke volume were analyzed. PHR0007 significantly increased atrial pulse pressure and atrial stroke volume in beating rabbit atria compared with control baseline levels. These effects of PHR0007 were completely blocked by pretreatment with either staurosporine (a nonspecific protein kinase inhibitor) or H-89 (a cAMP-dependent protein kinase A inhibitor). In addition, 3-isobutyl-1-methylxanthine (IBMX), a non-specific inhibitor of phosphodiesterases (PDEs), completely blocked the positive inotropic effect of PHR0007 on atrial dynamics, but forskolin, an activator of adenylyl cyclases (AC), failed to modulate PHR0007-induced increases in atrial pulse pressure and stroke volume. In conclusion, these data suggest that PHR0007 produces a positive inotropic effect in rabbit atria *via* the PDE-cAMP-PKA signaling pathway.

Keywords: Inotropic effect, PHR0007, milrinone, protein kinase A (PKA), cAMP, PDE

**Address correspondence to:*
Dr. Xun Cui, Department of Physiology and Pathophysiology, School of Basic Medical Sciences, Yanbian University, 1829 Juzi street, Yanji 133-000, Jilin, China.
e-mail: cuixun@ybu.edu.cn

1. Introduction

Medical treatment for severe heart failure commonly includes the use of digitalis glycosides, vasodilators, and catecholamines. However, these drugs exhibit only inotropic effects or only vasodilatory effects, while experimentally, a drug tolerance or arrhythmogenesis can also occur. Milrinone, a phosphodiesterase 3 (PDE3) inhibitor, is a potent cardiac bipyridine with inotropic and vasodilator properties (*1*,*2*), and is generally used for short-term management of heart failure (*3*). To develop more potent positive inotropic agents with less side effects, a series of positive inotropic agents were synthesized, and their biological activities were examined (*4*,*5*). Among the drugs tested, PHR0007 (2-(4-(4-(Benzyloxy)-3-methoxybenzyl)piperazin-1-)-*N*-(1-methyl-4,5-dihydro[1,2,4]triazolo[4,3-a]quinolin-7-yl)acetamide) exhibited a moderate positive inotropic activity.

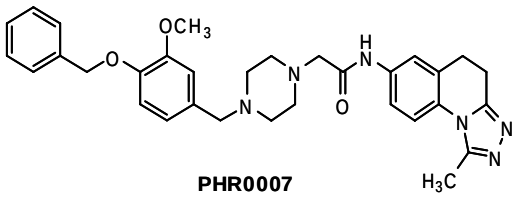

PHR0007

However, to the best of our knowledge, a detailed study of the positive inotropic activity of PHR0007 within the atria and the mechanisms of action has not been reported. Herein, we examined the positive inotropic effect of PHR0007 on atrial dynamics and the mechanism of action in beating rabbit atria.

2. Materials and Methods

2.1. *Preparation of rabbit perfused beating atria*

Atria were obtained from New Zealand white rabbits. The mean atrial weight was 193.1 ± 7.4 mg.

An isolated perfused atrial preparation was used as previously described (*7*). Briefly, hearts were removed from rabbits and the left atria were dissected free. A calibrated transparent atrial cannula containing two small catheters was inserted into the left atrium. The cannulated atrium was transferred to an organ chamber and perfused immediately with HEPES buffer solution (1.25 mL/min) at 34°C. The perfusate contained 0.1% bovine serum albumin, 118 mmol/L NaCl, 4.7 mmol/L KCl, 2.5 mmol/L $CaCl_2$, 1.2 mmol/L $MgCl_2$, 25 mmol/L $NaHCO_3$, 10.0 mmol/L glucose, and 10.0 mmol/L HEPES (pH adjusted to 7.4 with NaOH). Within 2-3 sec after the perfused atrium was set up, transmural electrical field stimulation with a luminal electrode was started at 1.5 Hz (duration 0.3 msec; voltage 30-40 V). The changes in atrial pulse pressure were measured by an electrophysiolograph, and changes in atrial stroke volume were monitored by reading the lowest levels of the water column in the calibrated atrial cannula during end diastole (*6,7*).

2.2. *Drugs*

PHR0007 was provided by Yanbian University College of Pharmacy. Milrinone, staurosporine, H-89, IBMX (3-isobutyl-1-methylxanthine) and forskolin were purchased from Sigma-Aldrich (St. Louis, MO, USA).

2.3. *Experimental protocol*

Atria were perfused for 60 min to stabilize atrial pulse pressure and atrial stroke volume, and the atria were paced at 1.5 Hz. The control period was followed by infusions of 1, 30, and 100 μmol/L PHR0007 in each atria, each for 12 min as one experimental cycle, and changes of atrial pulse pressure and stroke volume were recorded at each dose, and fractions were collected at 2 min intervals. The effects of 30 μmol/L PHR0007 on atrial pulse pressure and stroke volume were also directly compared with those of 30 μmol/L milrinone.

In another series of experiments to determine the mechanism of PHR0007 on atrial dynamics, 30 μmol/L forskolin [an activator of adenylyl cyclases (AC)] or 30 μmol/L IBMX [a non-specific inhibitor of phosphodiesterases (PDEs)] were infused for 12 min prior to infusion of 30 μmol/L PHR0007, and 1.0 μmol/L staurosporine (a non-specific protein kinase inhibitor) or 10 μmol/L H-89 [a specific inhibitor of cAMP-dependent protein kinase A (PKA)] were infused for 24 min prior to infusion of 30 μmol/L PHR0007. Atrial pulse pressure and stroke volume during the control period were compared with those during PHR0007 infusion.

2.4. *Statistical analysis*

Data are presented as means ± SEM. Differences between groups were determined by one-way ANOVA and student's unpaired *t*-test. Statistical significance was set at $p < 0.05$.

3. Results

3.1. *Effect of PHR0007 on atrial pulse pressure and stroke volume*

There were time- and dose-dependent effects of PHR0007 on both atrial pulse pressure and stroke volume, with a significant increase in both parameters compared with the control period at 30 μmol/L and 100 μmol/L PHR0007 (Figure 1, $n = 6$/group, $p < 0.001$), which peaked at 48 min of PHR0007 infusion.

3.2. *Role of phosphodiesterase (PDE)-cAMP-PKA pathway in the PHR0007-induced increase in atrial pulse pressure and stroke volume*

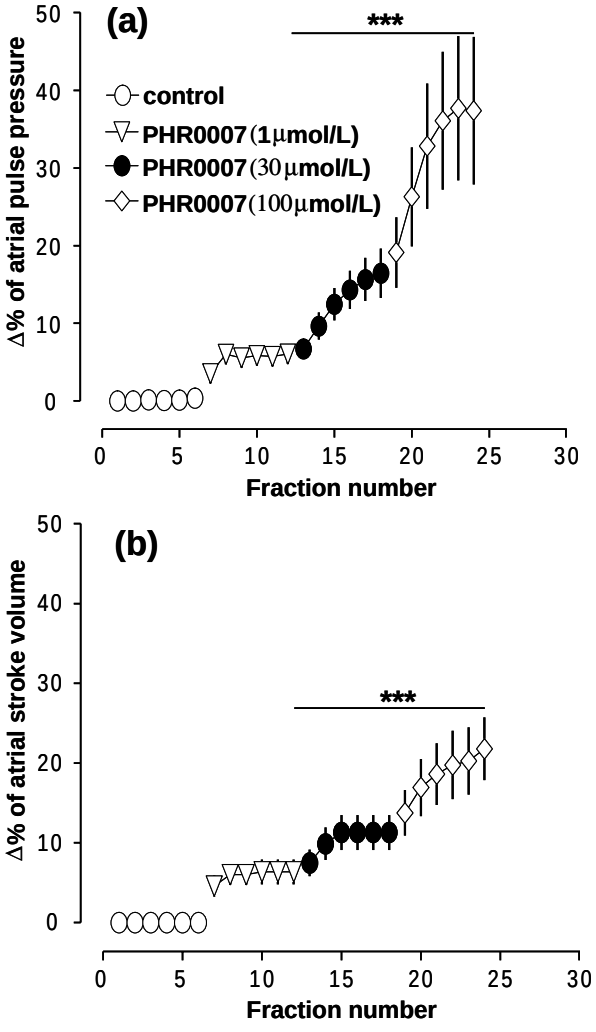

Figure 1. Effect of PHR0007 on atrial pulse pressure and stroke volume. Effects of 1, 30, and 100 μmol/L PHR0007 on atrial pulse pressure (**a**) and atrial stroke volume (**b**). Fractions were collected at 2 min intervals. Data are mean ± SEM ($n = 6$/group). *** $p < 0.001$ compared with the control period.

Staurosporine (1.0 μmol/L) or H-89 (1.0 μmol/L) significantly decreased atrial pulse pressure and stroke volume compared with the control period respectively (Figure 2, $n = 6$, both $p < 0.001$; Figure 3, $n = 6$, both $p < 0.05$). In the presence of staurosporine or H-89 plus PHR0007 (30 μmol/L) significantly decreased atrial pulse pressure and stroke volume compared with staurosporine or H-89 alone (Figure 2, $n = 6$, both $p < 0.001$; Figure 3, $n = 6$, both $p < 0.05$). Forskolin (30 μmol/L), an activator of adenylyl cyclases (AC), significantly increased atrial pulse pressure and stroke volume, but had no effect on PHR0007-induced increases in atrial pulse pressure and atrial stroke volume ($n = 6$; Figure 4). However, IBMX (30 μmol/L) completely blocked the positive inotropic effect of PHR0007 on atrial dynamics ($n = 6$; Figure 5).

3.3. *Effect of PHR0007 and milrinone on atrial pulse pressure and stroke volume*

PHR0007 (30 μmol/L) significantly increased atrial pulse pressure and atrial stroke volume compared with milrinone (30 μmol/L) in perfused beating atria (Figure 6; $n = 6$/group). The PHR0007-induced increase in atrial pulse pressure was time-dependent, and peaked at 12 min of PHR0007 infusion (Figure 6a; $n = 6$), then remained significantly higher than in the control group until the fourth experimental cycle. In contrast, the milrinone-induced increase in atrial pulse pressure peaked at 8 min of milrinone infusion, and then recovered throughout the remainder of the milrinone infusion (Figure 6a; $n = 6$). As such, both atrial pulse pressure and stroke volume were significantly higher in the PHR0007 group compared with the milrinone group in the fourth cycle ($p < 0.001$; Figure 6b).

4. Discussion

The present study showed that PHR0007 significantly increased atrial pulse pressure and atrial stroke

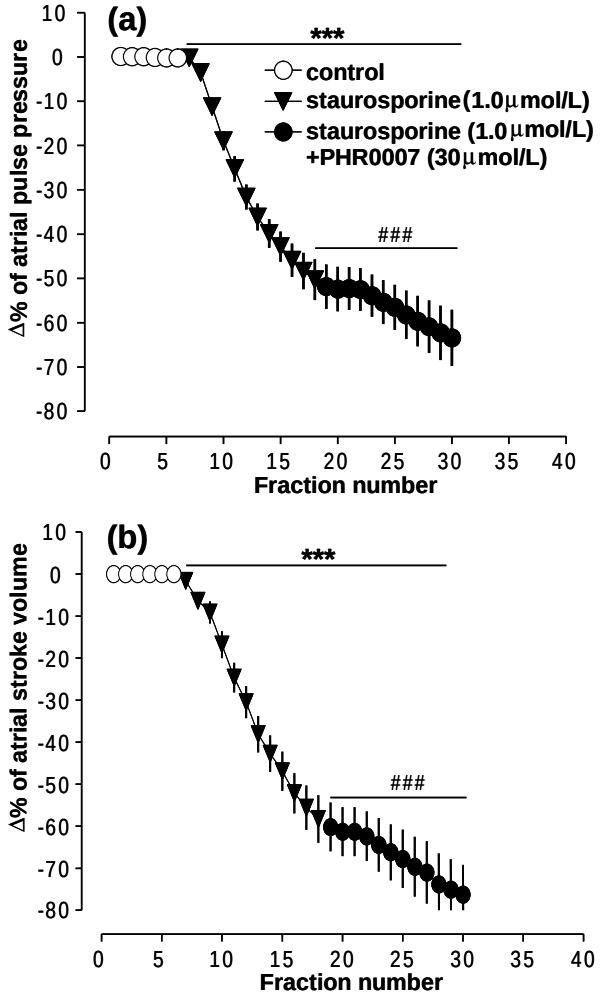

Figure 2. Role of phosphodiesterase (PDE)-cAMP-PKA pathway in the PHR0007-induced increase in atrial pulse pressure and stroke volume. Effects of the non-specific protein kinase inhibitor staurosporine (1.0 μmol/L) on PHR0007-induced atrial pulse pressure (**a**) and atrial stroke volume (**b**). Data are mean ± SEM ($n = 6$). *** $p < 0.001$ compared with the control period. ### $p < 0.001$ compared with staurosporine alone.

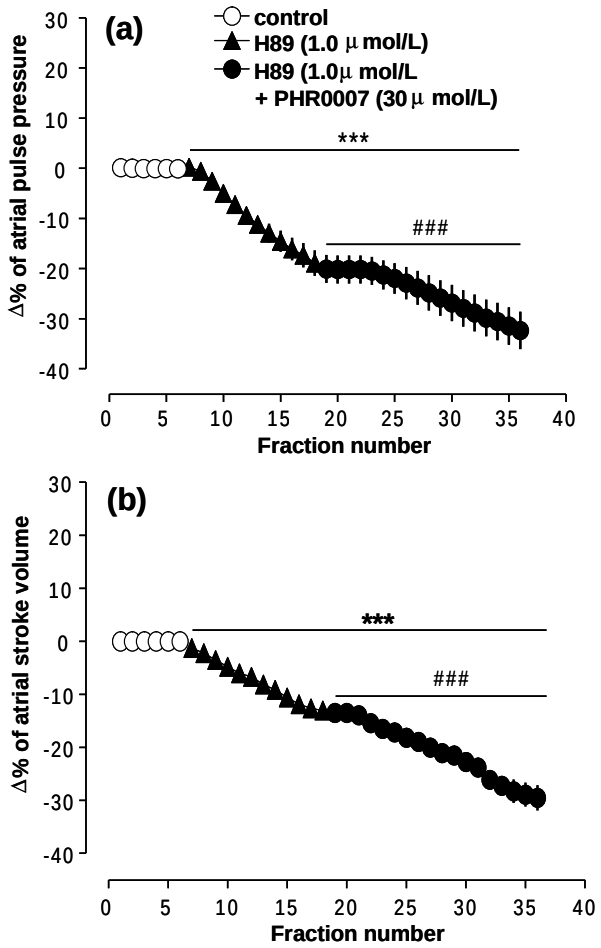

Figure 3. Role of phosphodiesterase (PDE)-cAMP-PKA pathway in the PHR0007-induced increase in atrial pulse pressure and stroke volume. Effects of the cAMP-dependent protein kinase inhibitor H-89 (10 μmol/L) on PHR0007-induced atrial pulse pressure (**a**) and atrial stroke volume (**b**). Data are mean ± SEM ($n = 6$). *** $p < 0.001$ compared with the control period. ### $p < 0.001$ compared with H-89 alone.

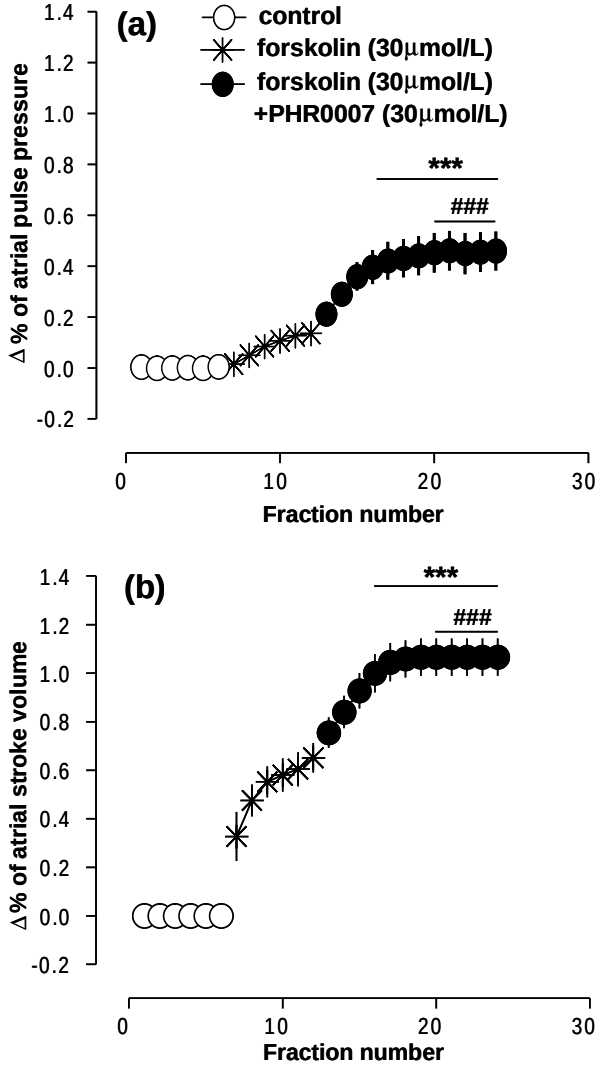

Figure 4. Role of phosphodiesterase (PDE)-cAMP-PKA pathway in the PHR0007-induced increase in atrial pulse pressure and stroke volume. Effects of the adenylyl cyclases (AC) potent activator forskolin (30 μmol/L) on PHR0007-induced atrial pulse pressure (**a**) and atrial stroke volume (**b**). Data are mean ± SEM (n = 6). *** p < 0.001 compared with the control period. ### p < 0.001 compared with forskolin alone.

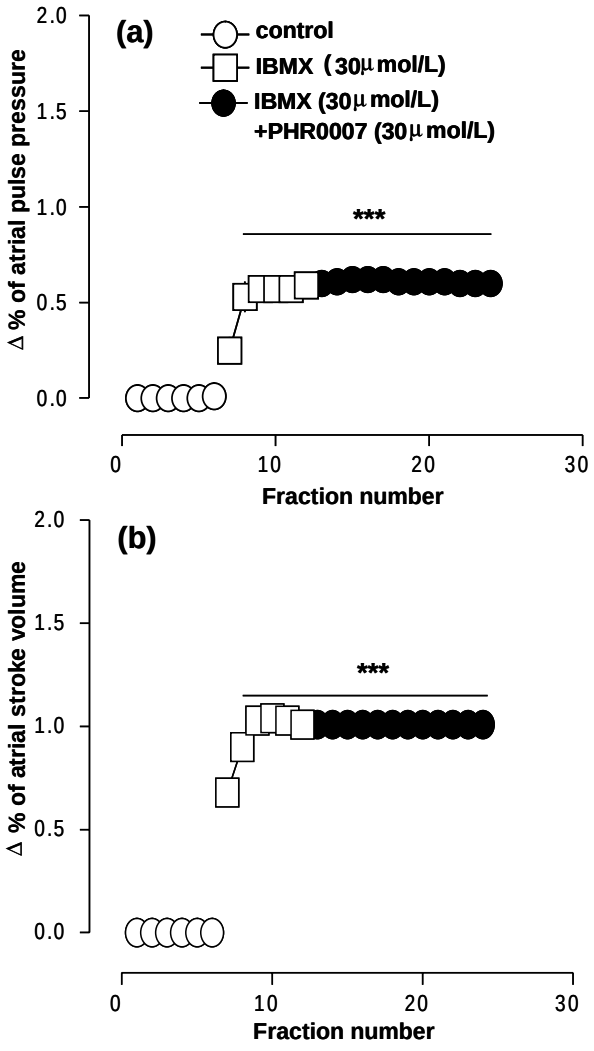

Figure 5. Role of phosphodiesterase (PDE)-cAMP-PKA pathway in the PHR0007-induced increase in atrial pulse pressure and stroke volume. Effects of the potent phosphodiesterase (PDE) inhibitor IBMX (30 μmol/L) on PHR0007-induced atrial pulse pressure (**a**) and atrial stroke volume (**b**). Data are mean ± SEM (n = 6). *** p < 0.001 compared with the control period.

volume, and general inhibition of protein kinases by staurosporine caused a reduction in both atrial pulse pressure and stroke volume that were further reduced using staurosporine plus PHR0007. Furthermore, selective inhibition of PKA by H-89 completely inhibited the PHR0007-induced increase in atrial pulse pressure and stroke volume. Because the cAMP signaling pathway is closely related to the protein kinases A (*8,9*) which increase cardiac contractility in beating atria, we hypothesized that cAMP would be related, *via* protein kinases, to the PHR0007-induced increase in atrial dynamics. Inhibition of protein kinases with staurosporine, or of PKA with H-89 (*10*), both blocked the PHR0007-induced increase in atrial pulse pressure and stroke volume, suggesting that the PHR0007-induced positive inotropic effect is cAMP-protein kinase A (PKA) pathway-dependent.

Growing evidence suggests that multiple spatially, temporally, and functionally distinct pools of cyclic nucleotides exist and regulate cardiac performance, from acute myocardial contractility to chronic gene expression and cardiac structural remodeling. The adenylyl cyclase (AC)-cAMP-PKA pathway has been shown to play an important role in determining the cellular response to outside stimuli (*11,12*). AC activity is inhibited or activated when a cell accepts an external stimulus, resulting in the regulation of intracellular cAMP levels (*13,14*) and the corresponding functional changes in cellular external metabolic signaling (*15, 16*). cAMP is a catalytic agent of PKA acting as a second messenger, which causes the regulation of cell function (*17-19*). Cyclic nucleotide phosphodiesterases (PDEs), by hydrolyzing cAMP and cyclic GMP, regulate the amplitude, duration, and compartmentation

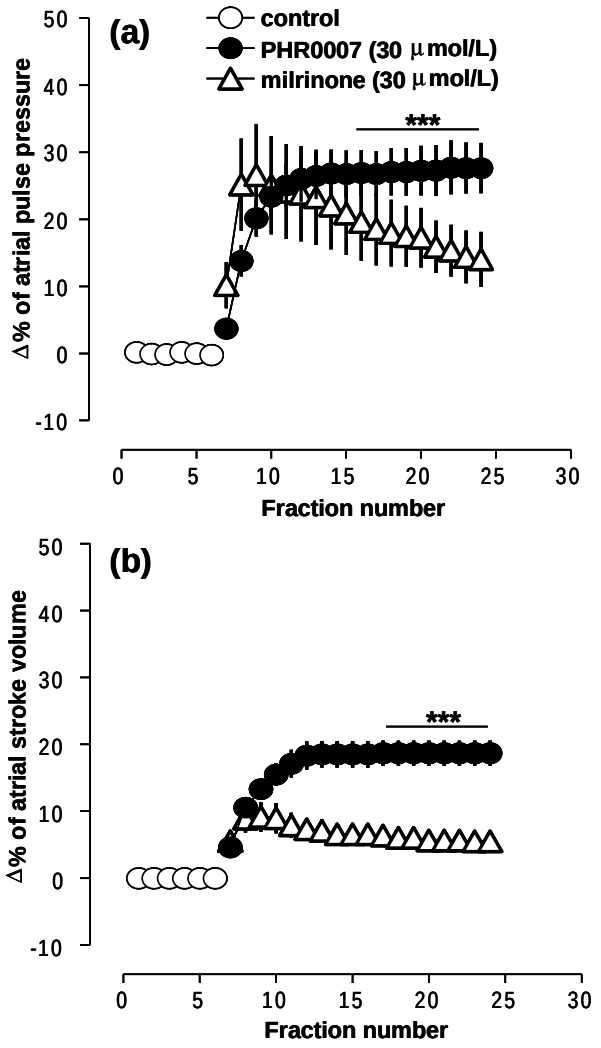

Figure 6. Effect of PHR0007 and milrinone on atrial pulse pressure and stroke volume. Effects of 30 μmol/L PHR0007 on atrial pulse pressure (**a**) and atrial stroke volume (**b**) compared with 30 μmol/L milrinone. Fractions were collected at 2 min intervals. Data are mean ± SEM (n = 6/group). *** $p < 0.001$ compared with milrinone.

of cyclic nucleotide-mediated signaling. In cardiac myocytes, multiple PDE isozymes from at least 5 different families have been described. These include PDE1, PDE2, PDE3, PDE4, and PDE5. In particular, PDE3 enzymes play a major role in regulating cAMP metabolism in the cardiovascular system. PDE3 inhibitors, by raising cAMP content, have acute inotropic and vasodilatory effects in treating congestive heart failure (*20*). Our data indicated that IBMX, a potent phosphordiesterase (PDE) inhibitor, completely blocked the positive inotropic effect of PHR0007 on atrial dynamics, but Forskolin, a potent activator of adenylyl cyclases (AC), had no effect on PHR0007-induced increases in atrial pulse pressure and atrial stroke volume. Therefore, the inotropic effect of PHR0007 is closely related to PDE but not AC.

In the present study, we compared the positive inotropic effect of PHR0007 *versus* milrinone on atrial dynamics in rabbit perfused beating atria. Milrinone is a PDE3 inhibitor known to enhance ventricular (LV) contractility by inhibiting the breakdown of cAMP *via* inhibition of PDE3 (*21*,*22*), and is used for short-term management of acutely decompensated heart failure, chronic hyperemia heart failure, and refractory heart failure. PHR0007 markedly increased both the atrial pulse pressure and stroke volume in beating rabbit atria in a dose-dependent manner. Furthermore, compared with 30 μmol/L milrinone, which itself increased atrial pulse pressure and stroke volume, these effects were significantly prolonged with 30 μmol/L PHR0007. These data suggest that the positive inotropic effect of PHR0007 is dependent on the PDE-cAMP-PKA signaling pathway. However, why did the general inhibition of protein kinases by staurosporine or H-89 cause a reduction in both atrial pulse pressure and stroke volume, that were further reduced using staurosporine or H-89 plus PHR0007. Those facts should be further investigated.

References

1. Alousi AA, Canter JM, Montenaro MJ, Fort DJ, Ferrari RA. Cardiotonic activity of milrinone, a new and potent cardiac bipyridine, on the normal and failing heart of experimental animals. J Cardiovasc Pharmacol. 1983; 5:792-803.
2. Alousi AA, Stankus GP, Stuart JC, Walton LH. Characterization of the cardiotonic effects of milrinone, a new and potent cardiac bipyridine, on isolated tissues from several animal species. J Cardiovasc Pharmacol. 1983; 5:804-811.
3. Sato N, Asai K, Okumura S, Takagi G, Shannon RP, Fujita-Yamaguchi Y, Ishikawa Y, Vatner SF, Vatner DE. Mechanisms of desensitization to a PDE inhibitor (milrinone) in conscious dogs with heart failure. Am J Physiol Heart Circ Physiol. 1999; 276:H1699-H1705.
4. Harada K, Supriatno, Yoshida H, Sato M. Vesnarinone inhibits angiogenesis and tumorigenicity of human oral squamous cell carcinoma cells by suppressing the expression of vascular endothelial growth factor and interleukin-8. Int J Oncol. 2005; 27:1489-1497.
5. Zhang CB, Cui X, Hong L, Quan ZS, Piao HR. Synthesis and positive inotropic activity of *N*-(4,5-dihydro-[1,2,4]triazolo[4,3-a]quinolin-7-yl)-2-(piperazin-1-yl)acetamide derivatives. Bioorg Med Chem Lett. 2008; 18:4606-4609.
6. Cho KW, Kim SH, Kim CH, Seul KH. Mechanical basis of atrial natriuretic peptide secretion in beating atria: Atrial stroke volume and ECF translocation. Am J Physiol. 1995; 268:R1129-R1136.
7. Zhang Y, Liu LP, Liang ZL, Li XL, Jin YZ, Cui X. cAMP produced by pituitary adenylate cyclase-activating polypeptide 27 inhibits atrial natriuretic peptide secretion in rabbit beating atria. Clin Exp pharmacol Physiol. 2008; 35:1233-1237.
8. Bauman AL, Scott JD. Kinase- and phosphatase-anchoring proteins: harnessing the dynamic duo. Nat Cell Biol. 2002; 4:203-206.
9. Fink MA, Zakhary DR, Mackey JA, Desnoyer RW,

Apperson-Hansen C, Damron DS, Bond M. AKAP-mediated targeting of protein kinase a regulates contractility in cardiac myocytes. Circ Res. 2001; 88:291-297.
10. Chijiwa T, Mishima A, Hagiwara M, Sano M, Hayashi K, Inoue T, Naito K, Toshioka T, Hidaka H. Inhibition of forskolin-induced neurite outgrowth and protein phosphorylation by a newly synthesized selective inhibitor of cyclic AMP-dependent protein kinase, *N*-[2-(p-bromocinnamylamino)ethyl]-5-isoquinolinesulfonaide (H-89), of PC12D pheochromocytoma cells. J Biol Chem. 1990; 265:5267-5272.
11. Bismuth G, Theodorou I, Gouy H, Le Gouvello S, Bernard A, Debré P. Cyclic AMP-mediated alteration of the CD2 activation process in human T lymphocytes. Preferential inhibition of the phosphoinositide cycle-related transduction pathway. Eur J Immunol. 1988; 18:1351-1357.
12. Kim DK, Nau GJ, Laucki DW, Dawson G, Fitch FW. Cholera toxin discriminates between murine T lymphocyte proliferation stimulated by activators of protein kinase C and proliferation stimulated by IL-2. Possible role for intracellular cAMP. J Immunol. 1988; 141:3429-3437.
13. Gilmore W, Weiner LP. The effects of pertussis toxin and cholera toxin on mitogen-induced interleukin-2 production: evidence for G protein involvement in signal transduction. Cell Immunol. 1988; 113:235-250.
14. Bourne HR, Lichtenstein LM, Melmon KL, Henney CS, Weinstein Y, Shearer GM. Modulation of inflammation and immunity by cyclic AMP. Science. 1974; l84:19-28.
15. Murray AW, Froscio M, Kemp BE. Histone phosphatase and cyclic nucleotide-stimulated protein kinase from human lymphocytes. Biochem J. 1972; 129:995-1002.
16. Anjard C, Zeng C, Loomis WF, Nellen W. Signal transduction pathways leading to spore differentiation in Dictyostelium discoideum. Dev Biol. 1998; 193:146-155.
17. Aubry L, Firtel R. Integration of signaling networks that regulate Dictyostelium differentiation. Annu Rev Cell Dev Biol. 1999; 15:469-517.
18. Meima M, Schaap P. Dictyostelium development-socializing through cAMP. Semin Cell Dev Biol. 1999; 10:567-576.
19. Yan C, Miller CL, Abe J. Regulation of phosphodiesterase 3 and inducible cAMP early repressor in the heart. Circ Res. 2007; 100:489-501.
20. Onodera S. Pulmonary vasoconstrictor responses. Nihon Kyobu Shikkan Gakkai Zasshi. 1992; 30 suppl:15-25. (in Japanese)
21. Remme WJ, van Hoogenhuyze DC, Kruijssen HA, Pieper PG, Bruggeling WA. Preload-dependent hemodynamic effects of milrinone in moderate heart failure. Cardiology. 1992; 80:609-615.
22. Chen EP, Bittner HB, Davis RD Jr, Van Trigt P 3rd. Milrinone improves pulmonary hemodynamics and right ventricular function in chronic pulmonary hypertension. Ann Thorac Surg. 1997; 63:814-821.

(*Received August 11, 2009; Revised October 27, 2009; Accepted November 2, 2009*)

Original Article

Spicatic acid: A 4-carboxygentisic acid from *Gentiana spicata* extract with potential hepatoprotective activity

Heba Handoussa[1], Natalia Osmanova[2], Nahla Ayoub[3,*], Laila Mahran[4,5,*]

[1] *Department of Pharmaceutical Biology, Faculty of Pharmacy and Biotechnology, German University in Cairo, Egypt;*
[2] *Department of Pharmaceutical Biology, Institute of Pharmacy, Hamburg University, Germany;*
[3] *Department of Pharmacognosy, Faculty of Pharmacy, Ain-Shams University, Cairo, Egypt;*
[4] *Department of Pharmacology and Toxicology, Faculty of Pharmacy and Biotechnology, German University in Cairo, Egypt;*
[5] *Department of Pharmacology and Toxicology, Faculty of Pharmacy, Cairo University, Cairo, Egypt.*

ABSTRACT: Due to our interest in bioactive plant derived materials, the hepatoprotective activity of the aqueous alcoholic extract of *Gentiana spicata* AEGS (Gentianaceae) on carbon tetrachloride treated rats was investigated. CCl_4 used at a concentration of 1 mL/kg.b.wt. significantly increased the levels of alanine aminotransferase (ALT) and aspartate aminotransferase (AST). However, pre-treatment with AEGS and its individual components significantly prevented the increase in these enzymes, which are the major indicators of liver injury. Biochemical assays of liver homogenate showed that AEGS and its components restored reduced glutathione (GSH) depletion reduced the level of thiobarbituric acid reactive substances (TBARS). Furthermore, liver histological observation also showed an obvious amelioration in liver cell necrosis, liver lesions, and fatty changes in pre-treated groups. Phytochemical investigation of the extract showed high phenolic content and led to the isolation and identification of the new carboxygentisic acid, 1,4-dicarboxy 2,5-dihydroxybenzene, for which we suggest the name spicatic acid, together with the known flavonoids, quercetin 3-*O*-[(2,3,4-triacetyl-α-rhamnopyranosyl)1‴→6″] 3-acetyl-β-galactopyranoside and quercetin 3-*O*-[(2,3,4-triacetyl-α-rhamnopyranosyl)1‴→6″]-4-acetyl-β-galactopyranoside, epicatechin, catechin and their gallolyated derivatives. All structures were elucidated on the basis of conventional analytical methods and confirmed by high resolution ESIMS, 1D- and 2D-NMR data. The new phenolic 4-carboxygentisic acid, spicatic acid is of special interest as it represents the first phenolic acid in nature which bears two carboxyl functions in one aromatic ring.

Keywords: *Gentiana spicata*, phenolics, hepatoprotective, 4-carboxygentisic acid, spicatic acid

1. Introduction

Gentiana spicata (Gentianaceae) is common in the tropics and subtropics of both hemispheres in sandy and loamy soils (*1*). It is commonly used as folk medicine for treating stomach disorders, hypertension, renal colic, rheumatic pains, and for elimination of stones from the kidney and the ureters (*2-4*).

Phytochemical studies reported the isolation of a number of metabolites from *Gentiana spicata*, quercetin 3-*O*-[(2,3,4-triacetyl-α-rhamnopyranosyl)-(1→6)]-3,4-diacetyl-β-galactopyranoside (*5*), quercetin 3-*O*-[(2,3,4-triacetyl-α-rhamnopyranosyl)-(1→6)]-β-galactopyranoside, quercetin 3-*O*-[(2,3,4-triacetyl-α-rhamnopyranosyl)1‴→6″]-3 acetyl-β-galacto-pyranoside, and quercetin 3-*O*-[(2,3,4-triacetyl-α-rhamnopyranosyl)1‴→ 6″]-4-acetyl-b-galactopyranoside (*6*), secoiridoid glucosides. sweroside (I), swertiamarin (II) and gentiopicroside (*7*) and alkaloids (*4*).

Liver damage in rats was induced using carbon tetrachloride (*8*) which causes severe xenobiotic-hepatotoxic effects. As it is metabolized in the body to a highly reactive trichloromethyl free radical (CCl_3) it leads to lipid peroxidation. Cell lysis leads to leakage of the two enzymes AST and ALT (*9*), and also depletion of cellular glutathione.

Administration of AEGS and its components (spicatic acid and flavonoids mixture) prior to CCl_4 intoxication has been used as a model to test the

*Address correspondence to:
Dr. Nahla Ayoub, Department of Pharmacognosy, Faculty of Pharmacy, Ain-Shams University, Cairo, Egypt.
e-mail: ayoub.n@link.net

Dr. Laila Mahran, Department of Pharmacology and Toxicology, Faculty of Pharmacy and Biotechnology, German University in Cairo, Egypt.
e-mail: Laila.Mahran@guc.edu.eg

potential preventive role of phytochemicals against acute oxidative stress as flavonoids (*10*), and catechins (*11*) besides spicatic acid, the phenolic compound which resembles salicylic acid (*12*), were reported to protect against liver injury.

The present study was conducted to examine the hepatoprotective activities of the extract, flavonoids and spicatic acid, against CCl_4-induced hepatotoxicity in rats, to evaluate the therapeutic claims of *Gentiana* species in the traditional practice of treating liver disorders.

2. Materials and Methods

2.1. *Instruments and materials*

^{1}H NMR spectra were measured using a Jeol ECA 500 MHz NMR spectrometer 500 MHz NMR spectrometer, at 500 MHz. ^{1}H chemical shifts (δ) were measured in ppm, relative to TMS and ^{13}C NMR chemical shifts to DMSO-d_6 and converted to the TMS scale by adding 39.5. Typical conditions: spectral width 8 kHz for ^{1}H and 30 kHz for ^{13}C, 64 K data points and a flip angle of 45. FTMS spectra were measured on a Finnigan LTQFTMS (Thermo Electron, Bremen, Germany) (Department of Chemistry, Humboldt-Universität zu Berlin). UV recordings were made on a Shimadzu UV-Visible-1601 spectrophotometer. $[a]^{25}D$ were measured on a Kruess polarimeter-8001 (A. Kruess Optronic, Germany). Paper chromatographic analysis was carried out on Whatman No. 1 paper, using solvent systems: (1) H_2O; (2) 6% HOAc; (3) BAW (*n*-BuOH-HOAc-H_2O, 4:1:5, upper layer). Solvent 3 was used for PPC.

2.2. *Plant material, extraction and isolation*

Plant material of *Gentiana spicata* is a wild plant collected from northern Sinai (Arab Republic of Egypt). The authenticity of species was confirmed by Professor Dr.Abdel Salam Mohamed Al-Nowiahi, Professor of Taxonomy, Faculty of Science, Ain-Shams University, Egypt. The aerial parts (1 kg) were exhaustively extracted with distilled water (5 L). The extract was evaporated *in vacuo* at low temperature until dryness followed by ethanolic extraction. The ethanol soluble extract was evaporated *in vacuo* until dryness. The dry residual powder of aqueous ethanolic extract (8 g) was fractionated using column chromatography (60 L × 4.5 ID cm) using Sephadex LH-20 (50 g) as a stationary phase. Elution started with water, and was then followed by water/ethanol mixtures of decreasing polarities. The elution process was monitored with UV light. Eluted fractions were screened using 2-DPC analysis on Whatmann paper No. 1, using BAW for the first direction, followed by 6% AcOH for the second direction. Elution with H_2O led to desorption of fraction **I**. Compound (**1**) was purely isolated (150 mg) through crystallization of the material of fraction **I** from MeOH. Fraction **II** eluted with 50% MeOH was fractionated on precoated silica gel plates developed with EtOAc-HOAc-HCOOH-H_2O (30:0.8:1.2:8) (upperphase); separated bands were eluted with $CHCl_3$-MeOH (85:15) and (80:20) and subjected to repeated column chromatography on Sephadex LH-20 using MeOH as eluent to give (40 mg) pure sample of compound (**2**), and (35 mg) of compound (**3**).

Fraction **III** was applied onto a polyamide S_6 column using methanol: toluene: H_2O (60:38:2) as an eluent which led to desorption of four sub-fractions. Compounds (**4-7**) were isolated as pure sample through preparative PC of the eluted sub-fractions using BAW as eluent. The detected bands from the dried preparative paper chromatograms eluted by ethanol gave pure compounds (**4**) 15 mg, (**5**) 10 mg, (**6**) 45 mg and 30 mg of compound (**7**).

2.3. *Spectral data of the new natural 1,4-dicarboxy 2,5-dihydroxybenzene (spicatic acid), compound (**1**)*

Faint yellow amorphous powder, R_f values (×100): 84 (H_2O), 78 (6% AcOH), 45 (BAW). UV λ_{max} (nm) in MeOH: 222 and 354. UV λ_{max} (nm) in MeOH after acid hydrolysis: 222 and 354. IR (cm^{-1}): 3440, 1705, and 1605 cm^{-1}. ESI/MS m/z = 197.123 $[M-H]^-$. EI/MS m/z = 198. ^{1}H-NMR (DMSO-d_6) δ (ppm): 7.07 (2H, S, H-3 and H-6). ^{13}C-NMR (DMSO-d_6) δ (ppm): 119.46 (dd, ^3J = 7.5 Hz and ^2J = 2.5 Hz, C-1 and C-4), 151.99 (dd, ^3J = 8 Hz and ^2J = 2.2 Hz, C-2 and C-5), 117.36 (d, J = 160 Hz, C-3 and C-6), 170.37 (d, ^3J = 6 Hz, C-7 and C-8).

2.4. *Animals*

Adult male Wistar albino rats, each weighing (200-250 g.) bred at National Scientific Research Center Laboratory, Giza, Egypt, were kept in groups of six per cage under controlled environmental conditions at a temperature of 25 ± 1°C and left for two weeks for acclimatization before use. The rats received standard laboratory chow and water.

2.5. *Chemicals for biochemical assays*

Carbontetrachloride (CCl_4), Ellman's reagent (5,5′-dithio-bis-2-nitrobenzoic acid)(DTNB), Ethylene diamine tetracetic acid disodium salt (EDTA), 1,1′,3,3′-tetramethoxypropane thiobarbituric acid (TBA), and trichloroacetic acid (TCA) were obtained from Sigma-Aldrich (St. Louis, MO, USA). All other chemicals and reagents used were of analytical grade.

2.6. *Biochemical assays*

ALT and AST activities were analyzed according to the method described by Reitman and Frankel (*13*).

In brief, blood samples were first centrifuged at 4,000 rpm at 4°C for 20 min to obtain the serum. The serum collected was then analyzed for ALT and AST activities.

Liver homogenate was prepared in ice cold 0.1 M potassium chloride (KCl), was homogenized with 1.15% potassium chloride to make 10% w/v homogenate, and the supernatant developed after centrifugation was used to determine reduced glutathione (*14*). The other part of this homogenate was centrifuged at 1,000 rpm for 10 min at 4°C and in the formed supernatant; lipid peroxidation was assayed as malondialhyde (MDA) (*15*).

2.7. *Histopathological examination of rat liver*

CCl_4-induced liver necrosis was evaluated using hematoxylin and eosin stain (*16*). After collecting the blood under ether anaesthesia, the rat liver was removed and fixed in 10% formalin. The liver was dehydrated with serial dilutions of alcohol (methyl, ethyl and absolute ethyl), cleared in xylene and embedded in paraffin. Paraffin bees wax tissue blocks were prepared for sectioning at 4 micron thickness. The tissue sections obtained were collected on glass slides, deparaffinized and stained using hematoxylin and eosin stain (*16*) for histopathological examination through the light microscope.

2.8. *Statistical analysis*

Data were expressed as means ± standard deviation. Differences between the studied groups were evaluated using a one-way ANOVA test. A value of $p < 0.05$ was considered as statistically significant (*17*).

2.9. D*etermination of the median lethal dose (LD_{50})*

LD_{50} was determined according to the procedure described by Paumgartten *et al.* (*18*).

3. Results

3.1. *Isolation and structure elucidation*

Following column chromatographic fractionation of the *G. spicata* extract, compounds (**1-7**) were isolated. Conventional and spectral analysis using NMR spectroscopy and mass spectrometry indicated that one of these compounds (**1**) was found to be new natural product (*see Appendix*).

Compound (**1**), isolated as a light yellow amorphous powder, it exhibited in EI-MS, a molecular ion $[M]^+$ at m/z: 198. The characteristic chromatographic properties (yellow spot on PC under UV light) UV absorption data in methanol [λ_{max}: 222 (inflection), 354 nm] and the result of acid hydrolysis the compound was recovered unchanged after being refluxed with 2 N aqueous HCl, 100°C for 3 h which suggested that (**1**) is most probably a phenolic carboxylic acid derivative. The ambiguity of the structure of this new compound was solved using the following aids; IR analysis which showed strong absorptions at 3440, 1705, and 1605 cm^{-1}, consistent with the presence of OH, carboxylic carbonyl and benzenoid C=C groups, respectively. The ^1H NMR spectrum (DMSO-d_6) of (**1**) disclosed a singlet aromatic resonance at δ ppm 7.07.

This result possesses a symmetrical tetra substituted benzene ring such that each of the two symmetrical protonated carbons is connected to a hydroxylate carbon from one side and to a carboxylated carbon on the other side 117.36 (d, J = 160 Hz). The site of attachment of the four substitutions attached to the benzene nucleus of (**1**) has been unraveled by performing de-coupled and ^1H coupled ^{13}C NMR spectral analysis. The spectra revealed the presence of carbon resonances at δ ppm 170.37 (d, ^3J = 6 Hz) attributable to the two carbonyl carbons of the two symmetrical carboxyl groups at C-7 and C-8.

It revealed also a resonance at 151.99 δ ppm (dd, ^3J = 8 Hz and ^2J = 2.2 Hz) assigned to the two symmetrical oxygenated carbons (C-2 and C-5). The two quaternary carbons appeared in this spectrum at δ ppm 119.46 (dd, ^2J = 2.5 Hz and ^3J = 7.5 Hz), while the two symmetrical protonated carbons had a resonance at δ ppm 117.36 (d, J = 160 Hz).

Results showed that AEGS contained 0.27% of 1,4-dicarboxy 2,5-dihydroxybenzene (**1**), for which we suggest the name spicatic acid (Figure 1), in addition to 0.13% of acetylated flavonoids; quercetin 3-*O*-[(2,3,4-triacetyl-α-rhamnopyranosyl)-1‴→6″]-3-acetyl-β-galactopyranoside (**2**) and quercetin 3-*O*-[(2,3,4-triacetyl-α-rhamnopyranosyl)-1‴→6″]-4-acetyl-β-galactopyranoside (**3**) were identified. The isolation and characterization of four known catechins: epicatechin (**4**), catechin (**5**), epigallo-catechin 3-*O*-gallate (**6**), gallocatechin 3-*O*-gallate (**7**) are reported for the first time from this species.

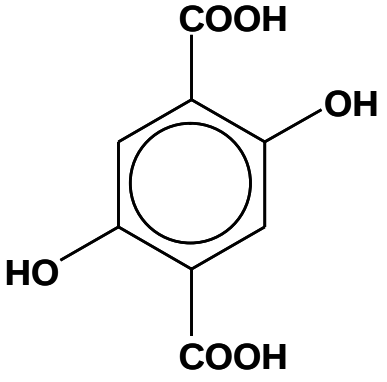

Figure 1. 4-Carboxygentisic acid (Spicatic acid).

3.2. *Evaluation of the biological activity*

3.2.1. *Determination of the median lethal dose (LD_{50})*

The median lethal dose (LD_{50}) of the tested extract was 6.7 g/kg.b.wt.

3.2.2. *Effects of aq. EtOH extracts of G. spicata, its components and silymarin on serum ALT and AST levels in rats subjected to CCl_4 as hepatotoxin*

Intraperitoneal dose of CCl_4 significantly elevated the levels of serum ALT and AST in comparison to the untreated group; 153% and 88.9%, respectively. Pretreatment with either the tested extract; its components (flavonoids mixture and spicatic acid), suppresses the leakage of serum enzyme activities of ALT; with values of 41.6%, 44%, and 46.5% levels, respectively, (Figure 2A) and AST with values of 60.8%, 35.3%, and 38.2%, respectively (Figure 2B). Silymarin as a standard reference resulted in a significant inhibition of cellular leakage of ALT and AST; 55.6% and 41.7%, respectively.

3.2.3. *Effects of aq. EtOH extracts of aerial parts of G. spicata on liver contents of thiobarbaituric acid reactive substances (TBARS) levels in rats subjected to CCl_4*

Administration of CCl_4 led to a significant increase in the levels of tissue lipid peroxidation marker TBARS. The MDA was significantly increased to 155% compared to the untreated group. However, this increase in TBARS was inhibited by pretreatment of rats with the tested extract and its components (flavonoids mixture and spicatic acid) with 57.9%, 68.5%, and 63.5%, respectively comparable to the CCl_4 treated group (Figure 2C). The extract has shown to impart significant hepatoprotective activities by modulation of free radical-induced lipid peroxidation where lipid peroxidation and reactive oxygen species are associated with hepatic injury. That hepatoprotective effect was assured when compared to the reference standard drug silymarin.

3.2.4. *Effects of aq. EtOH extracts of aerial parts of G. spicata on liver contents of reduced glutathione levels in rats subjected to CCl_4*

Hepatic tissue GSH levels were significantly decreased in animals treated with CCl_4 as compared to the untreated group (vehicle-treated) with values equal to 45%. The decreased level of liver GSH was significantly ameliorated by pretreatment of rats with the investigated extract and its components (flavonoids mixture and spicatic acid) with values of 75%, 52.9%, and 64.7%, respectively, compared to the CCl_4 group (Figure 2D).

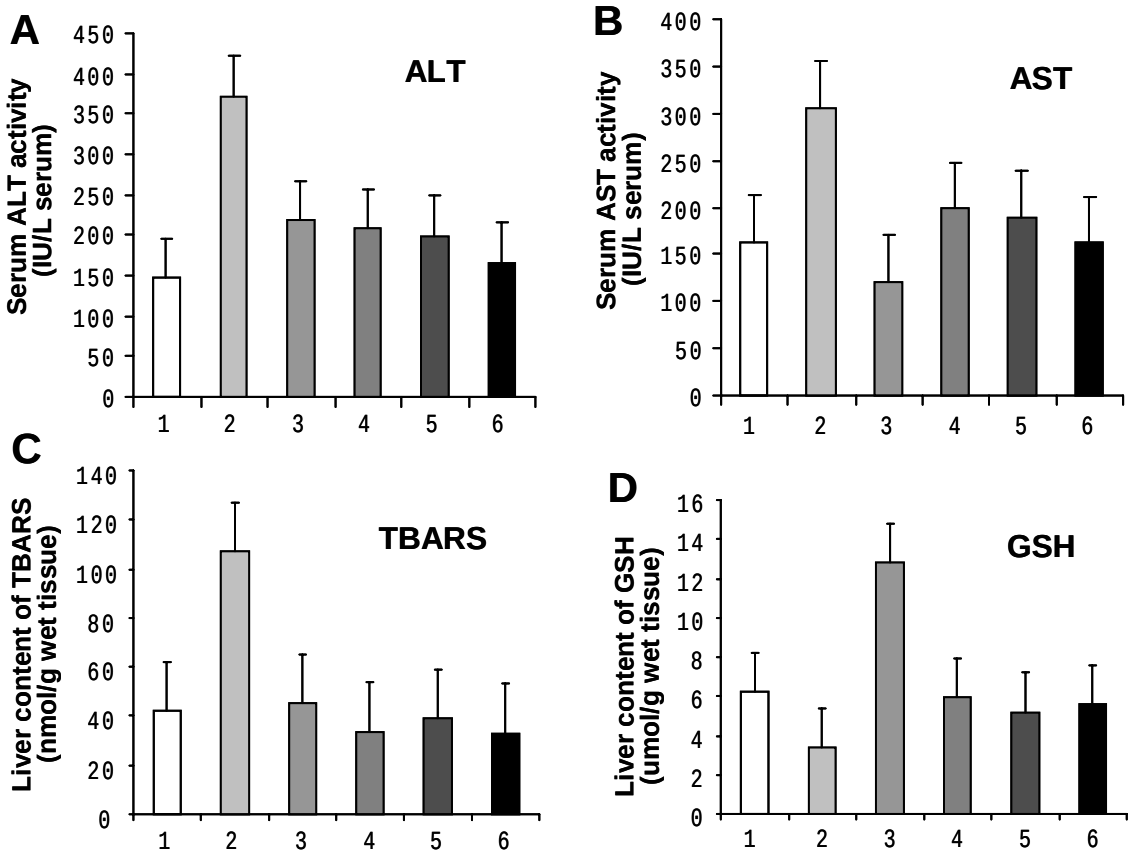

Figure 2. Effect of AEGS and its components on various enzymes in liver homogenate. 1, Untreated animals; **2**, Control animals given only CCl_4; **3-6**, CCl_4 (1 mL/kg)-intoxicated rats intraperitoneally administered for 14 successive days with aqueous ethanolic extract of aerial parts of *Gentiana spicata* (**3**), Flavonoids mixture (**4**), 4-carboxygentisic acid (spicatic acid) (**5**), silymarin (**6**). A, ALT; B, AST; C, TBARS; D, GSH.

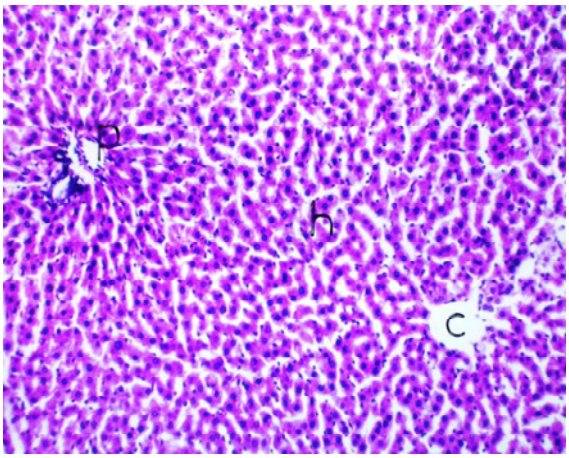

Figure 3. Liver of rat in control group showing the normal histological structure of the central vein (C), Portal area (P) and surrounding hepatocytes (H).

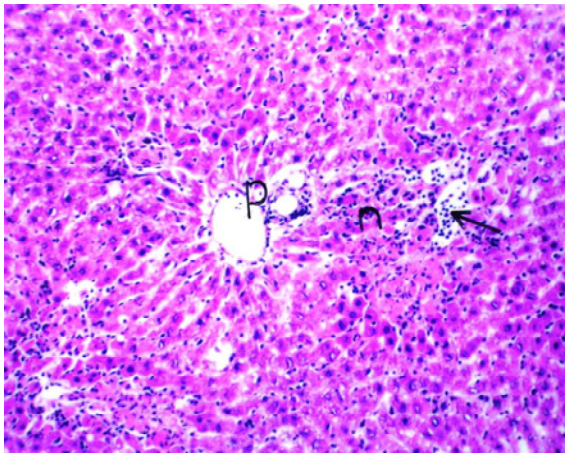

Figure 4. Liver of rat administrated spicatic acid and carbon tetrachloride. The photo shows few focal areas of coagulative necrosis (n) associated with focal inflammatory cells infiltration (arrow).

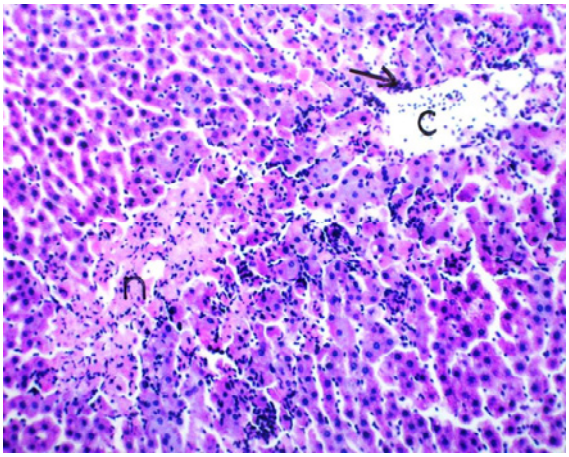

Figure 5. Liver of rat administrated flavonoids mixture and carbon tetrachloride. The photo shows focal cogulative necrosis (n) with inflammatory cells infiltration between the hepatocytes.

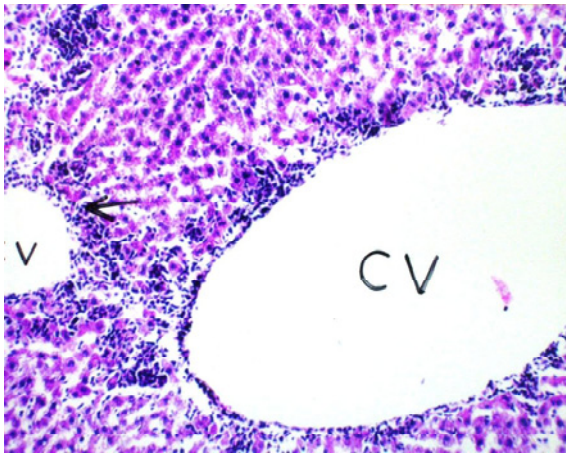

Figure 6. Liver of rat administrated silymarin and carbon tetrachloride. The photo shows massive numbers of inflammatory cells infiltration surrounding the dilated central vein (CV).

3.3. *Histopathological conditions of liver*

Figure 3 shows a representative photomicrograph of the protective effect of AEGS against CCl_4-induced liver injury in rats. Rats treated with normal saline showed no necrosis, inflammation, or vascular degeneration (Figure 3). Rats treated with AEGS and its components (spicatic acid and flavonoids) showed few focal areas of coagulative necrosis with inflammatory cell infiltration in the hepatic tissue with mild tubular dilatation (Figures 4 and 5, respectively), when compared to those treated with only silymarin used as a standard reference (Figure 6). In rats administered CCl_4 alone, focal necrosis was seen with degeneration associated with inflammatory cell infiltration and severe tubular dilation in the central vein (Figure 7) and middle zones prominent with many kupffer cells around the lesions.

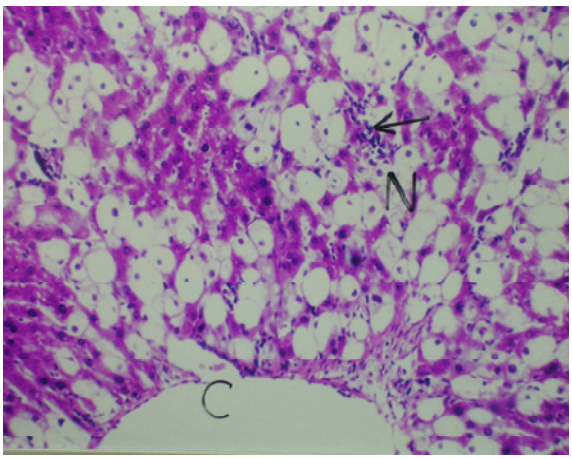

Figure 7. Liver of rat administrated carbon tetrachloride. The photo shows severe dilatation of central vein (C) with necrosis (N) and inflammatory cells infiltration (arrow) in the surrounding hepatocytes.

4. Discussion

A huge effort has been exerted to discover new antioxidants from natural compounds (*19,20*). Complementary and alternative medicine is becoming popular among patients with liver diseases (*21*). Different phenolic compounds used as folk medicine for several centuries have proven to ameliorate some inflammatory aliments as hepatitis in China (*22*).

Serum transferases (ALT and AST) are reliable markers of liver function (*23*). These enzymes are released into the blood as a result of cell membrane damage. The ease of liberation from liver hepatocytes of ALT and AST is considered a very sensitive indicator of necrotic lesions within the liver. Indeed they were significantly increased in control animals given only CCl_4; in group 2, administration of CCl_4 to rats induced severe xenobiotic-hepatotoxic effects. CCl_4 is metabolized in the body to a highly reactive trichloromethyl radical (CCl_3) which is responsible for initiation of a series of complex chain reactions. These reactions result in production of lipid peroxides which attack membrane phospholipids and stimulate lipid peroxidation and cell lysis, a decrease in membrane integrity and a loss in selective permeability (*9*).

In the present study, CCl_4-induced hepatotoxic effects could be attributed to free radical generation noted by an increased MDA level, one of several byproducts of the lipid peroxidation process. The increase in TBARS (MDA) levels in liver suggests enhanced lipid peroxidation leading to tissue damage and failure of antioxidant defense mechanisms to prevent formation of excessive free radicals.

Treatment with the ethanolic extract of *G. spicata* and its components group (3); aqueous ethanolic extract of aerial parts, group (4) flavonoids mixture, and group (5) 4-carboxgentisic (spicatic acid), significantly reversed these changes. Hence it may be possible that the mechanism of hepatoprotection of *G. spicata* is due to its antioxidant activity owing to the presence of polyphenolics contents. It was proven that the decreased MDA level was due to the flavonoids mixture in which it was comparable to silymarin. Flavonoids are known to exhibit a hepatoprotective effect (*24*). Flavonoid compounds were proven to protect against carbon tetrachloride-induced injury (*25*) and that was proven in this study as *Gentiana* is rich in flavonoids.

Glutathione is one of the most abundant biological antioxidants present in liver. It is a non protein cysteine reservoir in the liver and is involved in many cellular processes including the detoxification of endogenous and exogenous compounds. Glutathione is able to protect cellular constituents from the toxic effects of free radicals. This reflects the inability of liver cells to retain intracellular enzymes which indicates severe damage to the plasma membrane. Its functions are concerned with removal of free radical species and cytotoxic active oxygen species including hydrogen peroxide, superoxide radicals, hydroxyl radical, hydrogen peroxide, nitric oxide and alkoxy radicals. It also removes non radical species such as hydrogen peroxide and singlet oxygen and is involved with maintenance of membrane protein thiols and as a substrate for glutathione peroxidase (GPx) (*26*). As long as there is homeostatis between the rate of radical generation and radical dissipation, the cellular generation of free radicals is not considered harmful (*27*). Reactive oxygen radicals are involved in cell growth, differentiation, progression, and death. Therefore, low concentrations of reactive oxygen radicals are considered beneficial and even indispensable in processes such as intracellular signaling and defense against microorganisms. Nevertheless, higher amounts of reactive oxygen radicals contribute to the aging process and many diseases (*28*). Several biological molecules that are involved in cell signaling and gene regulation systems are very sensitive to the redox status of the cell. ROS within cells act as secondary messengers in intracellular signaling cascades. ROS can induce as well cellular senescence and apoptosis and therefore function as anti-tumorigenic species (*29*). Oxidative stress induces a cellular redox imbalance that has been found in various cancer cells when compared to normal ones. The redox imbalance thus may be related to oncogenic stimulation. Oxidative DNA lesions have been noted in many tumors (*29*). Antioxidants induce gene expression of detoxifying enzymes and small molecules that mimic antioxidant enzymes are known to be tools for treatment of many diseases (*30*). Although antioxidants from plant origins have proven to protect against hepatotoxicities, it's not recommended to rely on herbal supplements for routine treatment of any chronic liver disease because of the relative paucity of clinical studies (*21*).

The close resemblance in structure between spicatic acid and salicylic acid might explain its antioxidant effect against the hepatotoxicity of CCl_4. Salicylic acid was proven to inhibit lipooxygenase-catalyzed lipid peroxidation at therapeutic concentrations. These findings suggest possible inhibitory activity against enzymatic lipid peroxidation in clinical settings (*12*). Iron is essential for lipooxygenase activity and salicylic acid is known for its interference with iron. The present investigation is the first to separate the promising antioxidant spicatic acid that proved hepatoprotective and which resembles salicylic acid in its ability to neutralize reactive oxygen species through nonenzymatic mechanisms.

Gentiana spicata contains a mixture of biologically active constituents belonging chemically to flavonoids (*4*) which have antioxidant properties through a radical scavenging mechanism (*31-33*).

The suggested mechanism could also be due to the presence of the isolated catechins (catechin,

epicatechin and their gallate ester derivatives) that act as antioxidants even more than vitamin C (*34*). These catechins isolated from *G. spicata* were similar to the ones extracted from green tea (*35*) and proved to mediate antioxidant and free radical scavenging activities. *Gentiana spicata* is considered to be an excellent antioxidant source, which could contribute to the prevention of many diseases related to oxidative stress.

In conclusion, the results of the present study suggest that the aqueous ethanolic extract (250 mg/kg.b.wt.) of *Gentiana spicata* family Gentianaceae flavonoid mixture and spicatic acid possesses a potential activity to alleviate the hepatotoxic effects associated with CCl_4 administration. This was seen from normalization of serum ALT and AST. Liver MDA activity was highly reduced while liver reduced glutathione was elevated. This indicated a potent hepatoprotective activity against CCl_4-induced free radical species.

References

1. Britton NL, Brown A. An Illustrated Flora of The Northern United States and Canada, Academic Press, New York, USA, 1970; p. 3.
2. Cos P, Ying L, Calomme M, Hu JP, Cimanga K, Van Poel B, Pieters L, Vlietinck AJ, Vanden Berghe D. Structure-activity relationship and classification of flavonoids as inhibitors of xanthine oxidase and superoxide scavengers. J Nat Prod. 1998; 61:71-76.
3. Khafagy SM, Mnajed HK. Phytochemical investigation of Centaurium pulchellum Druce. Acta Pharm Suec. 1970; 7:667-672.
4. Khafagy SM, Mnajed HK. Isolation of a crystalline alkaloid from Centaurium spicatum growing in Egypt. Acta Pharm Suec. 1968; 5:135-142.
5. Shahat AA, Hassan RA, Nazif NM, Miert SV, Pieters L, Hammuda FM, Vlietinck A. Anticomplement and antioxidant activities of new acetylated flavonoid glycosides from Centaurium spicatum. Planta Medica. 2003; 69:1068-1070.
6. Shahat A, Apres S, Van Miert S, Claeys M, Pieters L, Vlietinck AJ. Structure elucidation of three new acetylated flavonoid glycosides from Centaurium spicatum. Res Chem. 2001; 39:625-629.
7. van der Sluis WG, Labadie RP. Secoiridoids and xanthones in the genus Centaurium. Planta Med. 1981; 41:150-160.
8. Klassen CD, Plaa GL. Comparison of the biochemical alteration elicited in liver of rats treated with CCl_4 and $CHCl_3$. Toxic Appl Pharmacol. 1969; 18:2019-2030.
9. Brent JA, Rumack BH. Role of free radicals in toxic hepatic injury II. Clin Toxicol. 1993; 31:173-196.
10. Wu Y, Wang F, Zheng Q, Lu L, Yao H, Zhou C, Wu X, Zhao Y. Hepatoprotective effect of total flavonoids from Laggera alata against carbon tetrachloride-induced injury in primary cultured neonatal rat hepatocytes and in rats with hepatic damage. J Biomed Sci. 2006; 13:569-578.
11. Katiyar S, Elmets CA, Katiyar SK. Green tea and skin cancer photoimmunology angiogenesis and DNA repair. J Nutr Biochem. 2007; 18:287-296.
12. Lapenna D, Ciofani G, Pierdomenico SD, Neri M, Cuccurulla C, Giamberardino MA, Cuccurullo F. Inhibitory activity of salicylic acid on lipooxygenase-dependent lipid peroxidation. Biochim Biophys Acta. 2009; 1790:25-30.
13. Reitman S, Frankel S. A colorimetric method for the determination of serum glutamic oxalacetic and glutamic pyruvic transaminases. Am J Clin Path. 1957; 28:56-63.
14. Ellman GL. Tissue sulfhydryl group. Arch Biochem Biophys. 1959; 82:70-76.
15. Uchiyama M, Mihara M. Determination of malonaldehyde precursor in tissues by thiobarbituric acid test. Anal Biochem. 1978; 86:271-278.
16. Banchroft JD, Stevens A, Turner DR. Theory and practice of histological techniques Fourth Ed., Churchill Livingstone, Philadelphia, PA, USA, 1996; pp. 25-90.
17. Armitage P, Berry G. Statistical methods in medical research. Oxford Blackwell Scientific Publications. 1987; 58:186-200.
18. Paumgartten F, Presgrave O, Menezes A, Fingola F, Freitas C, Carvalho R, Cunha Q. Comparison of five methods for the determination of lethal dose in acute toxicity studies. Braz J Med Biol Res. 1989; 22:987-991.
19. Lodhi G, Singh HK, Pant KK, Hussain Z. Hepatoprotective effects of Calotropis gigantean extract against carbon tetrachloride induced liver injury in rats. Acta Pharm. 2009; 59:89-96.
20. Saito K, Kohno M, Yoshizaki F, Niwano Y. Extensive screening for edible herbal extracts with potent scavenging activity against superoxide anions, Plant Foods Hum Nutr. 2008; 63:65-70.
21. Levy C, Seeff LD, Lindor KD. Use of herbal supplements for chronic liver disease. Clin Gastroenterol Hepatol. 2004; 2:947-956.
22. Wu Y, Yang F, Wu X, Zhou C, Shi S, Mo J, Zhao Y. Hepatoprotective and antioxidative effects of total phenolics from Laggera pterodonta on chemical-induced injury in primary cultured neonatal rat hepatocytes. Food Chem Toxicol. 2007; 45:1349-1355.
23. Friedman LS, Martin P, Mounz SJ. Hepatology. A textbook of liver disease. 3rd WB Saunders London. 1996; 28:791-810.
24. Wegener T, Fintelmann V. Pharmacological properties and therapeutic profile of artichoke (*Cynara scolymus L.*). Wien Med Wochenschr. 1999; 149:241-247. (in German)
25. Wu QX, Li Y, Shi YP. Antioxidant phenolic glucosides from *Gentiana piasezkii*. J Asian Nat Prod Res. 2006; 8:391-396.
26. Prakash J, Gupta SK, Kochupillai V, Singh N, Gupta YK, Joshi S. Chemopreventive activity of Withania somnifera in experimentally induced fibrosarcoma tumors in swiss albino mice. Phytother Res. 2001; 15:240-244.
27. Fujita T, Fujimoto Y. Formation and removal of active oxygen species and lipid peroxidase in biological systems. Nippon Yakurigaku Zasshi. 1992; 99:381-389.
28. Mates JM, Perez-Gomez C, Nunez de Castro I. Antioxidant enzymes and human diseases. Clin Biochem. 1999; 32:595-603.
29. Valko M, Rhodes CJ, Moncol J, Izakovic M, Mazur M. Free radicals, metals and antioxidants in oxidative stress-induced cancer. Chem Biol Interact. 2006; 160:1-40.
30. Mates JM. Effects of antioxidant enzymes in the molecular control of reactive oxygen species toxicology. Toxicology. 2001; 163:219- 221.
31. Yu F, Yu F, Li R, Wang R. Inhibitory effects of the

Gentiana macrophylla (Gentianaceae) extract on rheumatoid arthritis of rats. J Ethnopharmacol. 2008; 116:539-546.
32. Jayaraj R, Deb U, Bhaskar A, Prasad G, Rao P. Hepatoprotective efficacy of certain flavonoids against microcystin induced toxicity in mice. Environ toxicol. 2007; 22:472-479.
33. Awaad AS, Maitland DJ, Soliman GA. Hepatoprotective activity of Schouwia thebica. Bioorg Med Chem Lett. 2006; 16:4624-4628.
34. Mukai K, Mitani S, Ohara K, Nagaoka S. Structure-activity relationship of the tocopherol-regeneration reaction by catechins. Free Radic Biol Med. 2005; 38:1243-1256.
35. Kagaya N, Tagawa Y, Nagashima H, Saijo R, Kawase M, Yagi K. Suppression of cytotoxin-induced cell death in isolated hepatocytes by tea catechins. Eur J Pharmacol. 2002; 450:231-236.

(*Received August 2, 2009; Revised September 8, 2009; Re-revised October 20, 2009; Accepted October 24, 2009*)

Appendix 1

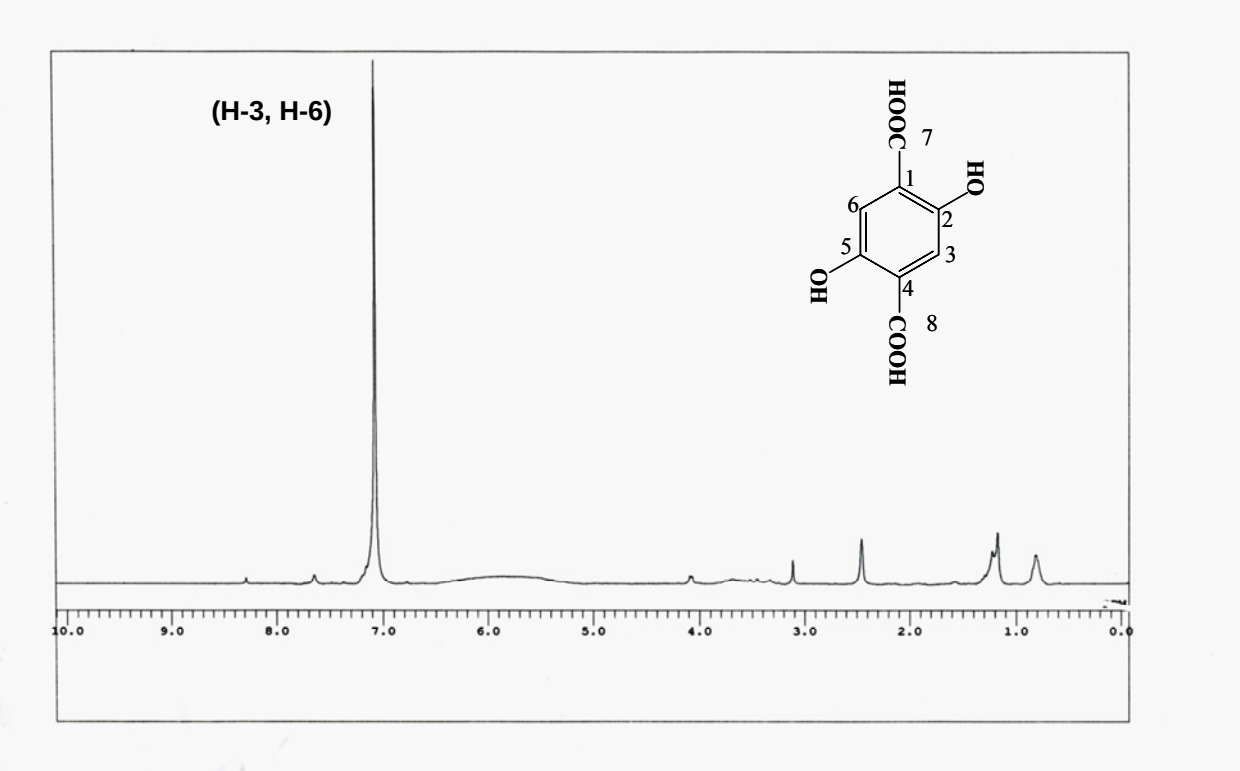

[1]H-NMR of compound (1): 1,4-dicarboxy 2,5-dihydroxy benzene (spicatic acid).

Appendix 2

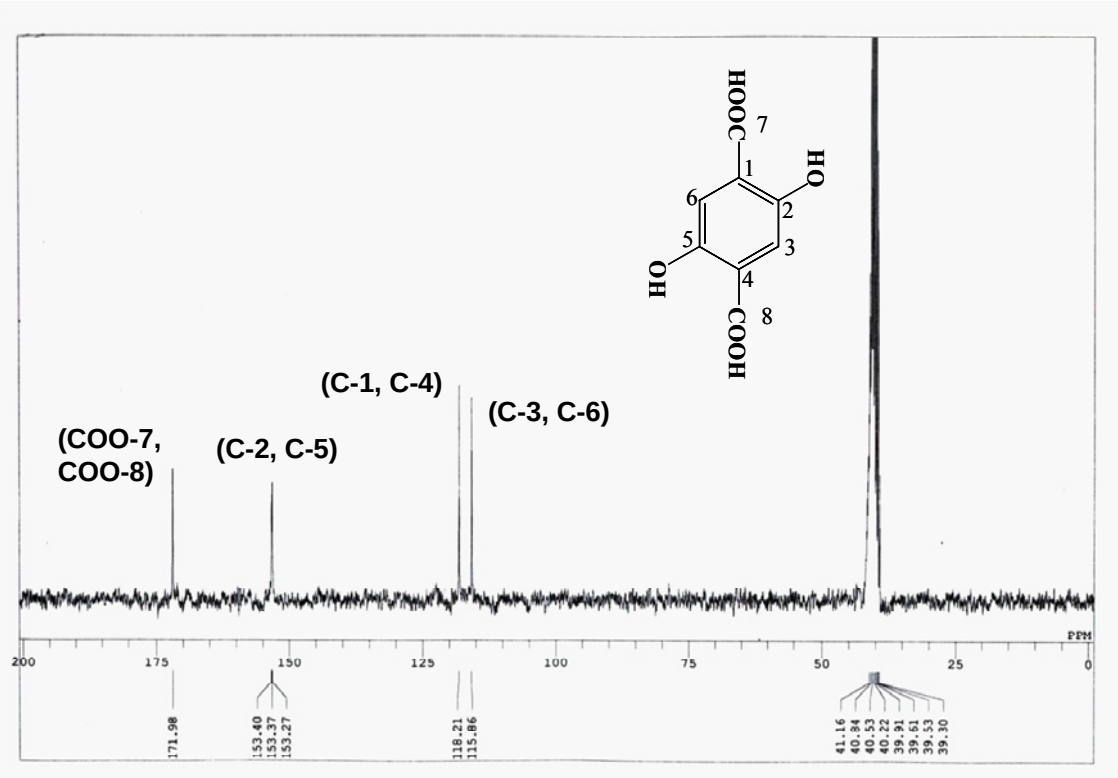

[13]C-NMR of compound (1): 1,4-dicarboxy 2,5-dihydroxy benzene (spicatic acid).

Original Article

Development of implants for sustained release of 5-fluorouracil using low molecular weight biodegradable polymers

Ahmed Fathy A. H. Hanafy[1,*], Adel M. El-Egaky[2], Sana A. M. Mortada[2], Abdulla M. Molokhia[1]

[1] *European Egyptian Pharmaceutical Industries, Alexandria, Egypt;*
[2] *Department of Industrial Pharmacy, Faculty of Pharmacy, University of Alexandria, Alexandria, Egypt.*

ABSTRACT: Anticancer drugs have poor efficacy especially against solid tumors that hinder drug penetration into the tumor. Thus, the dose has to be increased, but toxicity is a limiting factor. Local administration of a polymeric biodegradable poly-L-lactic acid (PLA) and poly(L-lactic acid-co-glycolic acid) copolymer (PLGA) implant containing an anticancer drug may be an acceptable method of concentrating the drug near the tumor site. This work sought to synthesize low molecular weight PLA and PLGA by polycondensation to yield polymers with good physical properties to make them suitable for use in implantable therapy. The synthesized polymers were characterized by determining their molecular weight, melting point, and percentage crystallinity using DSC. Fourier transformation-infra red spectrum (FT-IR), nuclear magnetic resonance (NMR) and specific optical rotation measurement were also used to characterize the synthesized polymers. Morphological characteristics were assessed using scanning electron microscopy (SEM). Implants were manufactured using compression (C) and injection molding (IM) and were loaded with 12 mg 5-fluorouracil (5-FU) per 120 mg implant. *In vitro* release patterns of all implants were assessed in phosphate buffered saline pH 7.4 (PBS 7.4) at 37°C. Factors affecting the release of 5-FU from implants were the polymer species, manufacturing technique, drug particle size, drug concentration, implant dimensions, and coating of the implant. Implants prepared with PLGA had significantly faster release of 5-FU than those prepared with PLA. Those manufactured using compression had significantly faster drug release than those prepared by injection molding. A PLA implant that contained 12 mg 5-FU/120 mg with a diameter of 0.3 cm and that was loaded with a drug particle size smaller than 150 µm and prepared by injection molding and then subsequently coated with PLA had the longest release period of 45 days.

Keywords: Poly-L-lactic acid (PLA), poly(L-lactic acid-co-glycolic acid) copolymer (PLGA), 5-fluorouracil (5-FU), implants, injection molding, compression, dissolution

1. Introduction

In the past decade, research has shown that the lack of sensitivity of most tumors to treatment lies in the inability of drugs to penetrate to the tumor interstitium. The poor efficacy of conventional anticancer drugs can be explained by solid tumors' special structure that includes stromal components that can represent up to 90% of tumor mass, the heterogeneous vasculature within the tumor that isolates tumor cells from the blood supply, and the absence of a well-differentiated lymphatic network. Therefore, a dosage form needed to be able to concentrate the drug close to the tumor site and avoid too wide a distribution (*1*). Local delivery of chemotherapeutic drugs is recognized as a potential method of delivering a drug to the target site with minimal systemic exposure. Because systemic administration of chemotherapeutic drugs can result in severe toxicity, the local delivery of these drugs to pathological tissues may provide an important means of improving both the safety and efficacy of cancer chemotherapy (*2*).

Biodegradable and non-biodegradable polymers are often utilized as implant base materials. Biodegradable polymers, and particularly poly-L-lactic acid (PLA) and poly(L-lactic acid-co-glycolic acid) copolymer (PLGA), disappear from the body during or after drug release and thus are superior in reducing the burden on patients (*3*). To a great extent, polymer synthesis determines the molecular weight, purity, polymeric chain orientation, and the microporous structure and crystallinity of the polymer. The release pattern from biodegradable implants can be controlled by composition, molecular weight of the polymer, morphology, manufacturing

**Address correspondence to:*
Dr. Ahmed Fathy A. H. Hanafy, European Egyptian Pharmaceutical Industries, Alexandria, Egypt.
e-mail: drafathy@gmail.com

technique, and structure of the implant (*4*).

This work sought to synthesize low molecular weight PLA and PLGA by polycondensation to yield polymers with good crystallinity and strength to make them suitable for implantation. Low molecular weight PLA and PLGA polymers were also synthesized in this study to prepare implants with a shorter degradation time in comparison to implants prepared from longer chain analogues as would be better suited to implantation in cancer tissue (*5*). Moreover, the synthesis process is much simpler and less costly, thus allowing preparation of implants on industrial large scale at an acceptable price. The synthesized polymers were used to manufacture implants loaded with a chemotherapeutic agent, 5-fluorouracil (5-FU), to achieve prolonged release *in vitro*. Different variables affecting drug release from implants were also studied to identify the factors that would prolong the drug release over a long period to decrease the frequency of implantation and thus increase patient compliance.

2. Materials and Methods

2.1. *Materials*

L-Lactic acid and glycolic acid were purchased from Merck. 5-FU was purchased from Beckmann Chemikalien KG. Sodium chloride, potassium dihydrogen phosphate, disodium hydrogen phosphate, potassium chloride, and zinc chloride were of analytical reagent grade.

2.2. *PLA and PLGA 50:50 polymer synthesis*

2.2.1. *Synthesis*

Low molecular weight PLA and PLGA 50:50 polymers were synthesized by a modified method of polycondensation (*6,7*) using L-lactic acid and glycolic acid as starting materials. Synthesis involves dehydration of the starting materials L-lactic acid and/or glycolic acid into oligo(L-lactic acid) or oligomer of L-lactic and glycolic acid at 125°C for 2 h and then boosting the polymerization process by adding a catalyst (0.4 wt% zinc chloride relative to the oligomer); the temperature is gradually increased to 180°C and then maintained for 22 h. This is followed by cooling to an intermediate temperature of 130°C and then maintaining this temperature for 2 h; afterwards, the polymer is molded into the required form for easy storage and later use.

2.2.2. *Characterization of synthesized biodegradable polymers*

Synthesized PLA and PLGA 50:50 polymers were characterized first by determining differential scanning calorimetry (DSC) (DSC PerkinElmer Thermal Analysis, USA) thermograms using a heating rate of 10°C/min, and the % crystallinity was calculated from the DSC thermograms. The viscosimetric molecular weights (Mv) for specimens of both PLA and PLGA synthesized polymers were determined from two samples with a Ubbelohde 0 viscosimeter (Ubbelohde viscometer, DC Scientific, USA). Chloroform was used as a solvent and eluent. Mark-Houwink constants k = 5.45×10^{-4} dL/g and a = 0.73 were used in molecular weight calculation (*8*). Fourier transformation infra red (FTIR-8400, Shimadzu, Japan) spectra were also measured. ^{13}C NMR and ^{1}H spectra of the synthesized polymers were recorded by a nuclear magnetic resonance (NMR) spectrometer (Joel NMR, 500 MHz, Japan) using chloroform as a solvent (*7*). Moreover, specific optical rotation, [α], was measured at 20°C for PLA and PLGA 50:50 synthesized polymers in a chloroform solution at a concentration of 0.5 g/dL with a spectropolarimeter (ADP 220, Bellingham + Stanly, Ltd., England) at a wavelength of 589 nm (*9*).

2.3. *Manufacture of implants*

Implants of both PLA and PLGA were prepared by two methods according to formulations in Table 1. Only one lot of PLA and PLGA was used to prepare all of the implants to prevent any possible variability due to polymer synthesis. Injection molding used a specially adapted injection molding instrument

Table 1. Composition of different 5-FU loaded implant formulations

Component (%, w/w)	F1	F2	F3	F4	F5	F6	F7	F8	F9	F10
PLA	90	90	95	80	90		90	89.75	90	90
PLGA 50:50						90				
5-FU (particle size smaller than150 µm)	10		5	20	10	10	10	10	10	10
5-FU (particle size 500-150 µm)		10								
Magnesium stearate								0.25		
Coating with PLA (mg/implant)									100	200
Heating time (min)	10	10	10	10	10	10	180			10
Diameter (cm)	0.3	0.3	0.3	0.3	0.6	0.3		0.6		0.3
Total surface area (cm^2)	1.27	1.27	1.27	1.27	1.7	1.27	1.27	1.32	1.27#	1.27#
Preparation technique	IM	IM	IM	IM	IM	IM	IM	C	IM	IM

IM, injection molding; C, compression, implant weight = 120 mg; #, total surface area for uncoated implant.

capable of producing implants with different diameters (0.3 and 0.6 cm).

The implants were prepared by melting synthesized polymers at 150°C and then adding of 5-FU to the melted polymer in different concentrations (5%, 10%, and 20%) with continuous stirring until complete homogeneity. The melted mixture was poured into the molding instrument and allowed to cool to room temperature; implants were then cut to the required length, corresponding to a weight of 120 mg.

Implants were prepared by compression using an Erweka single punch compression machine fitted with a 6 mm flat punch. The method involved sieving the polymer from a 500 µm sieve and dry mixing the polymer with the specified weight of 5-fluorouracil for 10 min and then blending this mixture with 0.25% magnesium stearate for 5 min. The final mixture was then compressed into disks weighing 120 mg with a hardness of approximately 6 KP.

Implants were coated by dipping them into melted PLA polymer and allowing solidification several times to reach the required coated weight. Solidification of the coat was assisted by a weak stream of nitrogen.

2.4. *In vitro characterization of the prepared implants*

2.4.1. *Drug content*

Three randomly selected implants of each formulation loaded with 5-FU were weighed and their average weight was calculated. The three implants were ground up and the weight equivalent to one implant (120 mg) was collected and sonicated in PBS, pH 7.4, for 15 min; then, its 5-FU content was measured using UV-VIS spectrophotometer (Cary 100 BIO spectrophotometer, Varian, Australia) at 265 nm.

Drug loading content (DLC%) was calculated as follows:

$$\text{DLC (\%)} = \frac{\text{measured amount of 5-Fu}}{\text{implant sample weight}} \times 100$$

2.4.2. *Water absorption and polymer erosion*

After the release test, water absorption and polymer erosion were determined as follows (*3,10*): the implant was taken out of the dissolution media, the excess medium on the surface was removed by brief absorption with filter paper, and the weight of the wet implant (WW) was measured. Then, the wet implant was dried to a constant weight using a vacuum pump, and the weight of the dried implant (WD) was measured. The amount of drug released (WPR-R) was calculated from the results of the *in vitro* release. The weight (WS) of the salts contained in PBS absorbed by the implant was calculated from the salt concentration (1.13%, w/w) and amount of PBS by assuming the density of PBS to be 1. The water absorbed by the implant was determined using the following equation (*3,10*):

$$\text{Water absorbed (\%, w/w)} = 100 \times (WW - WD) / (WD - WS)$$

When the initial polymer amount before the release test was WP0, the polymer erosion from the implant was calculated as follows (*3,10*):

$$\text{Polymer erosion (\%, w/w)} = 100 \times ((120 - WPR\text{-}R) - (WD - WS))/WP0$$

Furthermore, the change in weight of the implants was examined during the incubation of F1, F6, F8, and F10 under the same conditions as for *in vitro* release. At appropriate time intervals, the implants were collected and weighed, and the increase in weight was used as the apparent amount of medium absorption.

2.4.3. *Mechanical properties of 5-FU loaded implants*

The average hardness of implants of different formulations was determined by measuring the hardness of 3 implants for each formulation using a Dr. Schleuniger Pharmatron Tablet Hardness Tester (8 M, Switzerland).

2.4.4. *Scanning electron microscopy (SEM) and porosity measurement*

Changes in the surface morphology of implants before and during *in vitro* release were evaluated by scanning electron microscopy (SEM, Jeol Scanning Electron Microscope, Japan).

The implants were sputter-coated with gold under a vacuum using an electron beam (10 kV). The implant surface was viewed under low (×10.6) and high (×342) magnifications and representative photomicrographs obtained. The pore morphology and pore size distribution of the samples were investigated by SEM at ×1,000 magnification.

2.4.5. *Differential scanning calorimetry and thermal analysis of implants*

To follow implant degradation, implants were analyzed by DSC before release in PBS pH 7.4 and after 1 month of dissolution by observing changes in thermograms. The heating rate was 10°C/min.

2.4.6. *In vitro release of 5-FU from loaded implants*

A release study was performed using a shaking water bath kept at 37°C. The release medium was 20 mL of

phosphate buffer saline (PBS), pH 7.4, contained in a stoppered glass bottle shaken at 30 strokes per min (*10*). Aliquots (10 mL) were taken at predetermined time intervals and were immediately replaced with fresh PBS, pH 7.4. The 5-FU sample content was measured spectrophotometrically at 265 nm.

2.5. *Statistical analysis*

Results of 3 samples for the various tests are presented as mean ± standard deviation (S.D.). One-way analysis of variance (ANOVA) was used to determine significant differences between the formulations with respect to *in vitro* release of 5-FU from F1 implants.

3. Results and Discussion

3.1. *Characterization of synthesized PLA and PLGA 50:50 polymers*

The thermal properties of both synthesized polymers were assessed using differential scanning calorimetry. DSC showed that the synthesized PLA polymer had a glass transition temperature (T_g) of 45°C, a crystallization exotherm at T = 85.5°C, and melting endotherm at T = 133°C. Crystallinity for the polymer was calculated from the following equation (*8*):

$$\text{Crystallinity (\%)} = \frac{\Delta Hm - \Delta Hc}{93.1} \times 100$$

where ΔHm is heat of fusion, ΔHc is heat of crystallization, and the constant 93.1 J/g is the ΔHm for 100% crystalline PLLA or PDLA homopolymers. The % crystallinity for the PLA polymer was 25.1%. According to DSC, PLGA 50:50 had a T_g = 37°C and had no melting or crystallization endotherms, suggesting the amorphous nature of the PLGA copolymer (*10*).

The calculated viscosimetric molecular weight (Mv) was 2,511 g/mol for PLA and 2,455 g/mol for PLGA 50:50.

Figure 1a shows FTIR spectra of the PLA homopolymer with the following absorbance peaks: OH- stretch at approximately 3,500 cm^{-1}, C=O ester at 1,750 cm^{-1}, CH bend at 1,450 and 1,360 cm^{-1}, C-O stretch at 1,130 and 1,090 cm^{-1}, and CH bend at 750 cm^{-1}. These absorbance peaks almost matched those reported (*6*). The FTIR spectra of copolymer PLGA 50:50 were found to be similar to the FTIR spectra of the homopolymer PLA, as shown in Figure 1b (*7*).

The structure of the synthesized PLA polymer was elucidated using ^{13}C NMR spectra. Figures 2a and 2b show the ^{13}C NMR spectra for PLA and PLGA (50:50), respectively. The ^{13}C NMR signals were at 169.8 ppm (C=O), 69 ppm (C-H), and 16.6 (CH_3) for PLA and at 168-170 ppm (C=O), 69 ppm (C-H), 66.6 ppm (CH_2, weak signal), and 16.6 ppm (CH_3) for PLGA (*7*). ^1H NMR spectra for PLA exhibited signals at 1.46 ppm (CH_3) and 5 ppm (C-H). ^1H NMR spectra for PLGA exhibited similar signals at 1.5 ppm (CH_3) and 5.2 ppm with an extra signal at 5 ppm (*7*). The specific optical rotation, [α], for PLA and PLGA 50:50 synthesized polymers was -130 and -94, respectively.

3.2. *In vitro characterization of the prepared implants*

3.2.1. *Drug content*

The different implant formulas listed in Table 1 were analyzed and the drug content results were ± 5% of the labeled amount of 5-FU.

3.2.2. *Water absorption and polymer erosion of 5-FU loaded implants*

The extent of medium absorption and polymer erosion following *in vitro* drug release were compared at different time intervals among several selected formulas. Water absorption, polymer erosion, and the drug release profile were determined to help study the factors that would affect polymer degradation and thus help to formulate implants with prolonged drug release. Such implants would decrease the frequency of implantation and thus increase patient compliance. The results for water absorption and polymer erosion for the selected formulas after 1 month of *in vitro* release in PBS, pH 7.4, are presented in Table 2. Comparison of results for F1 and F6 implants indicated greater water absorption for PLGA implants than PLA implants; such absorption would cause greater polymer degradation and erosion, and substantial physical changes were visually apparent. Results for F8 indicated water absorption slightly less than for F1, revealing that F8 had greater polymer erosion than F1. These results show that compression (F8) can cause faster polymer erosion in comparison to injection molding. Comparing implant results (F1 and F10) indicated that coating an injection-molded PLA implant with PLA substantially reduced water absorption and polymer erosion. This great reduction in water absorption can have a positive effect on prolonging drug release and retarding polymer degradation (*3,10*).

3.2.3. *Mechanical properties of 5-FU loaded implants*

Hardness results for selected implant formulas are presented in Table 3. The PLA (F1) and PLGA (F6) implants have nearly the same hardness. Increasing implant diameter to 0.6 cm (F5) instead of 0.3 cm for the PLA implant (F1) caused a slight increase in hardness to 2.9 KP. Implants manufactured using compression (F8) were much harder than those manufactured using injection molding (F1). Coating

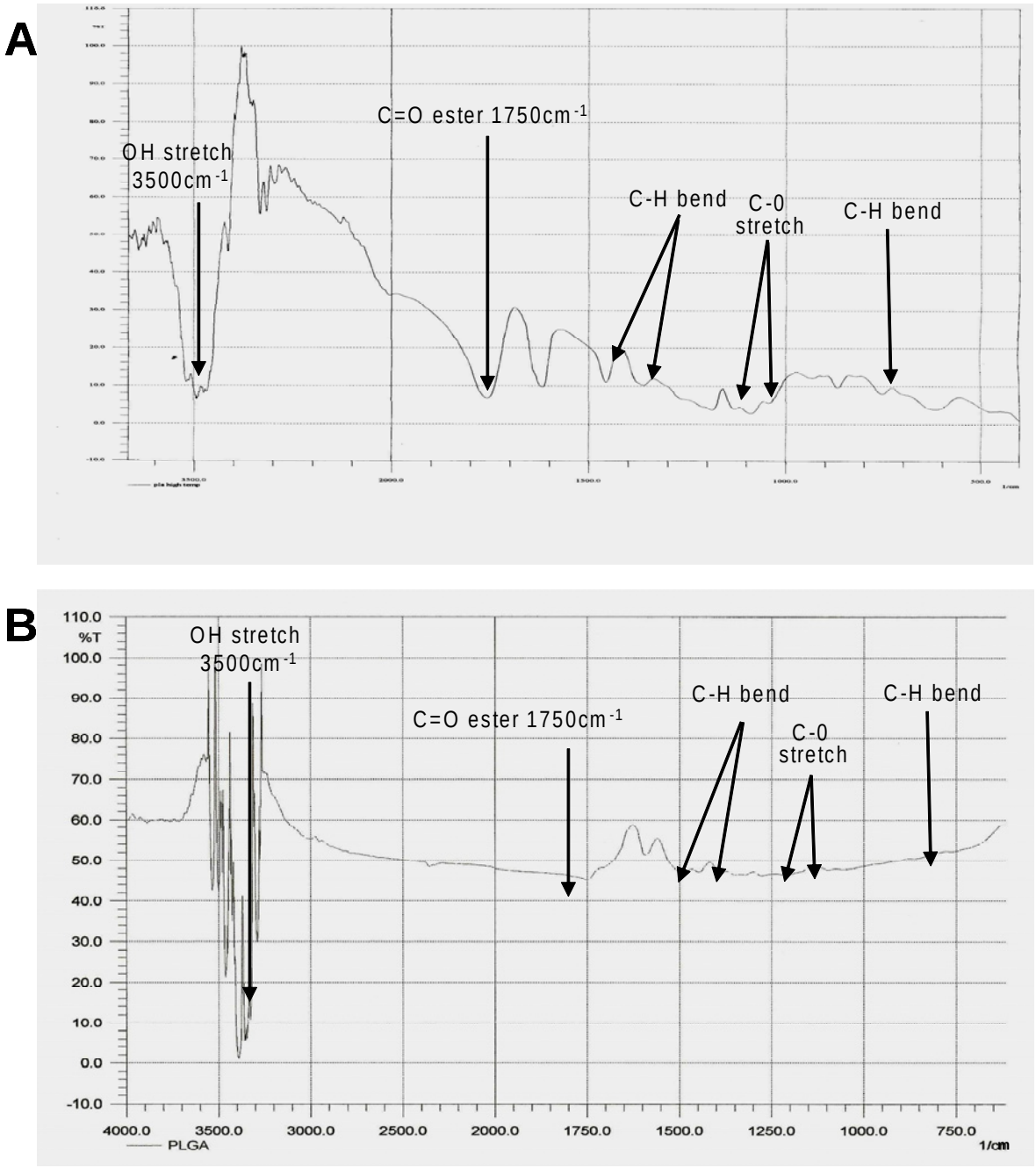

Figure 1. FTIR spectra for synthesized PLA (A) and PLGA 50:50 (B).

the implant (F10) also caused implant hardness to increase to 4 KP. Harder implants are better suited to the handling and insertion process.

3.2.4. *Scanning electron microscopy (SEM) and porosity measurement*

Porosity measurement using SEM was done one month after placing implants in PBS, pH 7.4 (*12*). Figure 3 shows that the manufacturing technique and particle size of loaded 5-FU had a substantial effect on implant pore size. Implants manufactured using compression (F8) and loaded with 5-FU with a smaller particle size had greater porosity (10-50 μm), while injection-molded (IM) implants loaded with 5-FU with the same particle size (F1) had less porosity (5 μm). Increasing the particle size of loaded 5-FU for IM implants (F2) resulted in increased porosity (10-30 μm). The IM technique produced implants with a condensed structure and lower porosity. Increasing the particle size of the loaded drug increased the porosity of implants due to pores left by the dissolved drug particles.

3.2.5. *Differential scanning calorimetry (DSC) and thermal analysis of implants*

DSC thermal analysis of implants was performed to follow polymer degradation during the release period.

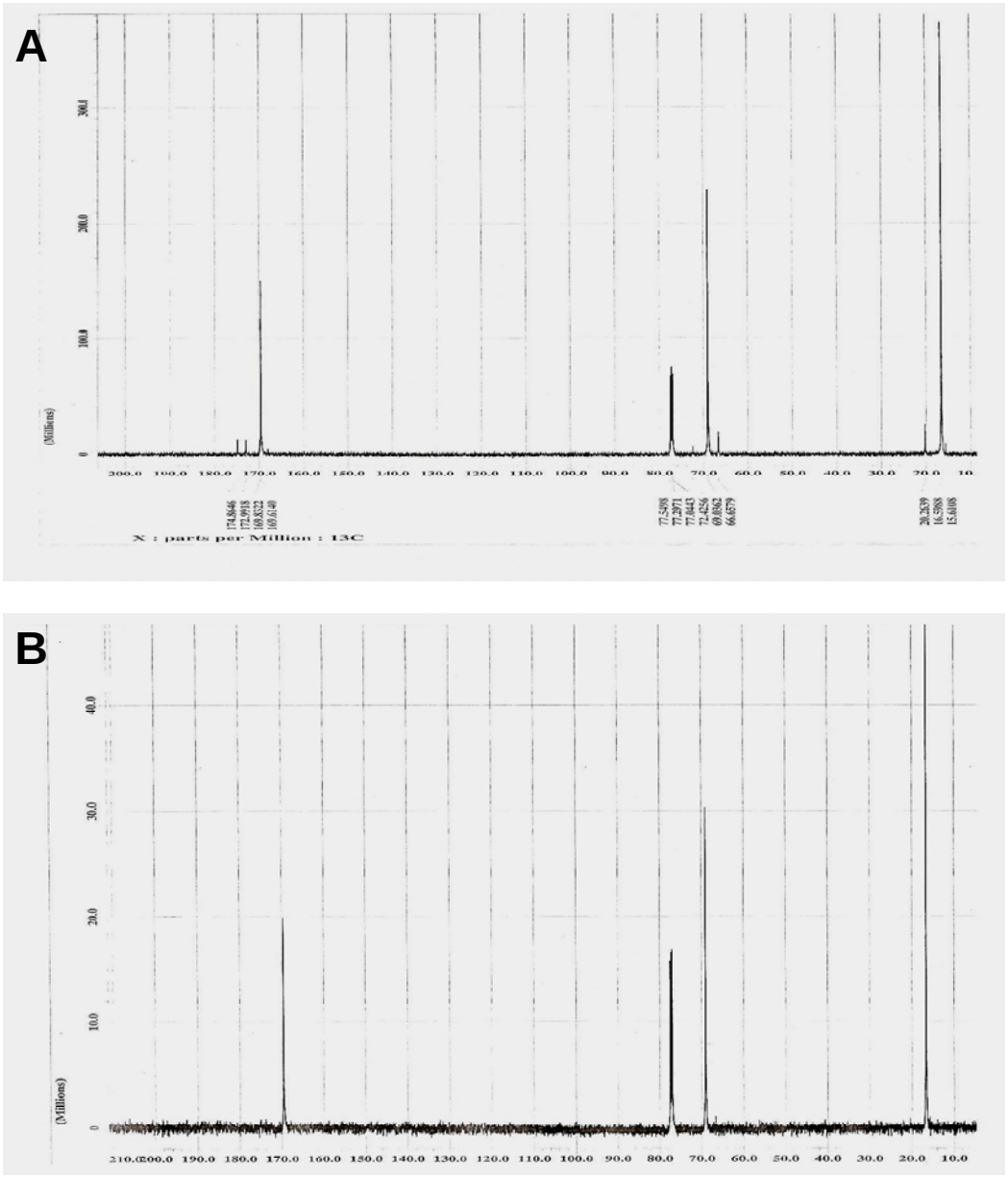

Figure 2. ^{13}C NMR for synthesized PLA (A) and PLGA 50:50 (B).

Table 2. Effect of polymer type and manufacturing technique on water absorption and polymer erosion

Implant formula (PT/MT)	*Water absorption (%, W/W)	*Polymer erosion (%, W/W)
F1 (PLA/IM)	81.9	14.7
F6 (PLGA/IM)	125.5	15.6
F8 (PLA/C)	78.2	19.8
F10 (PLA/IM+CT)	42	1

*: Water absorption and polymer erosion results 1 month after placement of implants in PBS, pH 7.4; PT: polymer type, MT: manufacturing technique; C: compression; CT: coating.

Table 3. Effect of polymer type and manufacturing technique on implant hardness

Implant formula (PT/MT)	Hardness (KP)
F1 (PLA/IM)	2.4
F5 (PLA/IM+ID)	2.9
F6 (PLGA/IM)	2.3
F8 (PLA/C)	6.1
F10 (PLA/IM+CT)	4

PT: polymer type; MT: manufacturing technique; C: compression; CT: coating; ID: increasing diameter.

PLA implants F1, F8, and F10 had a T_g of 40-45°C, recrystallization temperature (T_c) of 80-86°C, and melting temperature (T_m) of 120-133°C before placement in PBS, pH 7.4. After placement in PBS for one month, F1 and F8 had undetectable T_g and T_c and T_m of 80-90°C while F10 had a T_m of 114°C, which may indicate that implant coating decreased degradation of the implant as gauged by the shift in T_m of the PLA polymer (*2*,*8*). In DSC thermograms for PLGA implants (F6), no peaks were detected as a result of the amorphous nature of PLGA

(*11*). Thus, changes before and after implants were placed in PBS, pH 7.4, could not be studied.

3.2.6. *In vitro release of 5-FU by loaded implants*

Different implant formulas were assessed for drug release in PBS, pH 7.4, at 37°C. The release period of 5-FU was prolonged to approximately 45 days for some formulas. Drug particle size, implant surface area, and increasing heating time of drug-polymer dispersion did not produce significant changes in the *in vitro* release of 5-FU from implants. In contrast, polymer type, manufacturing technique, and implant coating had a marked effect on drug release. Figure 4 shows significantly faster release of 5-FU from PLGA implants (F6) than PLA implants (F1) ($p < 0.05$). This can be attributed to the amorphous nature of PLGA, as confirmed by DSC, that causes its faster degradation (*9*). Figure 5 illustrates the effect of the manufacturing technique on drug release of PLA implants prepared by injection molding and compression. A significantly faster release ($p < 0.05$) was noted from implants prepared by compression (F8) in comparison to those prepared by injection molding (F1) with almost the same surface area, although the latter (F8) had greater hardness than the former (F1) (Table 3). Increasing the 5-FU concentration per implant from 5% to 10% to 20% caused a significantly faster release ($p < 0.05$) due to the increase in matrix perforations by drug dissolution (*2*). Figure 6 shows that the release rate 5-FU was significantly reduced ($p < 0.05$) by coating the implants with PLA, and as the coat weight per implant increased, the retardation of the release rate increased.

These results can be explained using SEM pictures of different implants before and after they were placed in PBS pH 7.4 for one month. Figures 7 and 8 are SEM

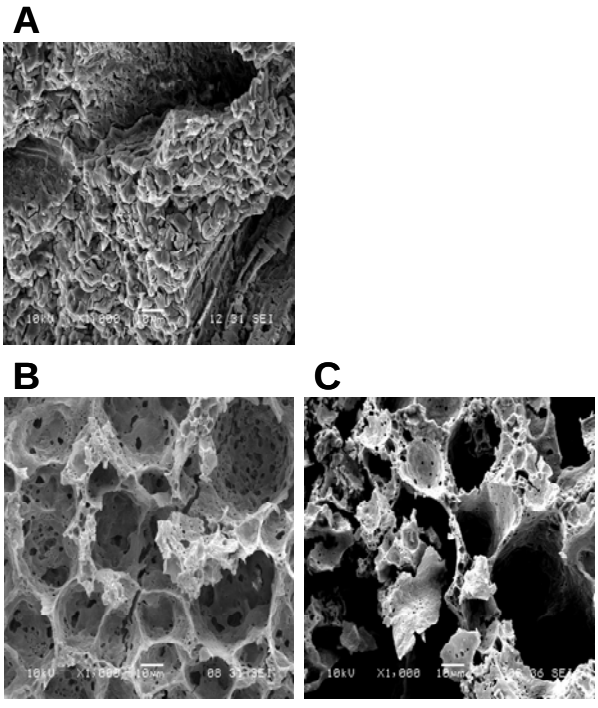

Figure 3. Effect of manufacturing technique on surface porosity of 5-FU loaded implants. (**A**) SEM picture of a PLA implant prepared by injection molding (F1). (**B**) SEM picture of a PLA implant prepared by injection molding (F2). (**C**) SEM picture of a PLA implant prepared by compression (F8).

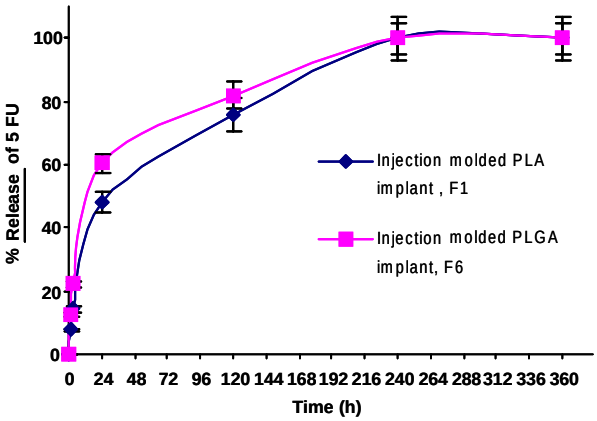

Figure 4. Effects of polymer type on 5-FU release from implants in PBS pH 7.4.

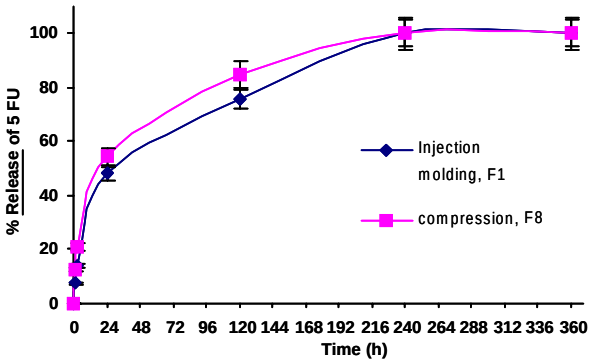

Figure 5. Effects of manufacturing technique on 5-FU release from PLA mplants in PBS pH 7.4.

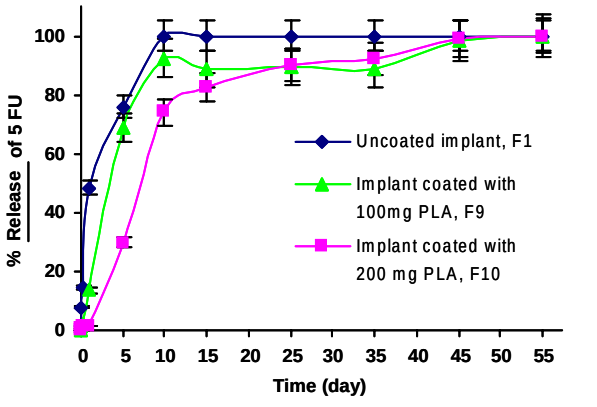

Figure 6. Effects of coating weight per implant on 5-FU release from coated PLA injection-molded implants in PBS pH 7.4.

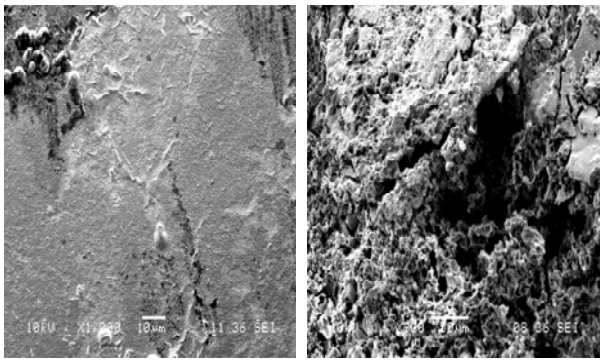

Figure 7. SEM picture of a PLA compressed implant loaded with 5-FU (F8) before and after placement in PBS, pH 7.4.

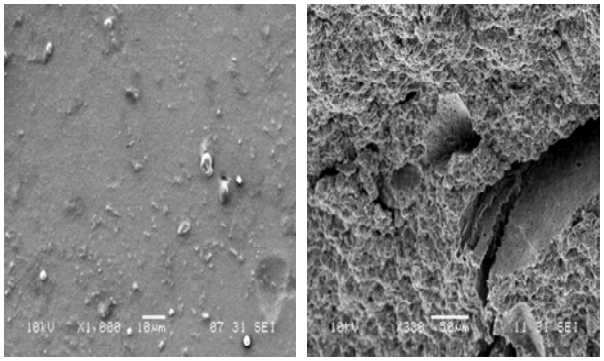

Figure 8. SEM picture of a PLA injection-molded implant loaded with 5-FU (F1) before and after placement in PBS, pH 7.4.

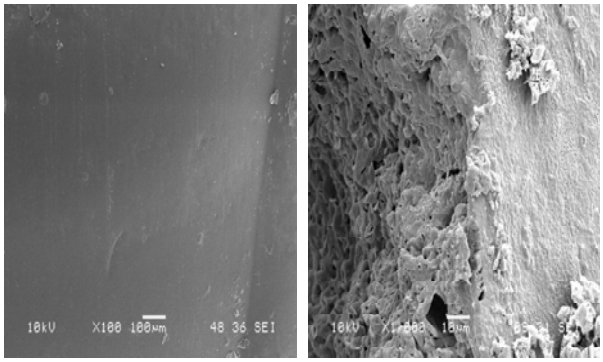

Figure 9. SEM picture of a PLA injection-molded implant loaded with 5-FU coated with 200 mg of PLA before and after placement in PBS, pH 7.4.

pictures of PLA implants prepared by compression and injection molding, respectively. While the surface of implants was smooth and non-porous at the beginning, SEM pictures of compressed implants revealed numerous microscopic perforations in comparison to injection molded implants one month after implants were placed in PBS, pH 7.4. This resulted in a spongy structure that caused an increase in polymer erosion and degradation (Table 2) and led to faster drug release from compressed implants than injection molded implants (*4*).

Coating implants with PLA caused a reduction in surface perforations (Figure 9), which helped to suppress the early release of hydrophilic drugs (*13*) like 5-FU, and reduced diffusion of water into the implant (Table 2). Implants coated with 100 mg per implant of PLA showed 90% of drug release after 10 days. When the coat weight was increased to 200 mg per implant, in contrast, the release of 90% of the drug took about 25 days. This coating process also caused the release period of 5-FU to be prolonged from 10 days to 45 days. The burst release (release after 1 day) of 5-FU was significantly reduced, causing a decrease in 5-FU release from 50% to only 2% ($p < 0.05$). The drug release mechanism of implants F9 and F10 is more complicated than that of others like F1 (*13*). This could be attributed to the change in the polymeric delivery system from a matrix type in uncoated tablets to a combination of a matrix and reservoir type in coated implants.

4. Conclusion

Synthesized polymers PLA and PLGA 50:50 prepared by polycondensation can be used successfully to prepare implants for use as a drug delivery system *via* injection molding and compression. Implants prepared from PLGA 50:50 had significantly faster release ($p < 0.05$) of 5-FU than those prepared with PLA. Implants manufactured using compression had significantly faster drug release ($p < 0.05$) than those prepared by injection molding. Coating an implant with PLA by dipping caused a significant reduction in burst release and a prolonged release period. An injected molded implant with PLA containing 12 mg of 5-FU with a particle size of less than 150 μm in 120 mg of implant that was then coated with 200 mg PLA had prolonged release for 45 days. The *in vitro* study will be expanded with an *in vivo* study on rats with induced liver cancer to further study *in vivo* release and the correlation with release *in vivo* and *in vitro*.

Acknowledgments

The authors would like to thank the European Egyptian Pharmaceutical Co. (Pharco Corporation) for their support and Prof. Dr. Mona Marie, head of the Tissue Engineering Department, Faculty of Dentistry, Alexandria University, for access to the scanning electron microscope at her facility.

References

1. Dubernet C, Fattal E, Couvreur P. Nanoparticulate controlled release systems for cancer therapy. In: Handbook of Extended Release, chapter 14 (eds). Publisher, USA, 2000; pp. 287-300.
2. Gao H, Gu Y, Ping Q. The implantable 5-fluorouracil-

loaded poly(L-lactic acid) fibers prepared by wet-spinning from suspension. J Control Release. 2007; 118:325-332.
3. Takahashi M, Onishi H, Machida Y. Development of implant tablet for a week-long sustained release. J Control Release. 2004; 100:63-74.
4. Rothen-Weinhold A, Besseghir K, Vuaridel E, Sublet E, Oudry N, Kubel F, Gurny R. Injection-molding *versus* extrusion as manufacturing technique for the preparation of biodegradable implants. Eur J Pharm Biopharm. 1999; 48:113-121.
5. Peltonen L, Koistinen P, Karjalainen M, Hakkinen A, Hirvonen J. The effect of cosolvents on the formulation of nanoparticles from low-molecular weight poly(l)lactide. AAPS PharmSciTech. 2002; 3:E32.
6. Moona SI, Leeb CW, Taniguchia I, Miyamotoa M, Kimuraa Y. Melt/solid polycondensation of l-lactic acid: an alternative route to poly(l-lactic acid) with high molecular weight. Polymer. 2001; 42:5059-5062.
7. Kiremitci-gumusderelioglu M, Deniz G. Synthesis, characterization and *in vitro* degradation of Poly(DL-lactide/poly(DL-lactide-co-Glycolide) films. Turk J Chem. 1999; 23:153-161.
8. Lim L-T, Auras R, Rubino M. Processing technologies for poly(lactic acid). Prog Polym Sci. 2008; 33:820-852.
9. Hyon S, Jamshidi K, Ikada Y. Synthesis of polylactides with different molecular weight. Biomaterials. 1997; 18:1503-1508.
10. Baro M, Sa´nchez E, Delgado A, Pererac A, Vora C. *In vitro-in vivo* characterization of gentamicin bone implants. J Control Release. 2002; 83:353-364.
11. Jain RA. The manufacturing techniques of various drug loaded biodegradable poly(lactide-co-glycolide) (PLGA) devices. Biomaterials. 2000; 21:2475-2490.
12. Kundu B, Sinha MK, Mitra MK, Basu D. Fabrication and characterization of porous hydroxyapatite ocular implant followed by an *in vivo* study in dogs. Bull Mater Sci. 2004; 27:133-140.
13. Gopferich A. Bioerodible implants with programmable drug release. J Control Release. 1997; 44:271-281.

(*Received July 16, 2009; Revised October 14, 2009; Accepted October 22, 2009*)

Original Article

Thymoquinone triggers anti-apoptotic signaling targeting death ligand and apoptotic regulators in a model of hepatic ischemia reperfusion injury

Ragwa M. Abd El-Ghany[1], Nadia M. Sharaf[1], Lobna A. Kassem[2,3], Laila G. Mahran[1,4], Ola A. Heikal[1,5,*]

[1] *Department of Pharmacology & Toxicology, Faculty of Pharmacy & Biotechnology, German University in Cairo, Cairo, Egypt;*
[2] *Department of Physiology, Faculty of Pharmacy & Biotechnology, German University in Cairo, Cairo, Egypt;*
[3] *Faculty of Medicine, Cairo University, Cairo, Egypt;*
[4] *Faculty of Pharmacy, Cairo University, Cairo, Egypt;*
[5] *Narcotics, Ergogenics & Poisons Department, National Research Center, Giza, Egypt.*

ABSTRACT: Thymoquinone (TQ) has been reported as a potent inducer of apoptosis in cancer cells. However, the role of TQ as an apoptotic or antiapoptotic has not been established yet in other types of cell injuries. Our objective was to explore whether TQ exerts a hepatoprotective effect against hepatic ischemia reperfusion injury (I/R) and to identify its potential effect on apoptotic pathways. Rats were divided into eight groups: group I: sham-operated; group II: I/R (45 min ischemia-60 min reperfusion). The other six groups were given PO administration of TQ aqueous solution at 5, 20, and 50 mg/kg/day dose levels for 10 days. At the end of treatment three groups were not subjected to any intervention (groups III, IV, and V: TQ control groups) or subjected to 45 min ischemia followed by one-hour reperfusion as in group II (groups VI, VII, and VIII: TQ pretreated I/R groups). Serum levels of liver enzymes, tissue levels of malondialdehyde (MDA), reduced glutathione (GSH) and TNF-α were measured. Activities of caspases 8, 9, and 3 were determined. Cytochrome c in cytosol was determined by solid phase ELISA. Expression of anti-apoptotic Bcl-2 and pro-apoptotic Bax proteins as well as nuclear factor κB (NF-κB) were assessed using polymerase chain reaction. Apoptosis end point was detected using electrophoresis for analysis of DNA fragmentation. TQ administration before I/R resulted in a significant decrease in liver enzymes, MDA and TNF-α tissue levels with increased GSH content. It also inhibited cytochrome c release into the cytosol, down regulated the expression of NF-κB and Bax and up regulated the Bcl-2 proteins. Hepatic apoptosis was significantly attenuated as indicated by a significant decrease in all caspase activities and by DNA fragmentation. In conclusion, TQ exerts an antiapoptotic effect through attenuating oxidative stress and inhibiting TNF-α induced NF-κB activation. Furthermore, it regulates the Bcl-2/Bax ratio and inhibits downstream caspases in this I/R model.

Keywords: Thymoquinone (TQ), liver enzymes, malondialdehyde, reduced glutathione, caspases activities, cytochrome c, TNF-α, Bcl-2, Bax and NF-κB proteins expression, DNA fragmentation

1. Introduction

Recent evidence that apoptosis of hepatocytes is a feature in a wide variety of liver diseases including viral hepatitis, hepatocellular carcinoma and autoimmune diseases, has raised hopes that inhibition of apoptosis provides a new target for treatment of liver diseases (*1*).

Apoptosis or programmed cell death can be induced through the death receptor-dependent pathway or the mitochondrial-dependent pathway. The former pathway is initiated in the liver by death ligands like TNF and Fas ligands following binding to their relevant death receptors. This leads to caspase 8 activation with subsequent activation of down stream caspases such as caspase 3 (*2*). In contrast, the latter pathway is triggered by a variety of intracellular stressors such as DNA damage and hypoxic conditions. These stimuli cause the release of cytochrome c from mitochondria into the cytosol. Released cytochrome c, in the presence of dATP, forms an activation complex with

**Address correspondence to:*
Dr. Ola Ahmed Heikal, Department of Pharmacology & Toxicology, Faculty of Pharmacy and Biotechnology, German University in Cairo, New Cairo City, Main Entrance Al Tagamoa Al Khames, Egypt.
e-mail: ola.heikal@guc.edu.eg

apoptotic protein activating factor-1 and caspase 9 that activates down stream caspases to execute the final morphological and biochemical alterations. A group of antiapoptotic proteins tightly regulates the mitochondrial pathway, such as Bcl-2, and proapoptotic proteins such as Bax; further downstream regulation occurs, by various inhibitors of caspases (*3,4*).

Nigella sativa (NS) (black seed or black cumin) has been used traditionally to promote health and fight disease for centuries and most of the known biological activities of the seeds have been attributed to its active constituent thymoquinone (*5*). Recently conducted research has shown many therapeutic effects of TQ such as an immunomodulator, anti-inflammatory and antioxidant agent (*6*). Moreover, TQ is a potential chemotherapeutic compound owing to its antineoplastic activity against various tumor cells such as neoplastic keratinocytes, colorectal cancer cells and ovarian adenocarcinoma cells (*7-9*). The promising antineoplastic effect of TQ is attributed to its ability to induce apoptosis in cancer cells. Other studies demonstrated that TQ disrupts mitochondrial membrane potential and triggers the activation of caspases 8, 9, and 3 in myeloblastic leukemia HL-60 cells (*10*).

Although, all the mentioned studies support the antineoplastic role of TQ as a potent inducer of apoptosis in cancer cells, conflicting reports also showed evidence of delayed apoptosis upon treatment of Hep-2, laryngeal carcinoma cells, with the black seed (*11*). Other studies have shown lack of TQ toxicity to normal cells as well as its selective growth inhibitory and apopotic effect in cancer cells (*9,12*). As far as we know, the modulatory effect of TQ on apoptosis in normal cells and in other types of cell injuries has not yet been established. Here, we hypothesize a controversial effect of TQ that it could exert an antiapoptotic effect in another model of injury other than cancer. Therefore, we designed our study to compare the potential effect of TQ on apoptosis in normal rats and in a model of hepatic ischemia reperfusion injury. We studied the effect of TQ on various steps in the apoptotic pathway including death ligand, down stream caspase signaling of the apoptotic cascade and apoptotic regulators. New apoptosis-modulating compounds could be useful in the treatment of most liver disorders.

2. Materials and Methods

2.1. *Chemicals and reagents*

TQ (2-isopropyl-5-methyl-1,4-benzoquinone) was prepared as a 1 M stock solution in hot water (60~80°C) and the appropriate working solutions were prepared in a total volume of 1 mL. TQ, agarose, and DNA ladders were purchased from Sigma-Aldrich, Germany. EGTA (ethylene glycol tetraacetic acid) and Triton X-100 were purchased from Sigma Chemical Co. (St. Louis, MO, USA). Ellman's reagent, 5,5`-dithio bis-(2-nitrobenzoic acid, was from MP Biomedicals, Inc. (Washington, DC, USA). Liver enzyme kits were purchased from Quimica Clinica (Aplicada S.A., Spain). Cytochrome c release assay kit and TNF-α ELISA kit were products from Quantikine® (R&D Systems, Inc., USA). Caspases colorimetric assay kits were purchased from R&D Systems Inc., USA. Total protein quantification kit was made by Stanbio Lab (San Antonio, TX, USA). The RNA extraction kit was obtained from Promega, Madison, WI, USA. Reverse transcriptase (AMV), primers and Taq DNA polymerase, DNTPs were also from Promega. DNAeasy tissue kit was a product of Qiagen Inc., USA. All other reagents were of analytical grade.

2.2. *Animals*

Forty-eight Sprague Dawley male albino rats were purchased from the animal house of National Research Center, Cairo, Egypt. All animals were housed in plastic cages, kept in a conditioned atmosphere at 25°C and fed standard laboratory pellets with tap water *ad libitum*. All experimental procedures were carried out in accordance with the guide for the care and use of laboratory animals published by the US National Institutes of Health (NIH publication, 1985) (*13*).

2.3. *Experimental design*

Rats were randomly divided into eight groups; each consisted of 6 rats. Rats underwent either no intervention (group I: sham-operated group) or 45 min ischemia followed by one-hour reperfusion (group II: ischemia reperfusion injury group {I/R}). The other six groups were given PO administration of TQ aqueous solution at 5, 20, and 50 mg/kg/day dose levels for 10 days. At the end of treatment three groups were not subjected to any intervention (groups III, IV, and V: TQ control groups) or subjected to 45 min ischemia followed by one-hour reperfusion as in group II (group VI, VII, and VIII: TQ pretreated I/R groups).

2.4. *Surgical procedure*

Rats were anaesthetized using sodium phentobarbital at a dose of 30 mg/kg, 24 h after the last dose. A complete midline incision was made. The hepatoduodenal ligament was separated after entry into the belly (sham-operated group). The animal model of hepatic ischemia reperfusion injury was established according to Nauta *et al.* (*14*). To induce hepatic ischemia, the hepatic pedicle including hepatic artery and portal vein, which supplies the left and median liver lobes (70% of liver mass), was occluded with a microvascular clamp for 30 min. This method of partial hepatic ischemia allows for portal decompression through right and caudate lobes and so

prevents mesenteric venous congestion. Reperfusion was initiated by removal of the clamps. After one hour reperfusion, blood samples were collected from the retro-orbital plexus for biochemical analysis. Animals were scarified and livers were excised, cut into smaller pieces and stored at –80°C for analysis. The mitochondria were separated from the tissue soluble cytosolic fraction.

2.5. *Isolation of rat liver mitochondria and cytosol*

Rat liver mitochondria and cytosol were isolated by differential centrifugation as described by Johnson and Lardy (*15*). After the animals were killed, their livers were excised quickly and 0.5 g of each rat liver was placed in a medium containing 0.25 M sucrose, 10 mM Tris-HCl, and 1 mM of the chelator EGTA, pH 8 at 4°C. The tissue was scissor minced and homogenized on ice using a Teflon Potter homogenizer. Liver homogenate was centrifuged at 1,000 × g for 5 min to pellet cell fragments, and the supernatant was centrifuged at 9,500 × g for 10 min to pellet the nuclei. The supernatant was further centrifuged at 14,000 × g for 25 min to obtain the mitochondrial fraction and the resulting supernatant was used as the soluble cytosolic fraction.

2.6. *Determination of liver functions*

Determination of serum alanine aminotransferase (ALT) and aspartate aminotransferase (AST) were determined according to manufacturer's instructions using test reagent kits (Quimica Clinica Aplicada S.A., Spain). The analysis was performed on a Shimadzu UVPC 2401v 3.9 spectrophotometer (Shimadzu, Kyoto, Japan).

2.7. *Determination of reduced glutathione content (GSH)*

GSH content was measured in 10% liver homogenate according to the method of Ellman (*16*). Analysis was performed on a Shimadzu UVPC 2401v 3.9 spectrophotometer. GSH concentrations are expressed in mg/g tissue.

2.8. *Determination of lipid peroxides*

Lipid peroxidation was measured in 10% liver homogenate by the thiobarbituric acid (TBA) assay according to the method of Uchiyama and Mihara (*17*). Thiobarbituric acid reactive substances (TBARS) content was calculated according to the standard curve using 1,1,3,3-tetraethoxypropane as a standard and expressed in nmol/g wet tissue. The absorbance was measured at 535 nm using a Shimadzu UVPC 2401v 3.9 spectrophotometer.

2.9. *Determination of caspases activities*

Caspases (8, 9, and 3) activities were determined colorimetrically using assay kits (R&D Systems Inc, USA). Analysis was performed according to the manufacturer's instructions. 0.1 g liver tissue was added to 1 mL of the lysis buffer then homogenized on ice using the Teflon Potter homogenizer. After liver homogenate was centrifuged at 1,000 × g for 15 min the supernatant was suitable for the assay.

2.10. *Determination of cytochrome c in cytosol by solid phase ELISA*

Cytochrome c was measured in the soluble cytosolic fraction of liver homogenate after differential centrifugation as described above. Analysis was performed according to the manufacturer's instructions using Quantikine Rat/Mouse Immunoassay solid phase ELISA commercial kit. Cytosolic cytochrome c concentration was determined by optical density using the Vector multiple ELISA plate reader (Perkin-Elmer, USA) set to 450 nm. The cytochrome c values were expressed as ng/mg protein. Total protein analysis was performed using the total protein diagnostic kit.

2.11. *Determination of tumor necrosis factor α by solid phase ELISA*

Tumor necrosis factor α (TNFα) was determined by the Quantikine Rat/Mouse Immunoassay ELISA commercial kit according to the manufacturer's instructions. Zero point five gram liver tissue was added to 2 mL saline and the tissues were scissor minced and homogenized on ice using the Teflon Potter homogenizer. Liver homogenate was centrifuged at 1,000 × g for 15 min, and the supernatant was used for the assay. TNFα concentration was determined as optical density using the Vector multiple ELISA plate reader (Perkin-Elmer, USA) set to 450 nm. Values were calculated as pg/mL from the constructed standard curve, and then expressed as pg/mg tissue protein. Total protein analysis was performed using the total protein diagnostic kit.

2.12. *Detection of DNA fragmentation by gel electrophoresis*

Thirty mg liver tissue was homogenized using the Teflon Potter homogenizer. DNAeasy tissue kits were used for rapid tissue DNA extraction and purification following the manufacturer's instructions using the DNAeasy spin column. Five µL DNA samples were electrophoresed on 1.5% agarose, stained with ethidium bromide and visualized using a UV transilluminator (Uvitec, UK). DNA cleavage becomes evident in agarose gel electrophoresis and DNA cleavage results

in characteristic fragments of oligonucleosomal size (180-200 bp) (*18*).

2.13. *Determination of Bcl-2, Bax, and NF-κB genes expression using polymerase chain reaction (PCR)*

About 30 mg of liver tissues were homogenized in 175 µL lysis buffer containing guanidium thiocyanate and β-mercaptoethanol for RNA extraction.

2.13.1. *RNA extraction*

Total RNA was extracted after homogenization according to manufacturer's instructions. The concentration of extracted RNA was measured spectrophotometrically at 260 nm.

2.13.2. *Reverse transcription and polymerase chain reaction (RT-PCR)*

For amplification of the target genes, reverse transcription and PCR were run in two separate steps. Briefly, equal amounts of total RNA (10 µg) were heat denatured and reverse transcribed at 37°C for 60 min with 50 U/µL Moloney murine leukemia virus reverse transcriptase (MMLV-RT enzyme; Promega Co., Madison, WI, USA), 40 U/µL human placental ribonuclease inhibitor (HPRI) (Promega Co.), 10 mM deoxy-nucleoside 5'-triphosphate mixture (dNTPs), and 1 nM oligo-dT primer in a final volume of 30 µL of 1× MMLV-RT enzyme buffer. The reactions were terminated by heating at 95°C for 10 min and cooling on ice. The formed cDNA (5 µL) samples were amplified in 50 µL of 1× PCR buffer in the presence of 5 U/µL Taq DNA polymerase (Promega Co.), 1 µL 10 mM dNTPs, and 1 µL of the appropriate primer pairs (2 primers, 50 pmol each), and 37 µL DEPC water. The 3 sets of primers of Bax, Bcl-2, and NF-κB were designed from GenBank (accession No. G35510 and 691379, respectively); PCR consisted of a first denaturing cycle at 97°C for 5 min, followed by a variable number of cycles of amplification defined by denaturation at 96°C for 1.5 min, annealing at 55°C for 1.5 min, and extension at 72°C for 3 min. A final extension cycle of 72°C for 10 min was included.

2.13.3. *Agarose gel electrophoresis*

All PCR products were electrophoresed on 2% agarose, stained with ethidium bromide and visualized by UV transilluminator.

2.13.4. *Semi-quantitative determination of PCR products*

β-Actin was used as an internal control and was also amplified using its specific primer. Semi-quantitation was performed using the gel documentation system (BioDO, Analyser) supplied by Biometra. According to the following amplification procedure, relative expression of each gene was calculated following the formula: R = densitometry units of each gene/ densitometry units of β-actin.

3. Results

3.1. *Effect of TQ on liver enzymes*

As it is shown in Table 1, I/R caused deterioration in liver functions as evidenced by a significant increase in AST and ALT activities as compared to sham-operated group ($p < 0.05$). Administration of TQ at doses of 5, 20, and 50 mg/kg for 10 days before I/R insult significantly reduced both AST and ALT activities as compared to the I/R group. The effect of 20 mg/kg TQ returned the AST activity to the sham-operated value ($p > 0.05$), while the 50 mg/kg TQ significantly decreased it below that of the sham-operated group ($p < 0.05$). The effect of TQ on liver enzyme activity in control rats was also studied (Table 2). We noticed that TQ significantly decreased the AST activity below that of the sham-operated group with no significant difference between groups III, IV, and V receiving different doses of TQ. For the ALT activity, TQ did not cause any significant change except for the dose of 20 mg/kg ($p < 0.05$ *vs*. sham group).

3.2. *Effect of TQ on lipid peroxidation*

As shown in Table 1, TQ markedly attenuated the increased MDA content, which is associated with hepatic I/R, in a dose dependent manner which reached

Table 1. Measurement of liver enzymes, MDA concentration, and GSH enzyme activities in TQ-IR pretreated groups

Groups	AST (U/L)	ALT (U/L)	GSH (mg/g)	MDA (nmol/g)
Control	87.90 ± 0.45	18.55 ± 0.54	2.47 ± 0.26	21.83 ± 0.80
I/R	141.96 ± 1.19[a]	65.90 ± 6.02[a]	0.58 ± 0.04[a]	63.4 ± 1.06[a]
VI	122.05 ± 1.05[a,b]	51.34 ± 3.73[a]	0.74 ± 0.02[a,b]	39.81 ± 1.88[a,b]
VII	90.08 ± 1.34[b]	29.83 ± 3.16[a,b]	0.99 ± 0.07[a,b]	30.56 ± 1.89[a,b]
VIII	75.16 ± 2.14[a,b]	22.76 ± 1.47[a,b]	1.49 ± 0.03[a,b]	11.03 ± 1.34[a,b]

Values are represented as mean ± SE, $n = 6$, [a] $p < 0.05$ *vs*. control, [b] $p < 0.05$ *vs*. I/R.

Table 2. Measurement of liver enzymes, MDA concentration and GSH enzyme activities in TQ-control groups

Groups	AST (U/L)	ALT (U/L)	GSH (mg/g)	MDA (nmol/g)
Control	87.90 ± 0.45	18.55 ± 0.54	2.47 ± 0.26	21.83 ± 0.80
III	64.53 ± 0.57[a]	17.85 ± 1.86	0.71 ± 0.06[a]	22.75 ± 1.18
IV	61.10 ± 0.68[a]	14.98 ± 0.68[a]	0.81 ± 0.05[a]	22.61 ± 1.54
V	62.46 ± 0.80[a]	16.67 ± 1.44	3.54 ± 0.03[a]	14.8 ± 0.76[a]

Values are represented as mean ± SE, $n = 6$, [a] $p < 0.05$ *vs*. control.

a significantly lower value than that of the sham group when the highest dose of 50 mg/kg ($p < 0.05$) was used. Results in Table 2 show that TQ at doses of 5 and 20 mg/kg, given to TQ control rats did not cause any significant reduction in MDA values as compared to the sham group ($p > 0.05$), while TQ at the 50 mg/kg dose significantly reduced the MDA content below that of the sham-operated group ($p < 0.05$).

3.3. *Effect of TQ on hepatic GSH content*

I/R caused a significant decrease in GSH ($p < 0.05$ *vs*. sham group) which was significantly elevated by TQ treatment in a dose dependent manner ($p < 0.05$ *vs*. I/R group). The increased level of GSH by TQ failed to return to sham-operated values for any of the doses used ($p < 0.05$). Interestingly, the antioxidant protective effect of TQ in the hepatic I/R model is reversed in the control groups of rats treated with TQ at doses 5 and 20 mg/kg. Results in Table 2 showed a significant decrease in the GSH level in groups III and IV as compared to the sham group ($p < 0.05$). On the other hand, the 50 mg/kg dose significantly increased the GSH level, which reached a higher level than the sham group ($p < 0.05$).

3.4. *Effect of TQ on caspases activities*

As shown in Figure 1, I/R induced apoptotic cell death was indicated by a significant increase in caspases 8, 9, and 3 activities. TQ administered at 5 mg/kg reduced apparently all caspases activities measured in the study but did not reach a significant level except for caspase 8. Meanwhile, TQ at doses of 20 and 50 mg/kg produced a dose-dependent decrease in caspase 3 (0.68 ± 0.05 and 0.50 ± 0.04, respectively; $p < 0.05$), caspase 8 (0.65 ± 0.04 and 0.40 ± 0.05, respectively; $p < 0.05$) and caspase 9 (0.63 ± 0.04 and 0.41 ± 0.05, respectively; $p < 0.05$) activities when compared to the I/R groups and values returned back to the corresponding sham operated situation with the 50 mg/kg dose of TQ. On the other hand, TQ did not cause any significant change in caspases 8, 9, and 3 activities at doses of 5 and 20 mg/kg in TQ control groups ($p > 0.05$ *vs*. sham). The 50 mg/kg TQ significantly reduced caspase 8 and 3 but had no effect on caspase 9 compared to the sham group (Figure 2).

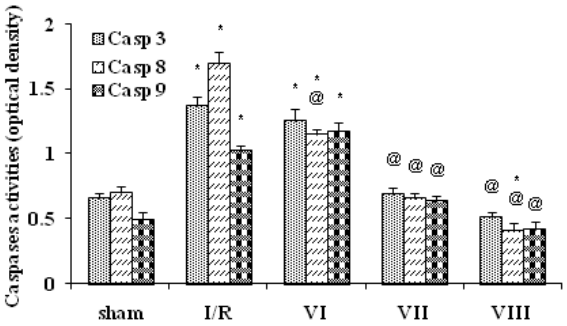

Figure 1. Effect of TQ on caspases activities in TQ-I/R groups. Values are represented as mean ± SE, $n = 6$, * $p < 0.05$ *vs*. control.

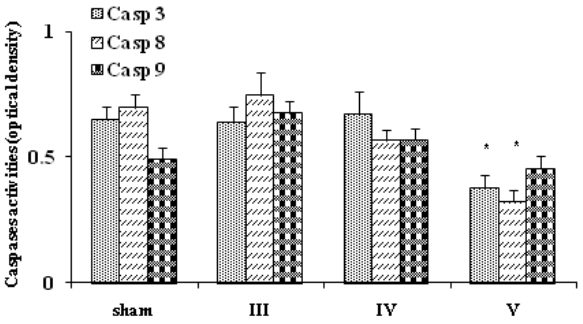

Figure 2. Effect of TQ on caspases activities in TQ groups. Values are represented as mean ± SE, $n = 6$, * $p < 0.05$ *vs*. control, @ $p < 0.05$ *vs*. I/R.

3.5. *Effect of TQ on cytochrome c*

As shown in Figure 3, I/R generated a significant increase in cytochrome c released into the cytosol as compared to the sham group ($p < 0.05$). TQ administration to TQ pretreated I/R groups VI, VII, and VIII resulted in a significant reduction in the released cytochrome c, in a dose dependent manner, as compared to the I/R group ($p < 0.05$). In TQ control groups III, IV, and V, no significant changes in the mean values of cytochrome c were detected as compared to the sham group ($p > 0.05$) (Figure 4).

3.6. *Effects of TQ on Bax and Bcl-2 protein levels*

As shown in Figures 5 and 11, I/R caused modulation of the apoptotic regulatory proteins towards apoptosis with a significant increase in the expression of proapoptotic

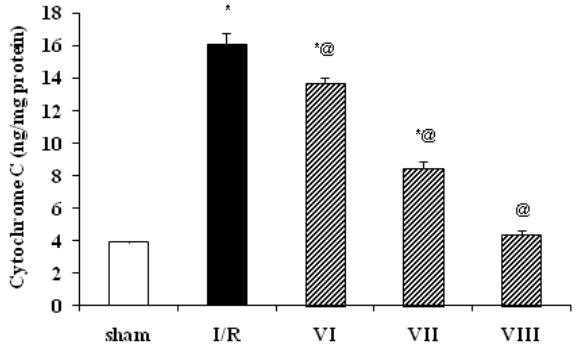

Figure 3. Effect of TQ on cytochrome C in TQ-I/R groups. Values are represented as mean ± SE, $n = 6$, * $p < 0.05$ *vs*. control, @ $p < 0.05$ *vs*. I/R.

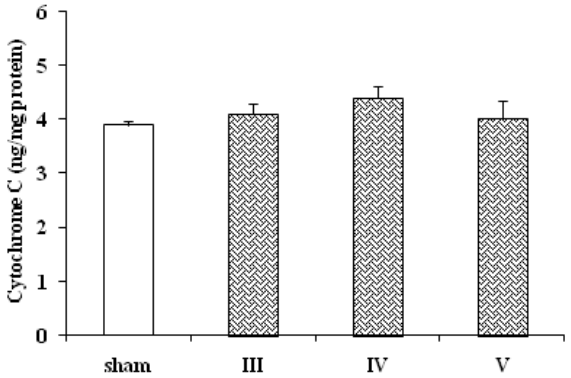

Figure 4. Effect of TQ on cytochrome C in TQ control groups. Values are represented as mean ± SE, $n = 6$, * $p < 0.05$ *vs*. control.

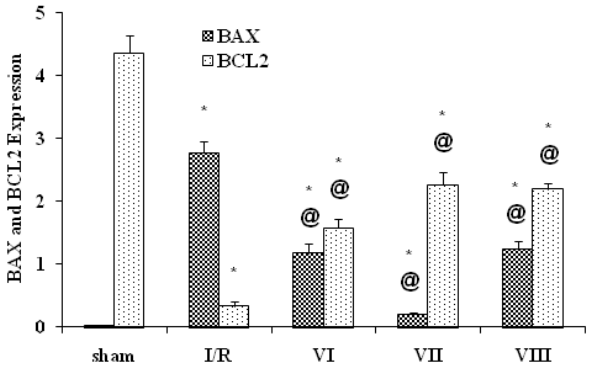

Figure 5. Effect of TQ on BAX and Bcl-2 proteins expression in TQ-I/R groups. Values are represented as mean ± SE, $n = 6$, * $p < 0.05$ *vs*. control, @ $p < 0.05$ *vs*. I/R.

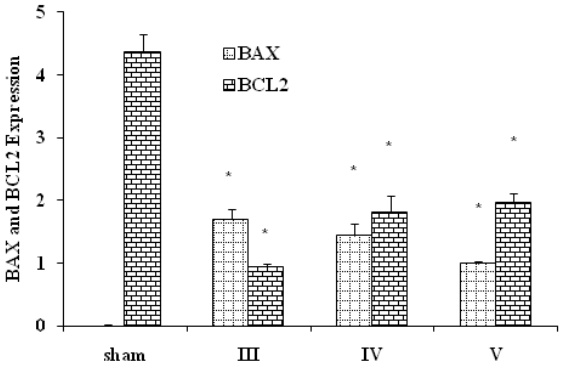

Figure 6. Effect of TQ on BAX and Bcl-2 proteins expression in TQ control groups. Values are represented as mean ± SE, $n = 6$, * $p < 0.05$ *vs*. control.

Bax protein and a significant decrease in the antiapoptotic Bcl-2 as compared to the sham group ($p < 0.05$). In groups VI, VII, and VIII receiving TQ at doses 5, 20, and 50 mg/kg, prior to I/R intervention, there was a significant decrease in Bax expression ($p < 0.05$) and a significant increase in Bcl-2 ($p < 0.05$). However, all doses of TQ used could not restore the Bax-to-Bcl-2 ratio to the control value ($p < 0.05$ *vs*. sham). On the other hand, administration of TQ to control rats in groups III, IV, and V resulted in a significant increase in the expression of Bax and a significant decrease in Bcl-2 as compared to the sham group ($p < 0.05$), raising the question whether TQ exerts an apoptotic effect on normal intact livers as shown in Figures 6 and 11.

3.7. *Effects of TQ on TNFα*

As shown in Figure 7, administration of TQ at doses of 20 and 50 mg/kg significantly reduced the TNFα levels compared to the I/R group. The hepatic content of TNFα was reduced from 0.79 ± 0.03 in the I/R group to 0.73 ± 0.04 and 0.58 ± 0.03 in groups VI and VII, respectively. The 50 mg/kg TQ given to group VIII returned the TNFα back to the control value in the sham-operated group ($p > 0.05$). Regarding the effect of TQ on TNFα in normal livers, TQ did not exert a significant effect in control rats at any of the doses used as illustrated in Figure 8 ($p > 0.05$ *vs*. sham group).

3.8. *Effects of TQ on NF-κB*

Figures 9 and 11 demonstrated the effect of TQ (5, 20, and 50 mg/kg) on NF-κB activation in the hepatic I/R model. TQ administered to rats at doses of 5 and 20 mg/kg prior to reperfusion injury significantly down regulated the increased expression of NF-κB by I/R ($p < 0.05$) but was still significantly higher than the control ($p < 0.05$). On the contrary, the 50 mg/kg dose did not cause any significant change in the NF-κB protein level as compared to the I/R group ($p > 0.05$). When control rats were treated with TQ, the expression of NF-κB was significantly increased at the 3 doses used in this study as compared to the sham group ($p < 0.05$), and opposite to the effect seen in the I/R model (Figures 10 and 11).

3.9. *DNA fragmentation*

Agarose gel analysis of fragmentation patterns of

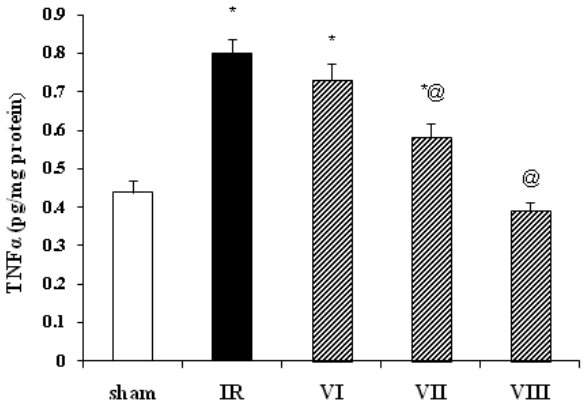

Figure 7. Effect of TQ on TNFα in TQ-I/R groups. Values are represented as mean ± SE, $n = 6$, * $p < 0.05$ *vs*. control, @ $p < 0.05$ *vs*. I/R.

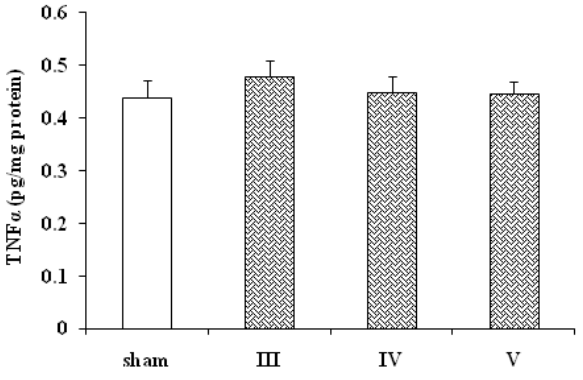

Figure 8. Effect of TQ on TNFα in TQ control groups. Values are represented as mean ± SE, $n = 6$, * $p < 0.05$ *vs*. control.

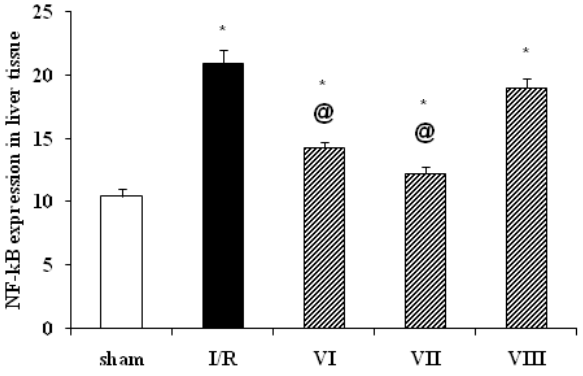

Figure 9. Effect of TQ on NF-κB in TQ-I/R groups. Values are represented as mean ± SE, $n = 6$, * $p < 0.05$ *vs*. control, @ $p < 0.05$ *vs*. I/R.

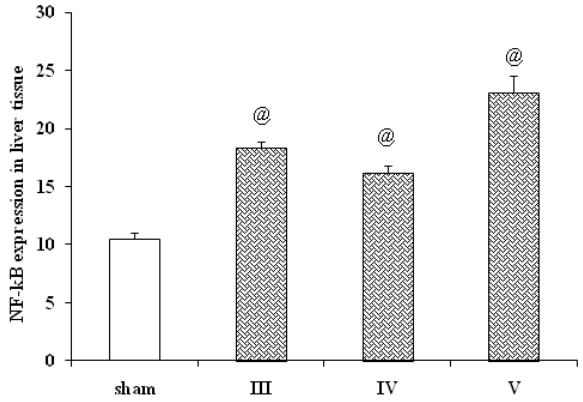

Figure 10. Effect of TQ on NF-κB in TQ control groups. Values are represented as mean ± SE, $n = 6$, * $p < 0.05$ *vs*. control.

cellular DNA isolated from I/R groups revealed the DNA ladder pattern of internucleosomal fragmentation. TQ pretreatment before the I/R insult decreased DNA fragmentation (Figure 12). Control groups treated with TQ were distinctly different from TQ pretreated I/R groups. There was a slight DNA fragmentation pattern only in TQ-control groups treated at 5 and 20 mg/kg doses while at the 50 mg/kg TQ dose, cellular DNA from rat group VIII showed no DNA ladder pattern when compared to the control group (Figure 13).

4. Discussion

Our results of TQ treatment on ALT and AST activities are in good agreement with a recent study by Yildiz *et al.* (*19*) who observed similar results with *Nigella* sativa (NS) extracts using the liver ischemic reperfusion model. In the present study, TQ treatment in groups VI, VII, and VIII significantly increased GSH levels in a dose dependent manner as compared to the I/R group. These results were consistent with the previous study on the effect of TQ on gastric mucosal I/R injury in rats. However, our

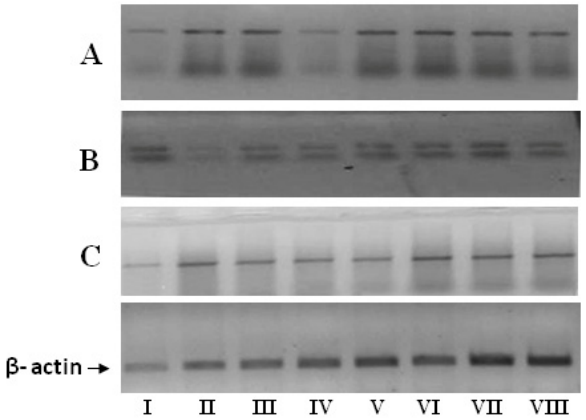

Figure 11. An agarose gel electrophoresis shows PCR products of BAX gene (A), BCL-2 gene (B), and NF-κB gene (C) in all animal groups (I-VIII).

results showed that GSH liver content in TQ control groups (III and IV) receiving 5 and 20 mg/kg of TQ were significantly decreased while the 50 mg/kg dose restored and significantly increased the GSH tissue content as compared to the sham-operated group ($p < 0.05$). This decrease in GSH content was reported in another *in vitro* study suggesting a TQ mediated-

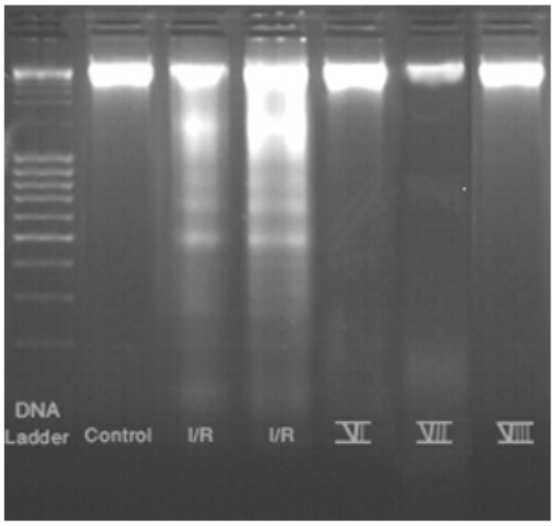

Figure 12. DNA fragmentation in TQ-I/R groups.

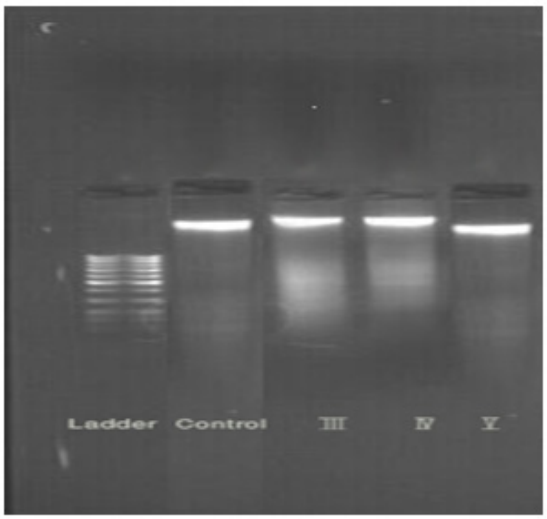

Figure 13. DNA fragmentation in TQ control groups.

GSH depletion effect in cancer cell lines (*20*). The effect of TQ on GSH content in different types of cell injuries is still questionable suggesting that the dose range used and the duration of treatment need further investigation.

The TQ effect on caspases cascade was first examined in the TQ control groups (Figure 2). Only the 50 mg/kg dose of TQ treatment caused a significant decrease in caspases 8 and 3 activities but had no effect on caspase 9 when compared to sham-operated group I. Therefore, the effect of TQ on caspases activities, in normal animal models, is only evident at the high dose and affected caspases 8 and 3. The TQ inhibitory effect on caspase 3 could be either through a direct effect or indirectly through deactivating up-stream caspase 8. The TQ negative effect on caspase 9 activities at all doses levels suggests that the TQ antiapoptotic effect in normal livers might be *via* targeting mainly inhibition of caspases 8 and 3 only. However, in TQ-I/R treated groups, we observed that the 20 mg/kg dose of TQ, resorted the caspases 8, 9, and 3 activities to normal values with complete protection against the I/R injury model especially with the 50 mg/kg dose. From these findings, we conclude that TQ inhibits downstream caspases and that caspase 8 is the most likely one targeted by TQ in the I/R model. This further supports our observations on the deactivation effect of TQ on caspase 8 in the normal animal groups.

TQ inhibited the release of mitochondrial cytochrome c into the cytosolic fraction in a dose dependent manner in all TQ-I/R groups compared to I/R groups but did not exert a significant change in the TQ control groups compared to the sham group. TQ deactivation of caspase 8 could be responsible for the inhibition of cytochrome c release from the mitochondria and thus the deactivation of caspase 3. The role of TQ and/or its metabolic reduced forms as free radical scavengers that result from I/R injury could lead to stabilization of the mitochondrial membrane permeability which regulates cytochrome c release and other caspase-induced pro-apopototic factors. This is further supported by our results in the present study where the gradual inhibition of lipid peroxidation measured as MDA hepatic tissue content are in agreement with the decrease of cytosolic cytochrome c levels in TQ pretreated groups VI, VII, and VIII. A conflicting *in vitro* study, conducted with isolated mitochondria from normal rat liver, showed the ability of TQ to induce mitochondrial O_2^- generation, suggesting that TQ enhances a mechanism of oxidative stress in mitochondria (*21*). However, in other studies, TQ has been reported to be a potent antioxidant that prevents oxidative injury in several tissues with the ability to inhibit lipid peroxidation and to preserve cell integrity (*22-24*).

This controversy could be explained by the ability of TQ to form a redox-couple consisting of the oxidized and semi-reduced forms of TQ similar to ubiquinone, a redox couple within the mitochondria, where the oxidized TQ becomes easily reduced and the semi-reduced form of TQ enhances O_2^- generation by accepting electrons from oxidizing species (*21*). In fact, these conflicting reports clarify the premise that the mechanism by which TQ induces changes in mitochondrial function *in vivo* might be different from that in *in vitro* studies.

Mitochondrial membrane permeability is tightly regulated by proteins from the Bcl-2 family which inhibit or promote mitochondrial membrane permeability depending on whether they belong to the pro- or anti- apoptotic branch of the family (*25-27*). Thus we determined changes in Bax and Bcl-2 protein expression levels upon TQ treatment. A significant increase in Bax protein with a similar decrease in Bcl-2 protein contents were found in all TQ-control

groups at all doses levels as compared to the sham-operated group. These data confirm previous results on the modulatory effect of TQ as proapoptotic in cancer cells. The reported mechanisms have been concluded in several studies to be p53-mediated where TQ induction of p53 was accompanied by down regulation of Bcl-2 (*8*). The Bax/Bcl-2 ratio changes, caused oligmerization of Bax on the outer mitochondrial membrane leading to permeabilization of the mitochondria with cytochrome c release (*28*). Interestingly our results showed that TQ causes up regulation of Bax and downregulation of Bcl-2 in normal animal groups, thus favoring the apoptotic pathway, while in the TQ-pretreated I/R groups, TQ caused a significant decrease in the Bax and concomitant increase in Bcl-2 levels as compared to the I/R group. However the values did not return to normal levels as in the sham-operated group. The mechanism is not fully understood and it needs further investigation. In a recent publication they reported upregulation of Bcl-2 using caspase 3 inhibitors to ameliorate ischemia reperfusion injury in a model of cardiac allograft in the rat. The inhibition of caspase 3 is concomitant with upregulation of Bcl-2 where caspase 3 inhibition mediates tryosine kinase activity allowing Bcl-2 overexpression (*29*). In the present study, results showed the inhibitory effect of TQ on caspase 3 activation at all doses levels in TQ pretreated I/R groups. Thus we might suggest that TQ deactivation of caspase 3 may allow for Bcl-2 overexpression that could provide partial protection against I/R injury-induced apoptosis. A distinct decrease in the DNA ladder pattern under TQ treatment supports our previous findings that TQ exerts an antiapoptotic effect against hepatic I/R injury.

Further findings on TQ's role in the death receptor pathway have to be highlighted (*30,31*). Ischemia reperfusion injury of the liver can lead to TNFα production, which can induce multiple mechanisms that initiate hepatocyte apoptosis (*32-34*). Bid, a proapoptotic protein, is activated by caspase 8 after TNFα binding to death receptor TNF-R1. The use of caspase 8 inhibitors to suppress Bid activation has been reported to inhibit cytochrome c release in TNFα-treated hepatocytes (*35*). This suggests the role of caspase 8 and the mitochondrial pathway in TNFα-induced apoptosis in hepatocytes. Further studies reported the role of TQ in attenuating pro-inflammatory responses *via* the inhibition of TNFα mRNA expression in a lipopolysaccaride-activated rat basophil cell line (*36*). In our present study TQ showed a significant dose dependent decrease in the TNFα content measured in liver homogenate of TQ pretreated I/R animal groups as compared to the I/R group. Thus we further suggest that the TQ anti-inflammatory effect could be through the deactivation of caspase 8, supporting the role of TQ administration in decreasing TNFα release in I/R injury. No distinct changes have been seen in all TQ-control groups as compared to the sham-operated group, indicating no effect of TQ on TNFα production under normal conditions.

On the other hand one of the multiple apoptotic pathways induced by TNFα has been linked to interference with the NF-κB signaling pathway. In our present study, we found that TQ at doses of 5 and 20 mg/kg induced a significant reduction in NF-κB expression in TQ pretreated I/R animal groups as compared to the I/R group, while the 50 mg/kg dose of TQ failed to cause any significant change in NF-κB expression.

The suppression in NF-κB values observed in groups administered TQ at doses of 5 and 20 mg/kg correlated with the TQ induced TNFα suppression in our hepatic I/R model. In agreement with our study, Sethi *et al*. investigated the effect of TQ on the NF-κB pathway. They found that TQ suppressed TNFα-induced NF-κB activation in a dose- and time-dependent manner and inhibited NF-κB activation induced by various carcinogens and inflammatory stimuli (*37*). Thus, we can conclude that the anti-apoptotic effect of TQ could be mediated in part through the suppression of TNFα and consequently suppression of the NF-κB activation pathway. On the other hand, the effect of TQ administration on the NF-κB expression protein levels in the normal animal model is opposite to its inhibitory effect in the I/R model. In TQ-control groups, TQ caused a significant NF-κB increase as compared to the sham-operated group. This increase is associated with a non detectable increase in TNFα content in TQ control groups, indicating that TQ activation of NF-κB is not only induced *via* the TNFα signaling pathway but also other pathways could be involved. Thus, it seems that in our study NF-κB activation observed in TQ-control groups induced an apoptotic effect especially because the Bax/Bcl-2 ratio in the TQ control groups is increased and the GSH level is depleted.

It can be concluded from this study that TQ exerts a potent antiapoptotic effect against hepatic I/R injury through attenuating oxidative stress and inhibiting TNFα-induced NF-κB activation. It inhibits caspases. It also inhibits cytochrome c release and targets the apoptotic regulators of the Bcl-2 family proteins. Concerning the effect of TQ on normal livers, TQ induced GSH depletion especially at the 5 and 20 mg/kg doses, increased the Bax to Bcl-2 ratio and activated transcription factor NF-κB, thereby promoting the apoptotic process. On the other hand, the 50 mg/kg dose of TQ decreased lipid peroxidation, increased the GSH hepatic content and inhibited caspase 8 and 3, favoring protection against apoptosis.

How TQ plays an anti-apopototic role in some conditions and a pro-apopototic in others requires further investigation.

References

1. Ghavami S, Hashemi M, Kadkhoda K, Alavian SM, Bay GH, Los M. Apoptosis in liver diseases – detection and therapeutic applications. Med Sci Monit. 2005; 11: RA337-345.
2. Yin XM, Din WX. Death receptor activation-induced hepatocyte apoptosis in liver injury. Curr Mol Med. 2003; 3:491-508.
3. Mitchell C, Mallet V, Guidotti JE, Mignon A, Couton D, Kahn A, Gilgenkrantz H. Experimental modulation of apoptosis. physiopathological and therapeutic targets. J Soc Biol. 2005; 199:243-246.
4. Bouchier-Hayes L, Lartigue L, Newmeyer Dd. Mitochondria: pharmacological manipulation of cell death. J Clin Invest. 2005; 115:2640-2647.
5. Ali BH, Blunden G. Pharmacological and toxicological properties of Nigella Sativa. Phytother Res. 2003; 17:299-305.
6. Iddamaldeniya SS, Thabrew MI, Wickramasinghe SM, Ratnatunge N, Hammitiyagodage MG. A long-term investigation of the anti-hepatocarcinogenic potential of an indigenous medicine comprised of Nigella sativa, Hemidesmus indicus and Smilax glabra. J Carcinog. 2006; 9:5-11.
7. Gali-Muhtasib HU, Abou Kheir WG, Kheir LA, Darwiche N, Crooks PA. Molecular pathway for thymoquinone-induced cell-cycle arrest and apoptosis in neoplastic keratinocytes. Anticancer Drugs. 2004; 15:389-399.
8. Gali-Muhtasib HU, Diab-Assef M, Boltze C, Al Hmaira J, Hartig R, Roessner A, Schneider SR. Thymoquinone extracted from black seed triggers apoptotic cell death in human colorectal cancer cells *via* a p53-dependent mechanism. Int J Oncol. 2004; 25:857-866.
9. Shoieb AM, Elgayyar M, Dudrick PS, Bell JL, Tithof PK. *In vitro* inhibition of growth and induction of apoptosis in cancer cell lines by thymoquinone. Int J Oncol. 2003; 22:107-113.
10. El-Mahdy MA, Zhu Q, Wang QE, Wani G, Wani AA. Thymoquinone induces apoptosis through activation of caspase-8 and mitochondrial events in p53-null myeloblastic leukemia HL-60 cells. Int J Cancer. 2005; 117:409-417.
11. Corder C, Benghuzzi H, Tucci M, Casen Z. Delayed apoptosis upon the treatment of hep-2 cells with black seed. Biomed Sci Instrum. 2003; 39:365-370.
12. Worthen DR, Ghosheh OA, Crooks PA. The *in vitro* anti-tumor activity of some crude and purified components of black seed, Nigella sativa L. Anticancer Res. 1998; 18:1527-1532.
13. "Animals in research": Heath Research extension act of 1985. Public law 99-158, November 20, 1985.
14. Nauta R, Tsimoyiannis E, Uribe M, Walsh D, Miller D, Butterfield A. Oxygen derived free radicals in hepatic ischemia and reperfusion injury in the rat. Surg Gynecol Obstet. 1990; 171:120-125.
15. Johnson D, Lardy HA. Isolation of liver and kidney mitochondria. In: Methods in Enzymology (Estabook RW, Pullman M, eds). Academic Press, New York, USA, 1967; pp. 94-96.
16. Ellman GL. Tissue sulfhydryl groups. Arch Biochem. 1959; 82:70-77.
17. Uchiyama M, Mihara M. Determination of malonaldehyde precursor in tissues by thiobarbituric acid test. Anal Biochem. 1978; 86:271-278.
18. Kerr JF, Wyllie AH, Currie AR. Apoptosis: a basic biological phenomenon with wide-ranging implications in tissue kinetics. Br J Cancer. 1972; 26:239-257.
19. Yildiz F, Coban S, Terzi A, Ates M, Aksoy N, Cakir H, Ocak AR, Bitiren M. Nigella sativa relieves the deleterious effects of ischemia reperfusion injury on liver. World J gastroenterol. 2008; 14:5204-5209.
20. Rooney S, Ryan MF. Modes of action of alpha-hedrein and thymoquinone, active constituents of Nigella sativa, against HEp-2 cancer cells. Anticancer Res. 2005; 25:4255-4259.
21. Roepke M, Diestel A, Bajbouj K, Walluscheck D, Schonfeld P, Rossner A, Stock RS, Muhtasib HG. Lack of p53 augments thymoquinone-induced apoptosis and caspase activation in human osteosarcoma cells. Cancer Biol Ther. 2007; 6:160-169.
22. Badary OA, Taha RA, Gamal El-Din AM, Abdel-Wahab MH. Thymoquinone is a potent superoxide anion scavenger. Drug Chem Toxicol. 2003; 26:87-98.
23. Mansour MA, Nagi Mn, El-Katib AS, Al-Bekairi AM. Effects of thymoquinone on antioxidant enzyme activities, lipid peroxidation and DT-diaphorase in different tissues of mice: a possible mechanism of action. Cell Biochem Funct. 2002; 20:143-151.
24. Houghton PT, Zarka R, De La Heras B, Hoult JR. Fixed oil of Nigella sativa and derived thymoquinone inhibit eicosanoid generation in leukocytes and membrane lipid peroxidation. Planta Medica. 1995; 61:33-36.
25. Kroemer G. Mitochondrial control of apoptosis: an introduction. Biochem Biophys Res Commun. 2003; 304:433-435.
26. Kluck RM, Bossy-Wetzel E, Green DR, Newmeyer DD. The release of cytochrome c from mitochondria: a primary site for Bcl-2 regulation of apoptosis. Science. 1997; 275:1132-1136.
27. Wei MC, Zong WX, Cheng EH, Lindsten T, Panoutsakopoulou V, Ross AJ, Roth KA, Macgregor GR, Thompson CB, Korsmeyer SJ. Proapoptotic BAX and BAK: a requisite gateway to mitochondrial dysfunction and death. Science. 2001; 292:727-730.
28. Zhao Y, Ding WX, Qian T, Watikins S, Lemasters JJ, Yin XM. Bid Activates multiple apoptotic mechanisms in primary hepatocytes after death receptors engagement. Gasterenterology. 2003; 12:854-867.
29. Gruenfelder J, Miniati DN, Murata S, Falk V, Hoyt G, Kown M, Koransky ML, Robbins RC. Upregulation of Bcl-2 through caspase-3 inhibitions ameliorates ischemia reperfusion injury in rat cardiac allograft. Circulation. 2001; 104:202-206.
30. Yin XM, Ding WX. Death receptors activation induced hepatocyte apoptosis and liver injury. Curr Mol Med. 2003; 3:491-508.
31. Yoon JH, Gores GJ. Death receptor-mediated apoptosis and the liver. J Hepatol. 2002; 37:400-410.
32. Rudiger HA, Clavien PA. Tumor necrosis factor alpha, but not Fas, mediates hepatocellular apoptosis in the murine ischemia liver. Gastroenterology. 2002; 122:202-210.
33. Ding WX, Ni HM, Difrancesca D, Stolz DB, Yin XM. Bid-dependent generation of oxygen radicals promotes death receptor activation-induced apoptosis in murine hepatocytes. Hepatology. 2004; 40:403-413.
34. Zhao Y, Li S, Childs EE, Kuharsky DK, Yin XM.

Activation of pro-death Bcl-2 family proteins and mitochondrial apoptosis pathway in tumor necrosis factor alpha-induced liver injury. J Biol Chem. 2001; 276:27432-27440.
35. Yin XM, Wang K, Gross A, Zhao Y, Zinkel S, Klocke B, Roth Ka, Korsmeyer SJ. Bid-deficient mice are resistant to Fas-induced hepatocellaur apoptosis. Nature. 1999; 400:886-891.
36. El Gazzar MA, El Mezayen R, Nicolls MR, Dreskin SC. Thymoquinone attenuates proinflammatory respones in lipopolysaccharide-activated mast cells by modulating NF-KappaB nuclear transactivation. Biochem Biophys Acta. 2007; 1770:556-564.
37. Sethi G, Ahn KS, Aggarwal BB. Targeting nuclear factor-kappa B activation pathway by thymoquinone: role in suppression of antiapoptotic gene products and enhancement of apoptosis. Mol Cancer Res. 2008; 6:1059-1070.

(*Received October 7, 2009; Accepted November 2, 2009*)

Original Article

Promising therapy for Alzheimer's disease targeting angiotensin-converting enzyme and the cyclooxygense-2 isoform

Nesrine S. El Sayed[1], Lobna A. Kassem[2], Ola A. Heikal[1,*]

[1] *Department of Pharmacology & Toxicology, Faculty of Pharmacy & Biotechnology, German University in Cairo, Egypt;*
[2] *Department of Physiology, Faculty of Pharmacy & Biotechnology, German University in Cairo, Egypt.*

ABSTRACT: Deposition of β-amyloid in brain is one of the pathological hallmarks of Alzheimer's disease (AD) that is often associated with inflammatory response. Much evidence also points to a link between the renin-angiotensin system, hypertension and dementia. Accordingly, the potential use of anti-inflammatory and antihypertensives might be beneficial agents in AD therapy. In this study, we investigated the possible mechanisms of Celecoxib (cyclooxygenase-2 (COX-2) inhibitor), Perindopril (angiotensin converting enzyme (ACE) inhibitor) and their combination in a lipopolysaccharide (LPS) model of AD. Mice were injected with LPS (0.8 mg/kg, *i.p.*) once then divided into three groups: the first was treated with Celecoxib (30 mg/kg/day, *i.p.*), the second with Perindopril (0.5 mg/kg/day, *i.p.*) and the last group with a combination of both drugs. Learning and memory function were tested using a Y-maze and locomotor activity was assessed using an open-field test. Cerebral specimens were subjected to histopathological studies. Brain tumor necrosis factor-alpha (TNF-α), and interleukin (IL)-1β levels were measured. LPS decreased locomotor activity and percentage of correct choices in the Y-maze test. It also produced a significant increase in the percentage area of vascular angiopathy, area of lamellated plaques, and apoptotic index. These were associated with increased TNF-α and IL-1β. Administration of either Celecoxib or Perindopril partially improved cognitive impairment, decreased inflammatory cytokines and amyloid deposition. Combined therapy of both drugs completely prevented LPS-induced neurodegenerative and cognitive changes. In conclusion, these findings establish a link between COX-2, ACE activity and cognitive impairment in AD and provided a promising strategy for the complete cure of AD.

*Address correspondence to:
Dr. Ola Ahmed Heikal, Department of Pharmacology & Toxicology, Faculty of Pharmacy and Biotechnology, German University in Cairo, New Cairo City – Main Entrance Al Tagamoa Al Khames, Egypt.
e-mail: ola.heikal@guc.edu.eg

Keywords: Alzheimer's disease, cyclooxygenase-2 inhibitor, angiotensin converting enzyme inhibitor, β-amyloid, inflammatory cytokines

1. Introduction

Alzheimer's disease (AD) is the most common neurodegenerative disorder marked by progressive loss of memory and cognitive ability. The pathology of AD is characterized by the presence of senile plaques that are deposits of amyloid β protein (Aβ) (*1*), and intracellular neurofibrillary tangles leading to pronounced cell death (*2*). Aβ deposited extracellularly or within the walls of the cerebrovasculature, caused cerebral amyloid angiopathy in 90% of patients with AD (*3*). In addition, the end-stage pathology of AD is also notable for the presence of numerous cellular and molecular markers of an inflammatory response that is often associated with the Aβ deposits. Accordingly, the role of inflammatory mechanisms in the pathogenesis of AD must be taken as a matter of convenience (*4*). In recent years, non-steroidal anti-inflammatory drugs (NSAIDs) have been suggested to be beneficial agents in delaying the onset and possibly reducing the risk of AD (*5-8*), but recommendations for their chronic use are tempered by the well documented risk of gastrointestinal bleeding and ulceration (*9*). Therefore, new classes of NSAIDs have emerged as treatment for AD, including selective inhibitors of cyclooxygenase-2 (COX-2). However, it may be worth noting that a definitive mechanism of action underlying their therapeutic effect remains completely uncertain and still, there is conflicting data regarding the expression of COX-2 in AD (*10,11*). Much epidemiological evidence points to a link between hypertension, risk factors for atherosclerotic vascular disease, and dementia; and in turn, the use of antihypertensive medications has been suggested to reduce the incidence of dementia including Alzheimer's disease, although through an unknown mechanism (*12*). Recent findings indicate that the brain has its own renin-angiotensin system (RAS), which

plays a role in neuronal plasticity as well as in learning and memory (*13*). There is conflicting evidence about the neurobiological links between the renin-angiotensin system and the pathogenesis of Alzheimer's (*14*). It has been reported that angiotensin converting enzyme (ACE) degrades the amyloid β-protein *in vitro*, and is a putative upstream initiator of Alzheimer's disease. This supports the hypothesis that ACE inhibitor (ACEI) treatment might increase Aβ concentrations and could increase Alzheimer's disease risk (*15*). This is in contrast to what has been reported in clinical studies that ACE inhibitors had a beneficial effect on the rate of cognitive decline, thought to be due partly to the presence of Aβ (*16*). Our goal was to investigate the effect of Perindopril, a brain penetrating ACE inhibitor on an Alzheimer's mouse model, to reveal the role of ACE in the pathogenesis of Alzheimer's. We also studied the effect of Celecoxib, a specific cyclooxygenase-2 inhibitor, aiming to explore its mechanism of action. We tested these drugs in terms of cognitive function, amyloidogenesis and inflammatory mediators. Furthermore, we proposed a promising therapeutic strategy based on a combination of ACEI and COX-2 inhibitors, which might be more beneficial in the treatment of Alzheimer's disease than either individual agent alone.

2. Materials and Methods

2.1. *Animals*

Adult male mice weighing 25-30 g were purchased from the animal house of the National Research Center. Mice were housed in separate cages with no more than 5 animals per cage, in the laboratory animal center of the German University in Cairo, under a controlled temperature (22-23°C), on a 12-hour light/dark cycle and supplied with food and water *ad lib*. All experimental procedures were conducted according to NIH guidelines for the treatment and care of laboratory animals published by the US National Institutes of Health (NIH publication 85-23 revised 1985) and approved by the animal and human ethics committee in the German University in Cairo (GUC).

2.2. *Chemicals*

LPS (Sigma Chemical Co., USA); Perindopril (Servier Pharmaceutical Co., Egypt) and Celecoxib (Pfizer Co., Egypt) were used in this study. All were dissolved in physiological saline. TNF-α and IL-1β levels were measured using Quantikine rat TNF-α and IL-1β ELISA kits (R&D Systems).

2.3. *Experimental protocol*

Mice were divided into five groups, each containing 10 mice. The first group received a daily dose of 1% Tween 80 intraperitoneally (*i.p.*), for 7 days and served as control group. The other four groups of animals were given a single injection of LPS at a dose of 0.8 mg/kg, *i.p.* to induce an Alzheimer's model (*17,18*). In addition to LPS, the four groups received concurrent treatment for 7 days with one of the following: 1% Tween 80, *i.p.* (LPS – treated group); Celecoxib at a dose of 30 mg/kg/day, *i.p.* (LPS + Celecoxib – treated group) (*19*); Perindopril at a dose of 0.5 mg/kg/day, *i.p.* (LPS + Perindopril – treated group) (*14*) and a combination therapy of both Celecoxib and Perindopril at the same doses previously used (LPS + Celecoxib + Perindopril – treated group). At the end of the experimental protocol, behavioral tests were carried out 1 h after the last injection of the tested drugs, and then 24 h later. Animals were anesthetized with sodium phentobarbital (60 mg/kg) and killed by decapitation. Brains were rapidly removed and cut into 2 symmetrical halves by midline incision. One half was fixed in 10% formol saline for histopathological studies, and the other half was stored at –80°C for estimation of TNF-α and IL-1β.

2.4. *Behavioral experiments*

On the day of testing, mice were transported to the testing facility (Behavioral Lab, Faculty of Pharmacy, Cairo University). A 30 min period was allowed prior to testing to adapt to the environment and to minimize the effect of stress due to transfer.

2.4.1. *The open field test*

Exploratory locomotor activity was measured using the open field test (*20*). This test was carried out during the morning daylight in a quiet lab in order to avoid interference from any external stimuli. It was performed using a special a squared-shape wooden box having red sides and a white floor. Each side is 80 × 80 cm and 40 cm in height (*21*). The floor field is divided by black lines into 16 equal squares (*22*). Rats were placed individually into the central point of the open field and observed during a 3 min period for the following items:

1) *Latency*: it is the time interval (in seconds) between placing the animal at the middle of the arena until the decision of the animal to move (*23*).

2) *Ambulation frequency*: which is the number of squares crossed by the animal and was recorded per minute. The total number during the 3 min period was used to compare groups (*22,24*).

3) *Grooming frequency*: it is defined as the number during 3 min of face washing and scratching with the hind leg, licking of the fur and genitals (*21,25*).

4) *Rearing frequency*: it is the number of times the animal stood and stretched on hind limbs with or without fore limb support (*24,26*).

2.4.2. *Spontaneous alternation Y-maze test*

Immediate working memory performance was assessed by recording spontaneous alternation behavior in a Y-maze (*27*). The maze was made of black-painted wood and each arm was 25 cm long, 14 cm high, 5 cm wide and positioned at equal angles. Each mouse was placed in the center of the Y maze and allowed to explore freely during an 8-min session without reinforcers such as food, water, or electric shock. The series of arm entries were recorded visually and an arm entry was considered to be completed when the hind paws of the mouse were completely placed in the arm. The alternation behavior (actual alternations) was defined as the consecutive entry into three arms, *i.e.*, the combination of three different arms, with stepwise combinations in the sequence. The maximum number of alternations was thus the total number of arms entered minus 2, and the percentage of alternation behavior was calculated as (actual alternations/maximum alternations) × 100% (*28*).

2.5. *Histopathological studies*

2.5.1. *Histochemical study*

Cerebral specimens of control and experimental groups were placed in 10% formol saline and prepared for paraffin block sections. Five μm serial sections were cut and stained with Congo red stain (*29*). The entire procedure was performed at room temperature in a fume hood. Counterstaining was performed with haematoxylin for demonstration of nuclei. Congo red labels amyloid in brain parenchyma and blood vessels.

2.5.2. *Morphometric study*

A Leica Quin 500 LTD image analysis computer assisted system (Histology Department, Kasr Al Aini) was used. The % area of amyloid angiopathy was determined per section using an interactive measurements menu. The area of amyloid plaques was assessed. The apoptotic index was recorded as the percentage of dark nuclei in neurons.

2.6. *Biochemical parameters: TNF-α and IL-1β*

TNF-α and IL-1β, as inflammatory cytokines, were measured in the brain tissue after homogenization in ice-cold saline using a Potter-Elvejham glass homogenizer. The homogenate was centrifuged at 1,200 × g for 20 min at 4°C and the supernatant was examined for TNF-α and IL-1β using Quantikine rat TNF-α and IL-1β ELISA kits (R&D Systems) according to the manufacturer's recommendations.

2.7. *Statistical analysis*

All data are expressed as means ± S.E.M. Statistical analysis for comparisons between different groups were carried out by one way analysis of variance (ANOVA) followed by "*t*" test used as a post hoc test. The level of significance was set at $p < 0.05$. Graph Pad Software InStat (version 2) was used to carry out these statistical tests.

3. Results

3.1. *Effect of COX-2 inhibitor "Celecoxib" and ACEI "Perindopril" on LPS-induced cognitive impairment in mice*

3.1.1. *Open field test*

In the current investigation, administration of LPS (0.8 mg/kg) resulted in a significant increase in the latency period and decrease in the grooming frequency as compared to the normal control values in the open field test. Treatment with Celecoxib (30 mg/kg/day) or combined therapy of both Celecoxib and Perindopril resulted in significant protection against LPS-induced changes in both parameters ($p < 0.05$ *vs.* LPS group) (Figures 1A and 1B). Perindopril significantly decreased the latency time but had no effect on grooming frequency. In the same test LPS administration significantly suppressed the ambulation and the rearing frequencies as compared to the normal control values. Treatment with Celecoxib, Perindopril (0.5 mg/kg/day) or both drugs resulted in a significant rise in both parameters as compared to that of the LPS group (Figures 1C and 1D). All parameters were significantly different from control values ($p < 0.05$) when each drug was used alone, but were not statistically significant from control ($p > 0.05$) when a combination therapy of both Celecoxib and Perindopril was used. This indicated complete memory recovery.

3.1.2. *Y-maze test*

LPS significantly decreased the % of alternation behavior, on the other hand Celecoxib, Perindopril or the combination of both drugs significantly reversed the LPS-induced reduction of alternation behavior (Table 1; Celecoxib group, Perindopril group: $p < 0.05$ *vs.* control; Celecoxib + Perindopril group: $p > 0.05$ *vs.* control group).

3.2. *Effect of Celecoxib and Perindopril on brain histopathology in LPS-induced Alzheimer's model*

3.2.1. *Histochemical results*

Concerning the histopathological findings, sections of normal mice showed cerebral cortex exhibiting pyramidal neurons with pale nuclei surrounded by

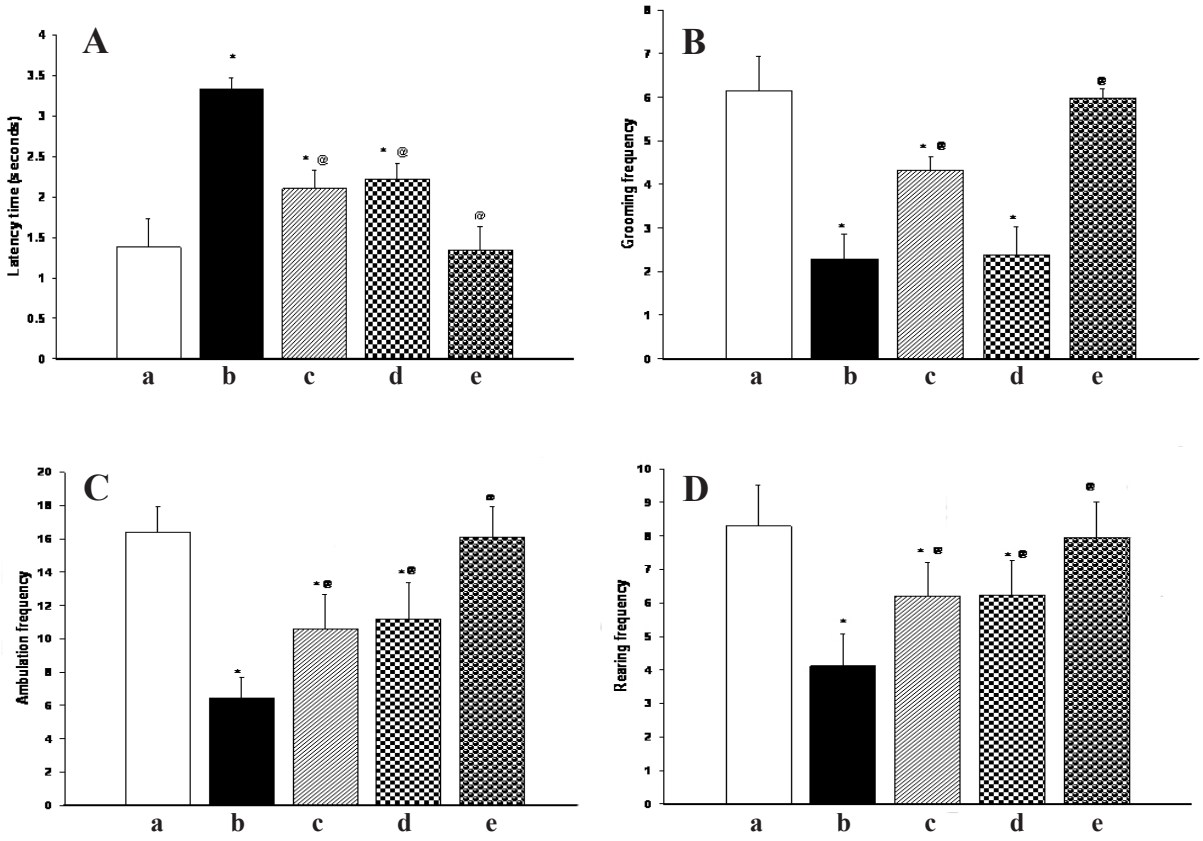

Figure 1. Effect of multiple treatment modalities on open field test in LPS-induced AD mice. Effect of lipopolysaccharide (LPS; 0.8 mg/kg, *i.p.*) with or without 7 days treatments with Celecoxib (30 mg/kg, *i.p.*), Perindopril (0.5 mg/kg, *i.p.*), Celecoxib (30 mg/kg, *i.p.*) + Perindopril (0.5 mg/kg, *i.p.*) was determined. LPS was administered as a single *i.p.* injection on the 1st day to all groups except the normal control one. The test agents were administered daily for 7 days. (**A**) Latency period of mice. (**B**) Grooming frequency of mice. (**C**) Ambulation frequency of mice. (**D**) Rearing frequency of mice. Each bar with vertical line represents the mean of 10 animals ± SE. * Significantly different from normal control group at $p < 0.05$. @ Significantly different from LPS-treated group at $p < 0.05$. **a**, Normal; **b**, LPS; **c**, LPS + Celecoxib; **d**, LPS + Perindopril; **e**, LPS + Celecoxib + Perindopril.

Table 1. Effect of multiple treatment modalities on spontaneous alternation behavior in the Y-maze test in LPS-induced AD mice

Groups	Alternation behavior %
Normal control	75.67 ± 6.45
Control LPS	42.37 ± 3.21[a]
LPS + Celecoxib	58.34 ± 4.23[a,b]
LPS + Perindopril	59.76 ± 3.09[a,b]
LPS + Celecoxib + Perindopril	73.36 ± 4.89[b]

LPS was administered as single *i.p.* injection (on the 1st day) to all groups except the normal one. The test drugs were administered for 7 days. The control and LPS groups received 1% Tween 80 daily for 7 days. Data are expressed as mean ± SE. [a] Significantly different from control group at $p < 0.05$. [b] Significantly different from LPS-treated group at $p < 0.05$.

nerve fibers, glial cells and blood vessels (Figure 2A). In mice receiving LPS, multiple plaques formed of lamellated fibrils were observed. Such plaques were surrounded by multiple apoptotic nuclei (Figures 2B1 and 2B2). Some areas revealed blood vessels with deposits of eosinophilic material (amyloid) in their wall and extravasated red blood corpuscles around as compared to the normal control group (Figure 2B3).

Administration of Celecoxib showed few small lamellated plaques and dense plaques and less prominent apoptotic nuclei (Figure 2C1). On the other hand, Perindopril revealed less multiple lamellated plaques, some dense plaques and still multiple apoptotic nuclei (Figure 2D1). Both Celecoxib and Perindopril sections recruited vessels with minimal deposits in their walls (Figures 2C2 and 2D2). On combined therapy occasional lamellated and occasional dense plaques as well as occasional apoptotic nuclei were detected. Moreover, the blood vessels were comparable to the control group (Figure 2E).

3.2.2. *Morphometric results*

The % area of vascular angiopathy and the area of lamellated amyloid plaques were significantly reduced by Celecoxib as well as by Perindopril compared to the LPS group ($p < 0.05$), while significant reduction was recorded on combined therapy *versus* each drug alone. The apoptotic index was significantly reduced after Celecoxib treatment ($p < 0.05$ *vs.* LPS group), but Perindopril showed no significant effect ($p > 0.05$ *vs.* LPS group). Combined therapy of both drugs revealed a further significant decrease in the apoptotic index (Table 2).

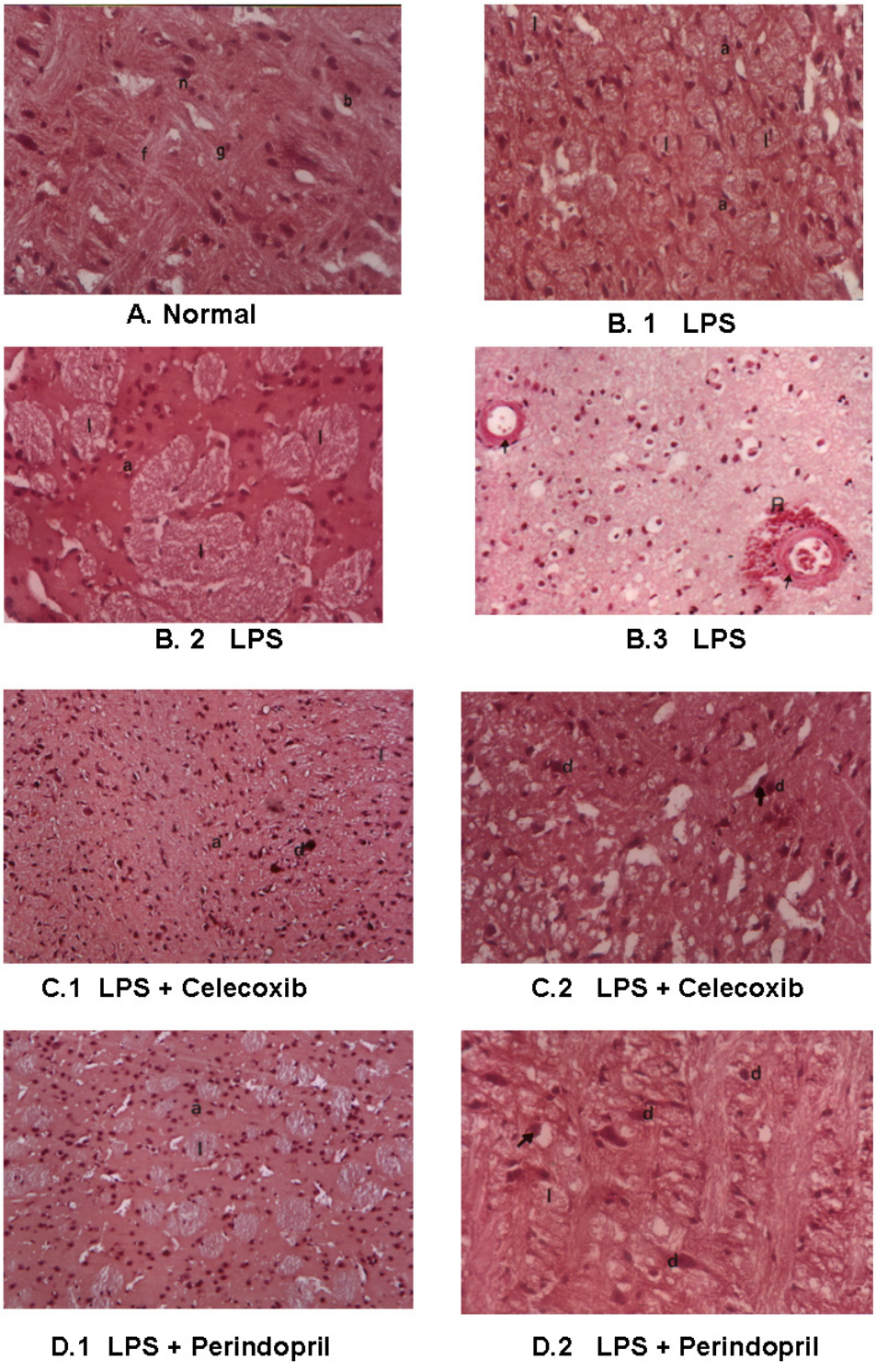

Figure 2. Effect of multiple treatment modalities on brain histopathology in LPS-induced AD mice. Photomicrograph of sections in the cerebral cortex of mice. Effect of lipopolysaccharide (LPS; 0.8 mg/kg, *i.p.*) alone (**B**) or with 7 days treatments by Celecoxib (30 mg/kg, *i.p.*) (**C**), Perindopril (0.5 mg/kg, *i.p.*) (**D**), and Celecoxib + Perindopril (**E**) on brain histopathology was determined. (**A**) Section of a control mouse showing pyramidal neurons (n), glial cells (g), nerve fibers (f), and blood vessels (b). Congo red, ×400. (**B1**) LPS-treated group showed multiple lamellated bodies (L) surrounded by apoptotic nuclei (a). Congo red, ×200. (**B2**) Higher magnification of lamellated bodies (L) and apoptotic nuclei around (a), Congo red, ×400. (**B3**) Two blood vessels with deposited eosinophilic material in their walls (arrows). Note extravasated red blood cells (R). Congo red, ×200. (**C1**) Celecoxib treatment showed few small lamellated bodies (L), some dense plaques (d) and apoptotic nuclei (a). Congo red, × 200. (**C2**) Deposited material in the wall of a capillary (arrow) and dense plaques (d). Congo red, ×400. (**D1**) Perindopril treatment showed less multiple lamellated plaques (L) and multiple apoptotic nuclei (a). Congo red, ×200. (**D2**) Same group showed lamellated plaques (L), some dense plaques (d) and deposited material in a capillary (arrow). Congo red, ×400. (**E**) Combined therapy with both Celecoxib and Perindopril showed occasional lamellated bodies (L), occasional apoptotic nuclei (a) as well occasional dense plaques (d). Congo red, ×400.

Table 2. Effect of multiple treatment modalities on % area of vascular angiopathy, area of lamellated plaques and apoptotic index in brain sections of LPS-induced AD mice

Groups	% Area of vascular angiopathy	Area of lamellated plaques	Apoptotic index
Control group	-	-	-
LPS group	4.65 ± 0.40[a]	5857.61 ± 361.5[a]	8.63 ± 0.42
Celecoxib group	1.47 ± 0.39[b]	1829.34 ± 116.49[b]	3.14 ± 0.19[b]
Perindopril group	1.68 ± 0.43[b]	1992.65 ± 52.69[b]	6.51 ± 0.60
Combined group	–	157.89 ± 32.16[b]	1.22 ± 0.11[b]

LPS was administered as a single *i.p.* injection (on the 1st day) to all groups except the control one. The test drugs were administered for 7 days. The control and LPS groups received 1% Tween 80 daily for 7 days. Data are expressed as mean of 10 animals ± SE. [a] Significantly different from control group at $p < 0.05$. [b] Significantly different from LPS-treated group at $p < 0.05$.

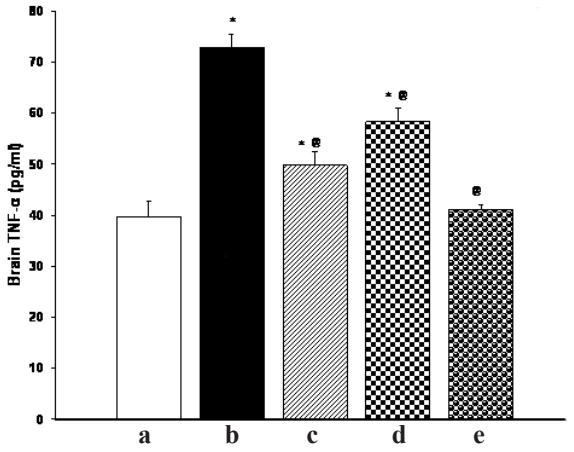

Figure 3. Effect of multiple treatment modalities on TNF-α concentration in brain homogenate samples LPS-induced AD mice. Effect of lipopolysaccharide (LPS; 0.8 mg/kg, *i.p.*) with or without 7 day treatment with Celecoxib (30 mg/kg, *i.p.*), Perindopril (0.5 mg/kg, *i.p.*), Celecoxib (30 mg/kg, *i.p.*) + Perindopril (0.5 mg/kg, *i.p.*) on the inflammatory cytokine TNF-α was determined. LPS was administered as single *i.p.* injection on the 1st day to all groups except the normal one. Each bar with vertical line represents the mean of 10 animals ± SE. * Significantly different from normal control group at $p < 0.05$. @ Significantly different from LPS-treated group at $p < 0.05$. **a**, Normal; **b**, LPS; **c**, LPS + Celecoxib; **d**, LPS + Perindopril; **e**, LPS + Celecoxib + Perindopril.

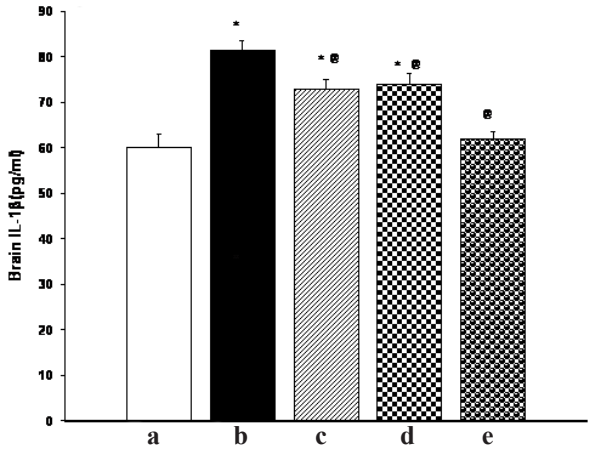

Figure 4. Effect of multiple treatment modalities on IL-1β concentration in brain homogenate samples of LPS-induced AD mice. Effect of lipopolysaccharide (LPS; 0.8 mg/kg, *i.p.*) with or without 7 day treatment with Celecoxib (30 mg/kg, *i.p.*), Perindopril (0.5 mg/kg, *i.p.*), Celecoxib (30 mg/kg, *i.p.*) + Perindopril (0.5 mg/kg, *i.p.*) on IL-1β. LPS was administered as a single *i.p.* injection on the 1st day to all groups except the normal one. Each bar with vertical line represents the mean of 10 animals ± SE. * Significantly different from normal control group at $p < 0.05$. @ Significantly different from LPS-treated group at $p < 0.05$. **a**, Normal; **b**, LPS; **c**, LPS + Celecoxib; **d**, LPS + Perindopril; **e**, LPS + Celecoxib + Perindopril.

3.3. *Effect of Celecoxib and Perindopril on TNF-α and IL-1β in AD brains*

TNF-α and IL-1β were quantified in brain supernatant extracted from the different studied groups. As shown in Figures 3 and 4, levels of both cytokines were significantly increased in the LPS treated group as compared to controls ($p < 0.05$), indicating that LPS induced a neuroinflammatory process which might contribute to AD. These cytokines were significantly attenuated after administration of either Celecoxib or Perindopril ($p < 0.05$ *vs.* LPS group) but there is still a statistical significant difference between each of these groups and the control ($p > 0.05$). Concomitant administration of the COX-2 inhibitor and the ACEI resulted in marked reduction of TNF-α and IL-1β, reaching the corresponding control values ($p > 0.05$ *vs.* control).

4. Discussion

Alzheimer's disease is the most common cause of progressive decline of cognitive function in aged humans (*30*). The pathophysiology of AD is not well understood; therefore, current therapeutic approaches for AD are merely symptomatic and offer only partial benefit without any disease modifying activity (*31*). Various complementary factors including the inflammatory cytokines (TNF and IL-1β), COX-2 as well as the renin angiotensin system seem to be involved in triggering the process of amyloidogenesis contributing to neuronal degeneration and death in AD. Our results revealed that the proposed combination therapy of both COX-2 inhibitor and ACEI proved to be more beneficial in the prevention of AD than the individual agents alone.

In the present study, we examined the effects of Celecoxib and Perindopril on LPS-induced behavioral changes in mice. The Y-maze test was employed to examine spatial learning performance based on working memory (*32*). The memory component in this task is that the mouse must remember which arm was most recently visited in order to alternate the arm choice. We observed that LPS significantly decreased spontaneous alternation, an effect that was in turn partially inhibited

by either Celecoxib or Perindopril and completely inhibited by their combination. Similar results were confirmed by Arai *et al.* (*17*), who proved that spatial memory was significantly impaired in rats injected by LPS. This suggested the induction of inducible nitric oxide synthase in the brain (*33*). The open field test has been widely used to measure behavioral responses such as anxiety-induced locomotor activity, hyperactivity, and exploratory behaviors (*34*). In our study LPS increased latency time and decreased grooming, rearing and ambulation frequencies. These locomotor changes were completely canceled by a concomitant administration of both Celecoxib and Perindopril. Similarly, Swiergiel and Dunn (*35*) reported that LPS decreased the number of line crossings in the center of the field, reflecting anxiety-like behavior. This effect was also accompanied by a similar decrease in line crossings in the periphery, as well as in rears and climbs indicating reduction in overall locomotor activity. They suggested that the ensuing cytokines could activate the hypothalamic-pituitary-adrenal axis and central noradrenergic systems and influence affective state, including anxiety-related behavior. In the present work, behavioral disturbances were accompanied by increased brain levels of both TNF-α and Il-1β in the LPS treated group. This is in agreement with previous workers who proved that peripheral administration of LPS increases the brain level of IL-1β, IL-6, and TNF-α (*6,7*) through activation of the immune system and increasing the concentrations of norepinephrine, dopamine, serotonin, and their metabolites in the hypothalamic paraventricular nucleus and in the dorsal hippocampus (*10,11*). Teeling *et al.* (*36*) found that the decrease in the locomotor behavior by LPS coincided with increased expression of cytokines in the periphery and selected regions of the brain.

Considering the concept that the AD affected brain may be in a chronic state of neuroinflammation, attempts to develop anti-neuroinflammatory compounds that attenuate neurodegeneration and improve cognitive impairment are feasible. Our study revealed that Celecoxib, a brain penetrating COX-2 inhibitor, protects against LPS-induced behavioral deficits. This has been associated with significant attenuation of TNF-α and IL-1β in the brain tissue. Our results were in agreement with the work of Cakata *et al.* (*37*), who found significant protection when using a COX-2 inhibitor in mice against memory deficit and locomotor disturbances induced by systemic administration of LPS and amyloid β.

The renin angiotensin system, already of recognized importance in the pathogenesis of hypertension, has become a source of interest in the pathogenesis of AD (*12,38*). In our study, a significant cognitive enhancing effect for the brain was observed with ACEI and Perindopril in LPS-treated mice, but it was still significantly lower than the control. A similar reduction in cognitive decline by ACEI has been reported by Hanon *et al.*, but in stroke related dementia (*39*). Jenkins and Chai (*40*) showed that groups of rats, treated with different concentrations of the ACE inhibitor, learned the location of the submerged platform in the water maze task significantly faster than control rats over 5 training days, reflecting some memory enhancing effects. This beneficial effect of ACEI could be explained by their effect on cholinergic activity *via* reduction of angiotensin II (AngII)-mediated depression of acetylcholine release (*12*). This is consistent with the documented role of the cholinergic system in learning and memory (*41*). Another possible explanation is that AngII suppresses long term potentiation, therefore, administration of ACEI could reverse cognitive deficits. On the contrary, another work demonstrated that intracerebroventricular injection of AngII enhances memory and learning suggesting a direct effect on brain angiotensin receptors including AT1 and AT4 (*42*). The current results demonstrated that Perindopril partially attenuated the LPS-induced increase in brain levels of TNF-α and IL-1β along with the improved behavioral parameters. Shimizu *et al.* (*43*) reported an involvement of peripheral AngII in the development of both fever and peripheral interleukin (IL-1β) production induced in rats by a systemic injection of lipopolysaccharide (LPS). A Miyoshi *et al.* work documented that endogenous AngII enhances LPS-induced microglial cell culture activity through stimulation of the microglial AT (*1*), which itself evokes activation of the transcription factor NF-κB (*44*). These findings could explain the inhibitory effect of Perindopril on the inflammatory response in our study.

It is interesting to note that the group of LPS-treated mice receiving concomitant administration of both Celecoxib and Perindopril displayed a complete improvement of cognitive performance as well as marked attenuation of the neuroinflammatory response. Taken together, all the previously mentioned data are indicative that each drug alone exerts a partial beneficial effect in our AD mice model and that their combination might have a synergistic effect and exert a more protective effect than each one alone. In the present work, some cerebral areas revealed blood vessels with deposited amyloid in their wall and an increased percentage area of vascular angiopathy after LPS injection. Furthermore, multiple lamellated amyloid plaques surrounded by apoptotic nuclei were observed. This is consistent with a study by Lee *et al.* who reported that systemic injection of LPS resulted in accumulation of Aβ1-42 (the major component of senile plaques of the AD brain) in both the cortex and hippocampus of mice brains accompanied with increased expression of amyloid precursor protein (*45*). A reciprocal relationship between amyloidogenesis and neuroinflammation exists (*4*), whereas certain inflammatory mediators induce and are induced by

Aβ. Therefore, in our study, we would expect that Aβ induced by LPS might stimulate glial and microglial production of IL-1 and TNF-α leading to an ongoing inflammatory cascade and contributing to synaptic dysfunction and loss, and later, neuronal death. On the other hand, increased tissue levels of IL-1 and TNF-α observed in this study could be responsible for Aβ synthesis resulting in deposition of amyloid plaques in cerebral areas and development of vascular angiopathy. In our study, the use of Celecoxib in the AD model, shows significant efficacy in decreasing the % area of vascular angiopathy with less deposition of lamellated plaques and decreased apoptotic index. Nevertheless, all these values were significantly lower that those of the control group. It has been reported that increased production of amyloid β results in vascular oxidative stress and loss of vasodilation function. The culprit molecule, superoxide, triggers the synthesis of other reactive oxygen species and the sequestration of nitric oxide (NO), which impairs resting cerebrovascular tone and NO-dependent dilation (*46*).

We observed from the present study that administration of the ACEI Perindopril partially protects the AD brain against cerebrovascular angiopathy and deposition of amyloid plaques. The apoptotic index tends to be lower than the corresponding value in the LPS group but did not reach a statistically significant level. Data from other Alzheimer models suggest that captopril and similar ACEIs do not cause Aβ accumulation *in vivo* (*15*). A more recent study by Miners *et al.* reported that ACE-1 activity is increased in AD, in direct relationship to parenchymal Aβ load and this increased ACE-1, probably of neuronal origin, accumulates perivascularly in severe cerebral amyloid angiopathy and colocalizes with vascular extracellular matrix. This effect could be attributed to increased upregulation of neprilysin (an Aβ degrading enzyme) (*48*) which also operates within the renin-angiotensin system (*16*). This possibility is further emphasized by the findings of a postmortem study that reported a significant reduction of neprilysin activity in brain homogenates of patients with AD compared to controls, and that loss of cerebrovascular-associated neprilysin in AD is inversely related to the severity of cerebral amyloid angiopathy (*49*).

A synergistic effect of both drugs, targeting wide varieties of pathophysiological mechanisms in the AD model has been observed. These data taken together with the previously discussed ones regarding complete cognitive recovery and inhibition of the neuroinflammatory cytokines support the potential use of such a combination as treatment for the pathophysiology of AD. However, there are enough clues to justify the use of such a combination as a promising strategy in treatment of AD. Many questions still remain regarding therapy.

Acknowledgement

Authors are very grateful to Professor Maha Zikry and Professor Gehan Abou El Fotouh (Histology Department, Faculty of Medicine, Cairo University) for their contributions to the histopathological studies of this work.

References

1. Marques CA, Keil U, Bonert A, Steiner B, Haass C, Muller W, Eckert A. Neurotoxic mechanisms caused by the Alzheimer's disease-linked Swedish amyloid precursor protein mutation. J Biol Chem. 2003; 278:28294-28302.
2. Keil U, Bonert A, Marques CA, Scherping I, Weyermann J, Strosznajder JB, Müller-Spahn F, Haass C, Czech C, Pradier L, Müller WE, Eckert A. Amyloid-β induced changes in nitric oxide production and mitochondrial activity lead to apoptosis. J Biol Chem. 2004; 279:50310-50320.
3. Love S. Contribution of cerebral amyloid angiopathy to Alzheimer's disease. J Neurol Neurosurg Psychiatry. 2004; 75:1-4.
4. Akiyama H, Barger S, Barnum S, *et al.* Inflammation and Alzheimer's disease. Neurobiol Aging. 2000; 21:383-421
5. Breitner JC. Inflammatory processes and antiinflammatory drugs in Alzheimer's disease: a current appraisal. Neurobiol Aging. 1996; 17:789-794.
6. Mackenzie IR. Antiinflammatory drugs in the treatment of Alzheimer's disease. J Rheumatol. 1996; 23:806-808.
7. Mackenzie IR, Munoz DG. Nonsteroidal anti-inflammatory drug use and Alzheimer-type pathology in aging. Neurology. 1998; 50:986-990.
8. Forette F, Hauw J. Alzheimer's disease from brain lesions to new drugs. Bull Acad Natl Med. 2008; 192:363-378.
9. James DS. The multisystem adverse effects of NSAID therapy. J Am Osteopath Assoc. 1999; 99(11 Suppl): S1-S7.
10. Yermakova AV, O'Banion MK. Downregulation of neuronal cyclooxygenase-2 expression in end stage Alzheimer's disease. Neurobiol Aging. 2001; 22:823-836.
11. Melnikova T, Savonenko A, Wang Q, Liang X, Hand T, Wu L, Kaufmann WE, Vehmas A, Andreasson KI. Cycloxygenase-2 activity promotes cognitive deficits but not increased amyloid burden in a model of Alzheimer's disease in a sex-dimorphic pattern. Neuroscience. 2006; 141:1149-1162.
12. Kehoe PG, Wilcock GK. Is inhibition of the renin-angiotensin system a new treatment option for Alzheimer's disease? Lancet Neurol. 2007; 6:373-378.
13. Takeda S, Sato N, Ogihara T, Morishita R. The renin-angiotensin system, hypertension and cognitive dysfunction in Alzheimer's disease: new therapeutic potential. Front Biosci. 2008; 13:2253-2265.
14. Hou DR, Wang Y, Zhou L, Chen K, Tian Y, Song Z, Bao J, Yang QD. Altered angiotensin-converting enzyme and its effects on the brain in a rat model of Alzheimer disease. Chin Med J. 2008; 121:2320-2323.
15. Hemming ML, Selkoe Dj, Farris W. Effects of prolonged angiotensin-converting enzyme inhibitor treatment on

amyloid beta-protein metabolism in mouse models of Alzheimer disease. Neurobiol Dis. 2007; 26:273-281.
16. Ohrui T, Matsui T, Yamaya M, Arai H, Ebihara S, Maruyama M, Sasaki H. Angiotensin converting enzyme inhibitors and incidence of Alzheimer's disease in Japan. J Am Geriatr Soc. 2004; 52:649-650.
17. Arai K, Matsuki N, Ikegaya Y, Nishiyama N. Deterioration of spatial learning performances in lipopolysaccharide-treated mice. Jpn J Pharmacol. 2001; 87:195-201.
18. Sheng JG, Bora SH, Xu G, Borchelt DR, Price DL, Koliatsos VE. Lipopolysaccharide-induced neuroinflammation increases intracellular accumulation of amyloid precursor protein and amyloid beta peptide in APPswe transgenic mice. Neurobiol Dis. 2003; 14:133-145.
19. Jantzen PT, Connor KE, DiCarlo G, Wenk GL, Wallace JL, Rojiani AM, Coppola D, Morgan D, Gordon MN. Microglial activation and beta -amyloid deposit reduction caused by a nitric oxide-releasing nonsteroidal anti-inflammatory drug in amyloid precursor protein plus presenilin-1 transgenic mice. J Neurosci. 2002; 22:2246-2254.
20. Tsujimura A, Matsuki M, Takao K, Yamanishi K, Miyakawa T, Hashimoto-Gotoh T. Mice lacking the kf-1 gene exhibit increased anxiety- but not despair-like behavior. Front Behav Neurosci. 2008; 2:4.
21. Cunha JM, Masur J. Evaluation of psychotropic drugs with a modified open field test. Pharmacology. 1978; 16:259-267.
22. Volosin M, Cancela I, Malina V. Influence of adrenocorticotrophic on the behavior in the swim test of rats treated chronically with desipramine. J Pharmacol. 1988; 40:74-76.
23. Zbinden G. Experimental methods in behavioral teratology. Arch Toxicol. 1981; 48:69-88.
24. van den Buuse M, de Jong W. Differential effects of dopaminergic drugs on open-field behavior of spontaneously hypertensive rats and normotensive Wistar-Kyoto rats. J Pharmacol Exp Ther. 1989; 248:1189-1196.
25. Chow HL, Beck HM. The effect of apomorphine on the open-field behavior of rats: alone and in pairs. Pharmacol Biochem Behav. 1984; 21:85-88.
26. Altman J, Sudarshan K, Das GD, McCormick N, Barnes D. The influence of nutrition on neural and behavioral development. 3. Development of some motor, particularly locomotor patterns during infancy. Dev Psychobiol. 1971; 4:97-114.
27. Sarter M, Bodewitz G, Stephens DN. Attenuation of scopolamine-induced impairment of spontaneous alteration behaviour by antagonist but not inverse agonist and agonist beta-carbolines. Psychopharmacology. 1988; 94:491-495.
28. Ueno K, Togashi H, Matsumoto M, Ohashi S, Saito H, Yoshioka M. Alpha 4 beta 2 nicotinic acetylcholine receptor activation ameliorates impairment of spontaneous alternation behavior in stroke-prone spontaneously hypertensive rats, an animal model of attention deficit hyperactivity disorder. J Pharmacol Exp Ther. 2002; 302:95-100.
29. Wilcock DM, Gordon MN, Morgan D. Quantification of cerebral amyloid angiopathy and parenchymal amyloid plaques with Congo red histochemical stain. Nat Neurosci. 2002; 1:1591-1595.
30. Yamada K, Toshitaka N. Therapeutic approaches to the treatment of Alzheimer's disease. Drugs Today. 2002; 38:631-637.
31. Mandel SA, Amit T, Kalfon L, Reznichenko L, Weinreb O, Youdim MB. Cell signaling pathways and iron chelation in the neurorestorative activity of green tea polyphenols: special reference to epigallocatechin gallate (EGCG). J Alzheimers Dis. 2008; 15:211-222.
32. Olton DS, Papas BC. Spatial memory and hippocampal function. Neuropsychologia. 1979; 17:669-682.
33. Yamada K, Komori Y, Tanaka T, Senzaki K, Nikai T, Sugihara H, Kameyama T, Nabeshima T. Brain dysfunction associated with an induction of nitric oxide synthase following an intracerebral injection of lipopolysaccharide in rats. Neuroscience. 1999; 88:281-294.
34. Prut L, Belzung C. The open field as a paradigm to measure the effects of drugs on anxiety-like behaviors: a review. Europ J Pharmacol. 2003; 463:3-33.
35. Swiergiel AH, Dunn AJ. Effects of interleukin-1beta and lipopolysaccharide on behavior of mice in the elevated plus-maze and open field tests. Pharmacol Biochem Behav. 2007; 86:651-659.
36. Teeling JL, Felton LM, Deacon RM, Cunningham C, Rawlins JN, Perry VH. Sub-pyrogenic systemic inflammation impacts on brain and behavior, independent of cytokines. Brain Behav Immun. 2007; 21:836-850.
37. Cakata M, Malik AR, Strosznajder JB. Inhibitor of cyclooxygenase-2 protects against amyloid β peptide-evoked memory impairment in mice. Pharm Rep. 2007; 59:164-172.
38. Zou K, Michikawa M. Angiotensin-converting enzyme as a potential target for treatment of Alzheimer's disease: inhibition or activation? Rev Neurosci. 2008; 19:203-212.
39. Hanon O, Seux ML, Lenoir H, Rigaud AS, Forette F. Prevention of dementia and cerebroprotection with antihypertensive drugs. Curr Hypertension Rep. 2004; 6:201-207.
40. Jenkins TA, Chai SY. Effect of chronic angiotensin converting enzyme inhibition on spatial memory and anxiety-like behaviours in rats. Neurobiol Learn Mem. 2007; 87:218-224.
41. Gard PR, Rusted JM. Angiotensin and Alzheimer's disease: therapeutic prospects. Expert Rev Neurother. 2004; 4:87-96.

(*Received October 7, 2009; Accepted November 8, 2009*)

Author Index (2009)

Subject Index (2009)

News

Reviews

Brief Reports

Original Articles

Correlation of *in vitro* dissolution rate and apparent solubility in buffered media using a miniaturized rotating disk equipment: Part I. Comparison with a traditional USP rotating disk apparatus.
Persson AM, Sokolowski A, Pettersson C
2009; 3(3):104-113.

Correlation of *in vitro* dissolution rate and apparent solubility in buffered media using a miniaturized rotating disk equipment: Part II. Comparing different buffer media.
Persson AM, Pettersson C, Sokolowski A
2009; 3(3):114-122.

Formulation and optimization of sustained release terbutaline sulfate microspheres using response surface methodology.
Khattab I, Bandarkar F, Lila A
2009; 3(3):123-135.

Stability studies of the effect of crosslinking on hydrochlorothiazide release.
Elmeshad AN, Darwish MK
2009; 3(3):136-142.

Effects of a hyaluronic acid and low molecular weight heparin injection on osteoarthritis in rabbits.
Ling PX, Zhang LN, Jin Y, He YL, Zhang TM
2009; 3(4):146-150.

Pterocarpus marsupium extract reveals strong *in vitro* antioxidant activity.
Mohammadi M, Khole S, Devasagayam TPA, Ghaskadbi SS
2009; 3(4):151-161.

Antiaggressive activity of hyperforin: A preclinical study.
Kumar N, Husain GM, Singh PN, Kumar V
2009; 3(4):162-167.

A novel liquid effervescent floating delivery system for sustained drug delivery.
Ibrahim HK
2009; 3(4):168-175.

Microspheres of tramadol hydrochloride compressed along with a loading dose: A modified approach for sustaining release.
Gonjari ID, Hosmani AH, Karmarkar AB, Kadam SB, Godage AS, Khade TS
2009; 3(4):176-180.

Buccal mucoadhesive tablets of flurbiprofen: Characterization and optimization.
Darwish MK, Elmeshad AN
2009; 3(4):181-189.

Beneficial effects of a standardized Hypericum perforatum extract in rats with experimentally induced hyperglycemia.
Husain GM, Singh PN, Kumar V
2009; 3(5):215-220.

Sedative and anxiolytic effects of different fractions of the Commelina benghalensis Linn.
Raquibul Hasan SM, Hossain MM, Akter R, Jamila M, Mazumder EHM, Rahman S
2009; 3(5):221-227.

Vaginal delivery of protein drugs in rats by gene-transformed Lactococcus lactis.
Kaushal G, Shao J
2009; 3(5):228-233.

Case Report

Drug Discoveries & Therapeutics

Guide for Authors

1. Scope of Articles

Drug Discoveries & Therapeutics mainly publishes articles related to basic and clinical pharmaceutical research such as pharmaceutical and therapeutical chemistry, pharmacology, pharmacy, pharmacokinetics, industrial pharmacy, pharmaceutical manufacturing, pharmaceutical technology, drug delivery, toxicology, and traditional herb medicine. Studies on drug-related fields such as biology, biochemistry, physiology, microbiology, and immunology are also within the scope of this journal.

2. Submission Types

Original Articles should be reports new, significant, innovative, and original findings. An Article should contain the following sections: Title page, Abstract, Introduction, Materials and Methods, Results, Discussion, Acknowledgments, References, Figure legends, and Tables. There are no specific length restrictions for the overall manuscript or individual sections. However, we expect authors to present and discuss their findings concisely.

Brief Reports should be short and clear reports on new original findings and not exceed 4000 words with no more than two display items. *Drug Discoveries & Therapeutics* encourages younger researchers and doctors to report their research findings. Case reports are included in this category. A Brief Report contains the same sections as an Original Article, but Results and Discussion sections must be combined.

Reviews should include educational overviews for general researchers and doctors, and review articles for more specialized readers.

Policy Forum presents issues in science policy, including public health, the medical care system, and social science. Policy Forum essays should not exceed 2,000 words.

News articles should not exceed 500 words including one display item. These articles should function as an international news source with regard to topics in the life and social sciences and medicine. Submissions are not restricted to journal staff - anyone can submit news articles on subjects that would be of interest to Drug Discoveries & Therapeutics' readers.

Letters discuss material published in *Drug Discoveries & Therapeutics* in the last 6 months or issues of general interest. Letters should not exceed 800 words and 6 references.

3. Manuscript Preparation

Preparation of text. Manuscripts should be written in correct American English and submitted as a Microsoft Word (.doc) file in a single-column format. Manuscripts must be paginated and double-spaced throughout. Use Symbol font for all Greek characters. Do not import the figures into the text file but indicate their approximate locations directly on the manuscript. The manuscript file should be smaller than 5 MB in size.

Title page. The title page must include 1) the title of the paper, 2) name(s) and affiliation(s) of the author(s), 3) a statement indicating to whom correspondence and proofs should be sent along with a complete mailing address, telephone/fax numbers, and e-mail address, and 4) up to five key words or phrases.

Abstract. A one-paragraph abstract consisting of no more than 250 words must be included. It should state the purpose of the study, basic procedures used, main findings, and conclusions.

Abbreviations. All nonstandard abbreviations must be listed in alphabetical order, giving each abbreviation followed by its spelled-out version. Spell out the term upon first mention and follow it with the abbreviated form in parentheses. Thereafter, use the abbreviated form.

Introduction. The introduction should be a concise statement of the basis for the study and its scientific context.

Materials and Methods. Subsections under this heading should include sufficient instruction to replicate experiments, but well-established protocols may be simply referenced. *Drug Discoveries & Therapeutics* endorses the principles of the Declaration of Helsinki and expects that all research involving humans will have been conducted in accordance with these principles. All laboratory animal studies must be approved by the authors' Institutional Review Board(s).

Results. The results section should provide details of all of the experiments that are required to support the conclusions of the paper. If necessary, subheadings may be used for an orderly presentation. All figures, tables, and photographs must be referred in the text.

Discussion. The discussion should include conclusions derived from the study and supported by the data. Consideration should be given to the impact that these conclusions have on the body of knowledge in which context the experiments were conducted. In Brief Reports, Results and Discussion sections must be combined.

Acknowledgments. All funding sources should be credited in the Acknowledgments section. In addition, people who contributed to the work but who do not fit the criteria for authors should be listed along with their contributions.

References. References should be numbered in the order in which they appear in the text. Cite references in text using a number in parentheses. Citing of unpublished results and personal communications in the reference list is not recommended but these sources may be mentioned in the text. For all references, list all authors, but if there are more than fifteen authors, list the first three authors and add "*et al.*" Abbreviate journal names as they appear in PubMed. Web references can be included in the reference list.

Example 1:
Hamamoto H, Akimitsu N, Arimitsu N, Sekimizu K. Roles of the Duffy antigen and glycophorin A in malaria infectionand erythrocyte. Drug Discov Ther. 2008; 2:58-63.

Example 2:
Zhao X, Jing ZP, Xiong J, Jiang SJ. Suppression of experimental abdominal aortic aneurysm by tetracycline: a preliminary study. Chin J Gen Surg. 2002; 17:663-665. (in Chinese)

Example 3:
Mizuochi T. Microscale sequencing of *N*-linked oligosacchaides of glycoproteins using hydrazinolysis, Bio-Gel P-4, and sequential exoglycosidase digestion. In: Methods in Molecular Biology: Vol. 14 Glycoprotein analysis in biomedicine (Hounsell T, ed.). Humana Press, Totowa, NJ, USA, 1993; pp. 55-68.

Example 4:
Drug Discoveries & Therapeutics. Hot topics & news: China-Japan Medical Workshop on Drug Discoveries and Therapeutics 2007. http://www.ddtjournal.com/hotnews.php (accessed July 1, 2007).

Figure legends. Include a short title and a short explanation. Methods described in detail in the Materials and methods section should not be repeated in the legend. Symbols used in the figure must be explained. The number of data points represented in a graph must be indicated.

Tables. All tables should have a concise title and be typed double-spaced on pages separate from the text. Do not use vertical rules. Tables should be numbered with Arabic numerals consecutively in accordance with their appearance in the text. Place footnotes to tables below the table body and indicate them with lowercase superscript letters.

Language editing. Manuscripts submitted by authors whose primary language is not English should have their work proofread by a native English speaker before submission. The Editing Support Organization can provide English proofreading, Japanese-English translation, and Chinese-English translation services to authors who want to publish in *Drug Discoveries & Therapeutics* and need assistance before submitting an article. Authors can contact this organization directly at http://www.iacmhr.com/iac-eso .

IAC-ESO was established in order to facilitate manuscript preparation by researchers whose native language is not English and to help edit work intended for international academic journals. Quality revision, translation, and editing services are offered by our staff, who are native speakers of particular languages and who are familiar with academic writing and journal editing in English.

4. Figure Preparation

All figures should be clear and cited in numerical order in the text. Figures must fit a one- or two-column format on the journal page: 8.3 cm (3.3 in.) wide for a single column; 17.3 cm (6.8 in.) wide for a double column; maximum height: 24.0 cm (9.5 in.). Only use the following fonts in the figure: Arial and Helvetica. Provide all figures as separate files. Acceptable file formats are JPEG and TIFF. Please note that files saved in JPEG or TIFF format in PowerPoint lack sufficient resolution for publication. Each Figure file should be smaller than 10 MB in size. Do not compress files. A fee is charged for a color illustration or photograph.

5. Online Submission

Manuscripts should be submitted to *Drug Discoveries & Therapeutics* online at http://www.ddtjournal.com. The manuscript file should be smaller than 10 MB in size. If for any reason you are unable to submit a file online, please contact the Editorial Office by e-mail: office@ddtjournal.com

Editorial and Head Office
Wei TANG, MD PhD
Executive Editor
Drug Discoveries & Therapeutics
TSUIN-IKIZAKA 410,
2-17-5 Hongo, Bunkyo-ku,
Tokyo 113-0033, Japan.
Tel: 03-5840-9697
Fax: 03-5840-9698
E-mail: office@ddtjournal.com

Cover letter. A cover letter from the corresponding author including the following information must accompany the submission: name, address, phone and fax numbers, and e-mail address of the corresponding author. This should include a statement affirming that all authors concur with the submission and that the material submitted for publication has not been previously published and is not under consideration for publication elsewhere and a statement regarding conflicting financial interests.

Authors may recommend up to three qualified reviewers other than members of Editorial board. Authors may also request that certain (but not more than three) reviewers not be chosen.

The cover letter should be submitted as a Microsoft Word (.doc) file (smaller than 1 MB) at the same time the work is submitted online.

6. Accepted Manuscripts

Proofs. Rough galley proofs in PDF format are supplied to the corresponding author *via* e-mail. Corrections must be returned within 4 working days of receipt of the proofs. Subsequent corrections will not be possible, so please ensure all desired corrections are indicated. Note that we may proceed with publication of the article if no response is received.

Transfer of copyrights. Upon acceptance of an article, authors will be asked to agree to a transfer of copyright. This transfer will ensure the widest possible dissemination of information. A letter will be sent to the corresponding author confirming receipt of the manuscript. A form facilitating transfer of copyright will be provided. If excerpts from other copyrighted works are included, the author(s) must obtain written permission from the copyright owners and credit the source(s) in the article.

Cover submissions. Authors whose manuscripts are accepted for publication in *Drug Discoveries & Therapeutics* may submit cover images. Color submission is welcome. A brief cover legend should be submitted with the image.

Revised April 20, 2009

IACMHR CO., LTD.

Drug Discoveries & Therapeutics

Editorial Office
TSUIN-IKIZAKA 410,
2-17-5 Hongo, Bunkyo-ku,
Tokyo 113-0033, Japan

Tel: 03-5840-9697
Fax: 03-5840-9698
E-mail: office@ddtjournal.com
URL: www.ddtjournal.com

IACMHR CO., LTD.

JOURNAL PUBLISHING AGREEMENT

Ms No:

Article entitled:

Corresponding author:

To be published in Drug Discoveries & Therapeutics

Assignment of publishing rights:

I hereby assign to International Advancement Center for Medicine & Health Research Co., Ltd. (IACMHR Co., Ltd.) publishing Drug Discoveries & Therapeutics the copyright in the manuscript identified above and any supplemental tables and illustrations (the articles) in all forms and media, throughout the world, in all languages, for the full term of copyright, effective when and if the article is accepted for publication. This transfer includes the rights to provide the article in electronic and online forms and systems.

I understand that I retain or am hereby granted (without the need to obtain further permission) rights to use certain versions of the article for certain scholarly purpose and that no rights in patent, trademarks or other intellectual property rights are transferred to the journal. Rights to use the articles for personal use, internal institutional use and scholarly posting are retained.

Author warranties:

I affirm the author warranties noted below.

1) The article I have submitted to the journal is original and has not been published elsewhere.
2) The article is not currently being considered for publication by any other journal. If accepted, it will not be submitted elsewhere.
3) The article contains no libelous or other unlawful statements and does not contain any materials that invade individual privacy or proprietary rights or any statutory copyright.
4) I have obtained written permission from copyright owners for any excerpts from copyrighted works that are included and have credited the sources in my article.
5) I confirm that all commercial affiliations, stock or equity interests, or patent-licensing arrangements that could be considered to pose a financial conflict of interest regarding the article have been disclosed.
6) If the article was prepared jointly with other authors, I have informed the co-authors(s) of the terms of this publishing agreement and that I am signing on their behalf as their agents.

Your Status:

☐ I am the sole author of the manuscript.

☐ I am one author signing on behalf of all co-authors of the manuscript.

Please tick one of the above boxes (as appropriate) and then sign and date the document in black ink.

Signature: **Date:**

Name printed:

Please return the completed and signed original of this form by express mail or fax, or by e-mailing a scanned copy of the signed original to:

Drug Discoveries & Therapeutics office
TSUIN-IKIZAKA 410, 2-17-5 Hongo,
Bunkyo-ku, Tokyo 113-0033, Japan
e-mail: proof-editing@ddtjournal.com
Fax: +81-3-5840-9698